

Bis(thiophenolate)pyridine Pincer Ligands and Trivalent Zirconocene  
Complexes Relevant to Early Transition Metal Polymerization Catalysts

Thesis by

Taylor Lenton

In Partial Fulfillment of the Requirements

For the Degree of

Doctor of Philosophy

California Institute of Technology

Pasadena, California

2014

(Defended September 10, 2013)

© 2014

Taylor Lenton

All Rights Reserved

## Acknowledgments

I must start by thanking my advisor, John Bercaw, who allowed me to join the group even as he was beginning to think about retirement. When I first arrived at Caltech, I didn't know exactly what kind of science I wanted pursue, but I knew I wanted to work for someone who would support and challenge me as a scientist. John has been an excellent advisor in that regard and I have learned to think about scientific problems in a much more rigorous manner.

Hans Brintzinger has been an unofficial co-advisor during my graduate career and much of the research in this thesis wouldn't have been possible without him. Although we were able to communicate results effectively through e-mail, phone, and video calls, I am so grateful to have had the opportunity to work with him in person, both in Pasadena and Konstanz, Germany. The ability to sit and exchange ideas over an afternoon cup of tea was invaluable and his enthusiasm for tackling difficult problems within the laboratory continues to inspire me.

The Bercaw Group has changed quite a bit over the years, but throughout my time here it has been filled with people I am happy to call friends and co-workers. Scientifically, the group is a tough crowd to please, but the critiques are mostly friendly and people are always willing to hang out in the wilderness for a few days or enjoy sunny California barbeque when we need a break from work.

Finally, I must thank my family, friends and Justin, who have provided so much support during my time here at Caltech and given me a life outside of the lab. I wouldn't have survived the ups and downs of graduate school without them.

## Abstract

Two major topics are covered: the first chapter is focused on the development of post-metallocene complexes for propylene polymerization. The second and third chapters investigate the consequences of diisobutylaluminum hydride ( $\text{HAl}^i\text{Bu}_2$ ) additives in zirconocene based polymerization systems.

The synthesis, structure, and solution behavior of early metal complexes with a new tridentate  $\text{LX}_2$  type ligand, bis(thiophenolate)pyridine ((SNS) =  $(2\text{-C}_6\text{H}_4\text{S})_2\text{-}2,6\text{-C}_5\text{H}_3\text{N}$ ) are investigated. SNS complexes of Ti, Zr, and Ta having dialkylamido coligands were synthesized and structurally characterized. The zirconium complex,  $(\text{SNS})\text{Zr}(\text{NMe}_2)_2$ , displays  $C_2$  symmetry in the solid state. Solid-state structures of tantalum complexes  $(\text{SNS})\text{Ta}(\text{NMe}_2)_3$  and  $(\text{SNS})\text{TaCl}(\text{NEt}_2)_2$  also display pronounced  $C_2$  twisting of the SNS ligand. 1D and 2D NMR experiments show that  $(\text{SNS})\text{Ta}(\text{NMe}_2)_3$  is fluxional with rotation about the Ta-N(amide) bonds occurring on the NMR timescale. The fluxional behavior of  $(\text{SNS})\text{TaCl}(\text{NEt}_2)_2$  in solution was also studied by variable temperature  $^1\text{H}$  NMR. Observation of separate signals for the diastereotopic protons of the methylene unit of the diethylamide indicates that the complex remains locked on the NMR timescale in one diastereomeric conformation at temperatures below  $-50\text{ }^\circ\text{C}$ .

Reduction of Zr(IV) metallocenium cations with sodium amalgam ( $\text{NaHg}$ ) produces EPR signals assignable to Zr(III) metallocene complexes. Thus, chloro-bridged heterobinuclear *ansa*-zirconocenium cation  $[\{(\text{SBI})\text{Zr}(\mu\text{-Cl})_2\text{AlMe}_2\}^+\text{B}(\text{C}_6\text{F}_5)_4^-]$  (SBI = *rac*-dimethylsilylbis(1-indenyl)), gives rise to an EPR signal assignable to the complex  $(\text{SBI})\text{Zr}^{\text{III}}(\mu\text{-Cl})_2\text{AlMe}_2$ , while  $(\text{SBI})\text{Zr}^{\text{III}}\text{-Me}$  and  $(\text{SBI})\text{Zr}^{\text{III}}(\mu\text{-H})_2\text{Al}^i\text{Bu}_2$  are formed by reduction of  $[\{(\text{SBI})\text{Zr}(\mu\text{-Me})_2\text{AlMe}_2\}^+\text{B}(\text{C}_6\text{F}_5)_4^-]$  and  $[\{(\text{SBI})\text{Zr}(\mu\text{-H})_3(\text{Al}^i\text{Bu}_2)_2\}^+\text{B}(\text{C}_6\text{F}_5)_4^-]$ ,

respectively. These products are also formed, along with  $(\text{SBI})\text{Zr}^{\text{III}}\text{-}i\text{Bu}$  and  $[(\text{SBI})\text{Zr}^{\text{III}}]^+ \text{AlR}_4^-$ , when  $(\text{SBI})\text{ZrMe}_2$  reacts with  $\text{HAl}^i\text{Bu}_2$ , eliminating isobutane en route to the Zr(III) complex. Studies concerning the interconversion reactions between these and other  $(\text{SBI})\text{Zr}(\text{III})$  complexes and reaction mechanisms involved in their formation are also reported.

The addition of  $\text{HAl}^i\text{Bu}_2$  to precatalyst  $[(\text{SBI})\text{Zr}(\mu\text{-H})_3(\text{Al}^i\text{Bu}_2)_2]^+$  significantly slows the polymerization of propylene and changes the kinetics of polymerization from 1<sup>st</sup> to 2<sup>nd</sup> order with respect to propylene. This is likely due to competitive inhibition by  $\text{HAl}^i\text{Bu}_2$ . When the same reaction is investigated using  $[(^n\text{BuCp})_2\text{Zr}(\mu\text{-H})_3(\text{Al}^i\text{Bu}_2)_2]^+$ , hydroalumination between propylene and  $\text{HAl}^i\text{Bu}_2$  is observed instead of propylene polymerization.

## Table of Contents

<b>Acknowledgment</b>	iii
<b>Abstract</b>	iv
<b>Table of Contents</b>	vi
<b>List of Figures</b>	vii
<b>List of Schemes</b>	ix
<b>List of Tables</b>	x
<b>Chapter 1</b>	1
General Introduction	
<b>Chapter 2</b>	7
Early Transition Metal Complexes Incorporating a Novel Bis(thiophenolate)pyridine Ligand	
<b>Chapter 3</b>	38
Formation of Trivalent Zirconocene Complexes from <i>ansa</i> -Zirconocene-Based Olefin-Polymerization Precatalysts	
<b>Chapter 4</b>	83
Hydroalumination versus Polymerization in Zirconocene Systems Containing Aluminum Hydrides	
<b>Appendix A</b>	105
Synthesis of (ONO)ZrMe <sub>2</sub> and (ONO)ZrNp <sub>2</sub> : Towards Stoichiometric Activation and Post-Metallocene Insertion Studies	

## List of Figures

### Chapter 1

Figure 1.1	Tacticity of polypropylene	2
Figure 1.2	Transition state model for polymerization	3
Figure 1.3	MAO activated zirconocene cations	4
Figure 1.4	Post-metallocene pincer complexes	5

### Chapter 2

Figure 2.1	Metallocene vs. $LX_2$ pincer ligand symmetries	10
Figure 2.2	Crystal structure of $(SNS)Zr(NMe_2)_2$	15
Figure 2.3	Crystal structure of $(SNS)Ta(NMe_2)_3$	18
Figure 2.4	1D-NOE $^1H$ NMR of $(SNS)Ta(NMe_2)_3$ at 25 °C	20
Figure 2.5	1D-NOE $^1H$ NMR of $(SNS)Ta(NMe_2)_3$ at 25 °C	21
Figure 2.6	Variable temperature $^1H$ NMR spectra of $(SNS)Ta(NMe_2)_3$	22
Figure 2.7	Crystal structure of $(SNS)Ta(NEt_2)_2Cl$	24
Figure 2.8	Variable temperature $^1H$ NMR spectra of $(SNS)Ta(NEt_2)_2Cl$	26
Figure 2.9	$^1H$ - $^1H$ ROESY NMR of $(SNS)Ta(NEt_2)_2Cl$	27

### Chapter 3

Figure 3.1	SBI <i>ansa</i> -zirconocene cations with discrete activators	40
Figure 3.2	EPR spectrum of $(SBI)Zr^{III}(\mu-Cl)_2AlMe_2$	44
Figure 3.3	EPR spectrum of reduction of $[(SBI)ZrMe][B(C_6F_5)_4]$	45
Figure 3.4	EPR spectrum of reduction of $[(SBI)Zr(\mu-Me)_2AlMe_2]^+$	45
Figure 3.5	$^1H$ NMR before and after reduction of $[(SBI)Zr(\mu-Me)_2AlMe_2]^+$	47
Figure 3.6	EPR spectrum of $(SBI)Zr^{III}(\mu-H)_2AlR_2$	48
Figure 3.7	Possible EPR simulations for $(SBI)Zr^{III}(\mu-H)_2AlR_2$	49
Figure 3.8	EPR time course of $(SBI)ZrMe_2$ and 10 $HAl^iBu_2$	52
Figure 3.9	$^1H$ NMR time course of $(SBI)ZrMe_2$ and 10 $HAl^iBu_2$	52
Figure 3.10	EPR spectrum of $(SBI)Zr^{III}-^iBu$	53
Figure 3.11	EPR time course of $(SBI)ZrMe_2$ and 2 $HAl^iBu_2$	54

Figure 3.12	$^1\text{H}$ NMR time course of (SBI)ZrMe <sub>2</sub> and 2 HAl <sup><i>i</i></sup> Bu <sub>2</sub>	54
Figure 3.13	EPR spectrum of (SBI)Zr <sup>III</sup> - <i>i</i> Bu + PMe <sub>2</sub> Ph	55
Figure 3.14	EPR of (SBI)Zr <sup>III</sup> - <i>i</i> Bu and (SBI)Zr <sup>III</sup> (μ-H) <sub>2</sub> AlR <sub>2</sub> + ClAlMe <sub>2</sub>	57
Figure 3.15	Crystal structure of (SBI)Zr <sup>III</sup> (μ-Cl) <sub>2</sub> AlMe <sub>2</sub>	59
Figure 3.16	EPR time course of (SBI)ZrMe <sub>2</sub> and 1 HAl <sup><i>i</i></sup> Bu <sub>2</sub>	61
Figure 3.17	EPR spectrum of [(SBI)Zr <sup>III</sup> ] <sup>+</sup>	62
Figure 3.18	EPR spectrum of (SBI)Zr <sup>III</sup> -Me	64
Figure 3.19	$^1\text{H}$ NMR spectra of [(SBI)Zr <sup>III</sup> ] <sup>+</sup> + [(SBI)Zr(μ-Me) <sub>2</sub> AlMe <sub>2</sub> ] <sup>+</sup>	65
Figure 3.20	$^1\text{H}$ NMR spectra of possible intermediates during reduction	67
<b>Chapter 4</b>		
Figure 4.1	$^1\text{H}$ NMR spectrum of [(SBI)Zr(μ-H) <sub>3</sub> (Al <sup><i>i</i></sup> Bu <sub>2</sub> ) <sub>2</sub> ][B(C <sub>6</sub> F <sub>5</sub> ) <sub>4</sub> ]	87
Figure 4.2	Polymerization with [(SBI)Zr(μ-H) <sub>3</sub> (Al <sup><i>i</i></sup> Bu <sub>2</sub> ) <sub>2</sub> ] <sup>+</sup>	88
Figure 4.3	Polymerization with [(SBI)Zr(μ-H) <sub>3</sub> (Al <sup><i>i</i></sup> Bu <sub>2</sub> ) <sub>2</sub> ] <sup>+</sup> and 10 HAl <sup><i>i</i></sup> Bu <sub>2</sub>	89
Figure 4.4	Polymerization with various concentrations of HAl <sup><i>i</i></sup> Bu <sub>2</sub>	90
Figure 4.5	Polymerization with [( <sup><i>n</i></sup> BuCp) <sub>2</sub> Zr(μ-H) <sub>3</sub> (Al <sup><i>i</i></sup> Bu <sub>2</sub> ) <sub>2</sub> ] <sup>+</sup>	93
Figure 4.6	$^1\text{H}$ NMR spectra of HAl <sup><i>i</i></sup> Bu <sub>2</sub> and hydroalumination products	94
<b>Appendix A</b>		
Figure A.1	Crystal structure of (ONO)ZrCl <sub>2</sub> (HNMe <sub>2</sub> )	107
Figure A.2	$^1\text{H}$ NMR spectrum of (ONO)ZrCl <sub>2</sub> (THF)	107
Figure A.3	$^1\text{H}$ NMR spectrum of (ONO)ZrMe <sub>2</sub>	108
Figure A.4	$^1\text{H}$ NMR spectrum of (ONO)ZrNp <sub>2</sub>	109
Figure A.5	Crystal Structure of (ONO)ZrNp <sub>2</sub>	109
Figure A.6	$^1\text{H}$ NMR spectra of (ONO)ZrNp <sub>2</sub> + B(C <sub>6</sub> F <sub>5</sub> ) <sub>3</sub>	110

## List of Schemes

### Chapter 2

Scheme 2.1	Synthesis of (SNS)H <sub>2</sub>	12
Scheme 2.2	Synthesis of (SNS)Ti(NMe <sub>2</sub> ) <sub>2</sub> and (SNS)Zr(NMe <sub>2</sub> ) <sub>2</sub>	14
Scheme 2.3	Rotation about Ta–N bonds of (SNS)Ta(NMe <sub>2</sub> ) <sub>3</sub>	19
Scheme 2.4	Possible mechanism for R group exchange in (SNS)Ta(NMe <sub>2</sub> ) <sub>3</sub>	23
Scheme 2.5	Summary of fluxional processes in (SNS)Ta(NEt <sub>2</sub> ) <sub>2</sub> Cl	29

### Chapter 3

Scheme 3.1	Summary of (SBI)Zr <sup>III</sup> species and their reactivities	70
------------	--	----

### Chapter 4

Scheme 4.1	Equilibrium between [(SBI)Zr(μ-H) <sub>3</sub> (Al <sup>i</sup> Bu <sub>2</sub> ) <sub>2</sub> ] <sup>+</sup> and [(SBI)Zr(μ-Me) <sub>2</sub> AlMe <sub>2</sub> ] <sup>+</sup>	85
Scheme 4.2	Hydroalumination of propylene by [(SBI)Zr(μ-H) <sub>3</sub> (Al <sup>i</sup> Bu <sub>2</sub> ) <sub>2</sub> ] <sup>+</sup>	86
Scheme 4.3	Possible steady state equilibrium in polymerization mechanism	91
Scheme 4.4	Polymerization of propylene by [( <sup>n</sup> BuCp) <sub>2</sub> Zr(μ-H) <sub>3</sub> (Al <sup>i</sup> Bu <sub>2</sub> ) <sub>2</sub> ] <sup>+</sup>	92
Scheme 4.5	Possible hydroalumination mechanism under high [HAl <sup>i</sup> Bu <sub>2</sub> ]	95
Scheme 4.6	Possible hydroalumination mechanism under low [HAl <sup>i</sup> Bu <sub>2</sub> ]	95
Scheme 4.7	Hydroalumination vs. polymerization of propylene	97

### Appendix A

Scheme A.1	Activation of (ONO)ZrNp <sub>2</sub>	
------------	--------------------------------------	--

## List of Tables

### Chapter 3

Table 3.1	Bond lengths and angles in Zr(III) compounds	60
Table 3.2	Bond lengths and angles in aluminum chloride compounds	60
Table 3.3	Polymerization activities of Zr(III) and Zr(IV) complexes	69

### Chapter 4

Table 4.1	Reactivity of trihydride zirconocenes with propylene and $\text{HAl}^i\text{Bu}_2$	96
-----------	--	----

## Chapter 1

### General Introduction

## Chapter 1

### *Polypropylene Properties and Uses*

The polymerization of propylene by early metal catalysts is an important reaction in both academia and industry. Revenue from the production of polypropylene continues to rise and is projected to reach \$145 billion by 2019, with products finding use in flexible and rigid packaging, medical supplies, and automotive parts.<sup>1</sup> Traditionally, heterogeneous Ziegler-Natta catalysts were used industrially while homogenous catalysts were reserved for academic pursuits, but in recent years, the unique polymer properties imparted by homogenous metallocene catalysts have allowed them to gain traction in industrial processes.<sup>2</sup>

From a chemical standpoint, polypropylene is an interesting material as the tacticity is defined by the relative orientation of neighboring methyl groups. Thus, the physical properties of material are defined by the microstructure of the polymer. Highly stereoregular polymers like isotactic polypropylene form crystalline solids while stereoirregular polypropylene remains amorphous (Figure 1.1).

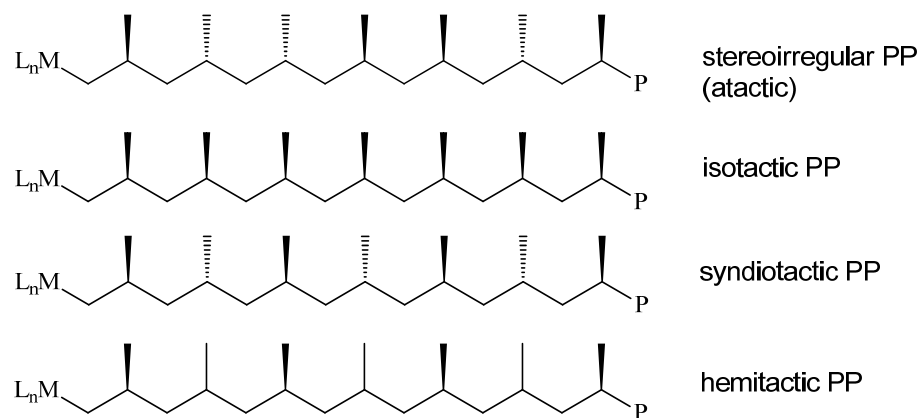


**Figure 1.1.** Polypropylene tacticity is defined by the relative orientation of methyl groups

### Zirconocene Polymerization Catalysts

In zirconocene-based catalysis, the stereochemistry of the polymer is controlled by the overall symmetry of the catalyst. Olefin insertion occurs into a metal–carbon bond, stabilized by an  $\alpha$ -agostic interaction, with the growing polymer chain directed away from the bulk of the ligand.<sup>3</sup> The coordination and insertion of each olefin moves the growing polymer chain back and forth between the two sides of the metallocene wedge with the stereochemistry of each insertion being dictated by the relative ligand environment. Isotactic polypropylene is produced from  $C_2$  symmetric complexes because both sides are identical with respect to the incoming olefin whereas  $C_s$  symmetric complexes lead to syndiotactic polymer (Figure 1.2).

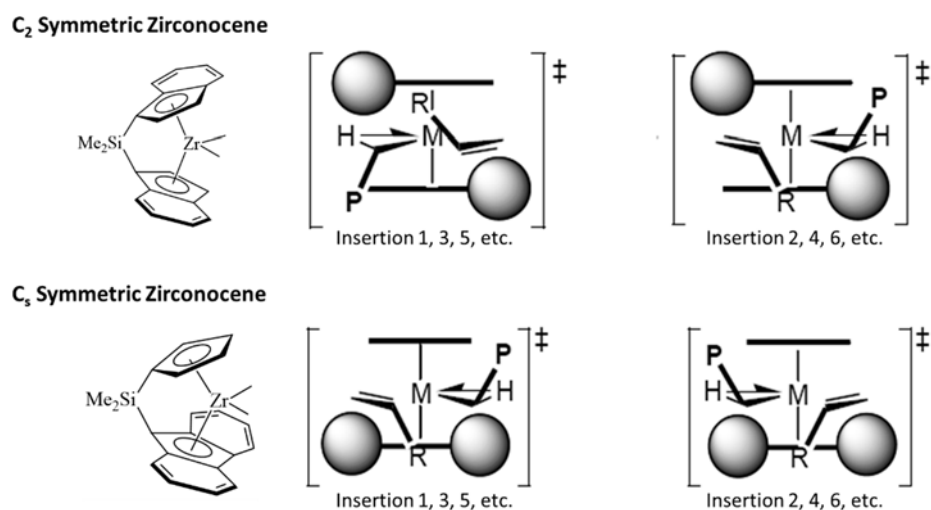


**Figure 1.2.** Transition states in the polymerization of propylene by *ansa*-zirconocene catalysts. The steric bulk of the ligand is represented by shaded circles in the diagrams on the right which orient the polymer chain. The R group of the incoming monomer is oriented away from the polymer chain in each case.<sup>3c</sup>

Activation of neutral Zr(IV) complexes to cationic Zr(IV) monoalkyl species is necessary for catalysis and is typically achieved with methylaluminoxane (MAO), an ill-

defined species formed through the hydrolysis of trimethylaluminum. MAO serves as both an alkylating agent and activator, creating cationic zirconocene complexes through methide abstraction.<sup>4</sup> Despite the ill-defined nature of the MAO, <sup>1</sup>H NMR studies have provided information about the speciation of zirconium upon activation. Three complexes have been identified as the major products after activation of *ansa*-zirconocene (SBI)ZrMe<sub>2</sub> (SBI = *rac*-dimethylsilylbis(1-indenyl)) with MAO (Figure 1.3).<sup>5</sup>

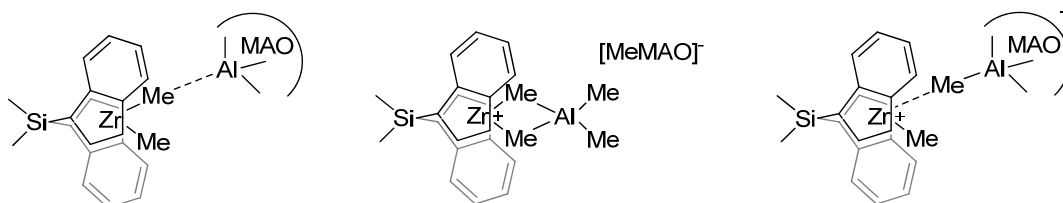


**Figure 1.3.** Cationic species formed upon activation of (SBI)ZrCl<sub>2</sub> or (SBI)ZrMe<sub>2</sub> with MAO.

Recently, zirconocene-based polymerization research has focused on the nature of catalytic resting states, and the relative rates of initiation, propagation, and termination, which are still not well understood.<sup>6,7</sup> These studies have uncovered the fact that significant portions of starting zirconocene concentration is unaccounted for during the course of the reaction. For example, Brintzinger and coworkers have identified a polymer bound compound, [(SBI)Zr(μ-R)(μ-Me)AlMe<sub>2</sub>]<sup>+</sup> (R = polyhexyl), that exists as a possible resting state during polymerization of 1-hexene by [(SBI)Zr(μ-Me)<sub>2</sub>AlMe<sub>2</sub>]<sup>+</sup>. However, upon addition of olefin, the concentration of these and other zirconocene species in solution – as measured by <sup>1</sup>H NMR – drops by up to 60%.<sup>6</sup> The nature of this missing zirconium and the interaction between dormant and active species during catalysis continues to be of great interest.

*Post-metallocene polymerization catalysts*

Although metallocene catalysts are highly active and capable of excellent stereocontrol, an active search continues for promising ‘post-metallocene’ catalyst frameworks that combine the high activities and stereocontrol of metallocenes with easier ligand syntheses, metallation protocols, and higher temperature stability. Our lab has begun to investigate complexes with  $LX_2$  type pincer ligands which are generated through a modular synthesis and display  $C_2$ ,  $C_{2v}$ , and  $C_s$  symmetry in metal complexes (Figure 1.4).<sup>8</sup> Modulation of the X and L donors has produced several active polymerization precatalysts but further studies are necessary to understand the relationship between the steric parameters of the ligand, overall symmetry of the complex, and resulting polymer microstructure.

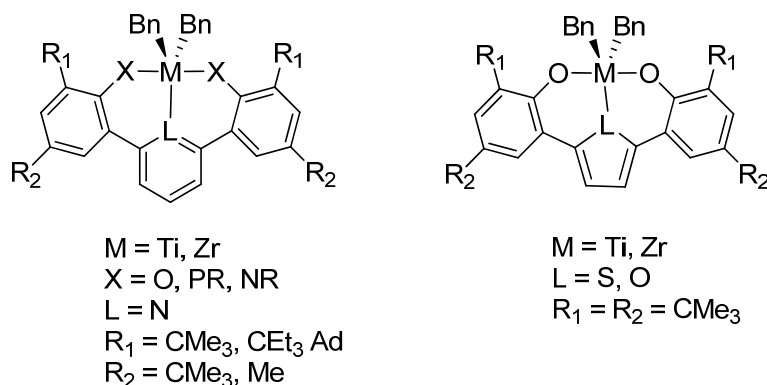


**Figure 1.4.** Post-metallocene complexes synthesized with  $LX_2$  pincer ligands.

## References

1. a.) Market Study: Polypropylene - 2nd ed. overview (UC-4205) Ceresana **2012**.  
Accessed Aug 15, 2013  
<http://www.ceresana.com/en/market-studies/plastics/polypropylene/>
2. Tullo, A. H., Metallocenes Rise Again. *C&E News* Oct. 18, 2010, pp 10.
3. a.) Grubbs, R. H.; Coates, G. W.; *Acc. Chem. Res.* **1996**, *29*, 1412. b.) Piers, W. E.; Bercaw, J. E. *J. Am. Chem. Soc.* **1990**, *112*, 9406. c.) Pino, P.; Cioni, P.; Wei, J. *J. Am. Chem. Soc.* **1987**, *109*, 6189.
4. a.) Bochmann, M. *Organometallics* **2010**, *29*, 4711. b.) Chen, E. Y. X.; Marks, T. J. *Chem. Rev.* **2000**, *100*, 1391.
5. a.) Tritto, I.; Donetti, R.; Sacchi, M. C.; Locatelli, P. Zannoni, G. *Macromolecules*, **1999**, *32*, 264 b.) Babushkin, D. E.; Naundorf, C. Brintzinger, H. H. *Dalton Trans.*, **2006**, 4539. c.) Bryliakov, K. P.; Semikolenova, N. V.; Panchenko, V. N.; Aakharov, V. A.; Brintzinger, H. H.; Talsi, E. P. *Macromol. Chem. Phys.*, **2006**, *207*, 327.
6. Babushkin, D. E.; Brintzinger, H. H. *J. Am. Chem. Soc.* **2010**, *132*, 452.
7. Liu, Z. X.; Somsook, E.; White, C. B.; Rosaaen, K. A.; Landis, C. R. *J. Am. Chem. Soc.* **2001**, *123*, 11193
8. a.) Agapie, T.; Henling, L. M.; DiPasquale, A. G.; Rheingold, A. L.; Bercaw, J. E. *Organometallics* **2008**, *27*, 6245. b.) Golisz, S. R.; Bercaw, J. E. *Macromolecules* **2009**, *42*, 8751. c.) Winston, M. S.; Bercaw, J. E. *Organometallics* **2010**, *29*, 6408. d.) Tonks, I. A.; Tofan, D.; Weintrob, E. C.; Agapie, T.; Bercaw, J. E. *Organometallics*, **2012**, *31*, 1965.

## Chapter 2

### Early Transition Metal Complexes Incorporating a Novel Bis(thiophenolate)pyridine Ligand

Adapted in part from:

Lenton, T. N.; VanderVelde, D. G.; Bercaw, J. E. *Organometallics* **2012**, *31*, 7492.

© American Chemical Society

## Chapter 2

**ABSTRACT:** A precursor to a new tridentate LX<sub>2</sub> type ligand, bis(thiophenol)pyridine ((SNS)H<sub>2</sub> = (2-C<sub>6</sub>H<sub>4</sub>SH)<sub>2</sub>-2,6-C<sub>5</sub>H<sub>3</sub>N), was prepared. Bis(thiophenolate)pyridine complexes of Ti, Zr, and Ta having dialkylamido coligands were synthesized and structurally characterized. The zirconium complex, (SNS)Zr(NMe<sub>2</sub>)<sub>2</sub> (**4**), displays C<sub>2</sub> symmetry in the solid state, unlike the related bis(phenolate)pyridine compound, C<sub>s</sub>-symmetric (ONO)Ti(NMe<sub>2</sub>)<sub>2</sub>. This change is likely the result of strain about the sulfur atom in the six membered chelate with longer metal-sulfur and carbon-sulfur bonds. Solid-state structures of tantalum complexes (SNS)Ta(NMe<sub>2</sub>)<sub>3</sub> (**5**) and (SNS)TaCl(NEt<sub>2</sub>)<sub>2</sub> (**6**) also display pronounced C<sub>2</sub> twisting of the SNS ligand. 1D and 2D NMR experiments show that **5** is fluxional with rotation about the Ta-N(amide) bonds occurring on the NMR timescale that interchange the equatorial amide methyl groups ( $\Delta G^\ddagger_{393} = 25.0(3)$  kcal/mol). The fluxional behavior of **6** in solution was also studied by variable temperature <sup>1</sup>H NMR. Observation of separate signals for the diastereotopic protons of the methylene unit of the diethylamide indicates that the complex remains locked on the NMR timescale in one diastereomeric conformation at temperatures below -50 °C, fast rotation about the equatorial amide Ta-N bonds occurs at higher temperatures ( $\Delta G^\ddagger_{298} = 13.4(3)$  kcal/mol), and exchange of diastereomeric methylene protons occurs via inversion at Ta that interconverts antipodes ( $\Delta G^\ddagger_{298} \approx 14(1)$  kcal/mol).

## Introduction

Much of our current knowledge on the control of polypropylene microstructure stems directly from the development and understanding of early metal catalysts based on metallocene platforms, which have relatively well-defined frontier orbitals and coordination sites restricted to the equatorial plane.<sup>1</sup> Predictable changes in polymer stereochemistry and co-monomer incorporation have been achieved by manipulating the structures of variously substituted metallocenes, particularly *ansa*-metallocenes of group 4 metals.<sup>2</sup> Recently, there has been a large effort to develop “post-metallocene” single site catalysts which would offer advantages compared to metallocene catalysts such as relative ease of ligand synthesis, more general metallation of the ligand, and the potential to effect new types of stereo-controlled polymerizations.<sup>3</sup>

Our group has previously described precatalysts having a pincer ligand framework of the LX<sub>2</sub> type, bis(phenolate)pyridine (ONO = pyridine-2,6-bis(4,6-*t*Bu<sub>2</sub> phenolate). ONO ligands normally coordinate in a meridonal fashion, and depending upon the relative twisting of phenolate rings, (ONO)MX<sub>2</sub> complexes may adopt *C*<sub>1</sub>, *C*<sub>s</sub>, *C*<sub>2</sub>, or *C*<sub>2v</sub> symmetries with frontier orbitals similar to those of metallocenes (Figure 2.1).<sup>3a, 4</sup> Early experiments revealed that group 4 ONO complexes exhibit moderate to good activities for ethylene and propylene polymerization.<sup>4,5</sup> Although isotactic enhancement is observed in some cases, stereo-irregular polypropylene is commonly produced. This is likely due to racemization of the catalyst site, a consequence of similar energies of the *C*<sub>2</sub>, *C*<sub>2v</sub>, and *C*<sub>s</sub> isomers and their facile interconversions.<sup>4</sup>

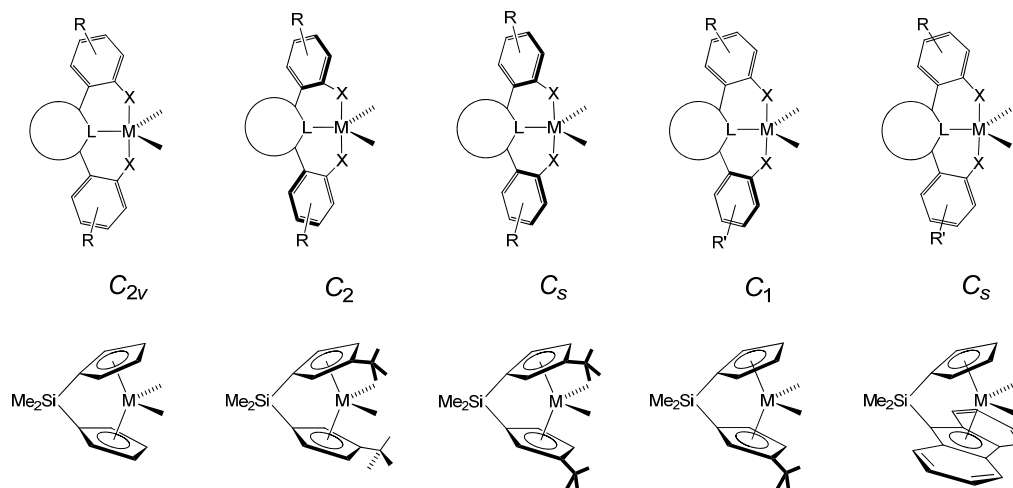


**Figure 2.1.** Comparison of possible bonding geometries of LX<sub>2</sub> type pincer ligands (top) and metallocene precatalysts (bottom).

We reasoned that with a more rigid ligand system, stereoregular polyolefins might be obtained.<sup>6,7</sup> A modified pincer ligand, bis(thiophenolate)pyridine (SNS), was anticipated to offer a possible solution, because the larger sulfur atom would increase ring strain in the metal chelate and lead to a stronger preference for a twisted  $C_2$  as opposed to a flat  $C_{2v}$  geometry. Indeed, the analogous early transition metal complexes with a bis(phosphido)pyridine (PNP) ligand, display very twisted  $C_2$  symmetry, as compared with the analogous bis(anilide)pyridine (NNN) complexes, due to the long metal-phosphorus and carbon-phosphorus (*vis-à-vis* M-N and C-N) bonds.<sup>13b</sup>

Furthermore, this ligand would provide insight into the bonding characteristics of X type sulfur donors in early metal complexes. Examples of group 4 and 5 transition metals bearing anionic thiolate ligands are relatively rare, and their scarcity has been attributed to a hard/soft mismatch.<sup>8</sup> Most examples of early transition metal thiolates are stabilized by cyclopentadienyl ancillary ligands or are clusters with sulfur bridges.<sup>9</sup> There appears to be little evidence supporting strong sulfur metal  $\pi$  bonding for the complexes that have been

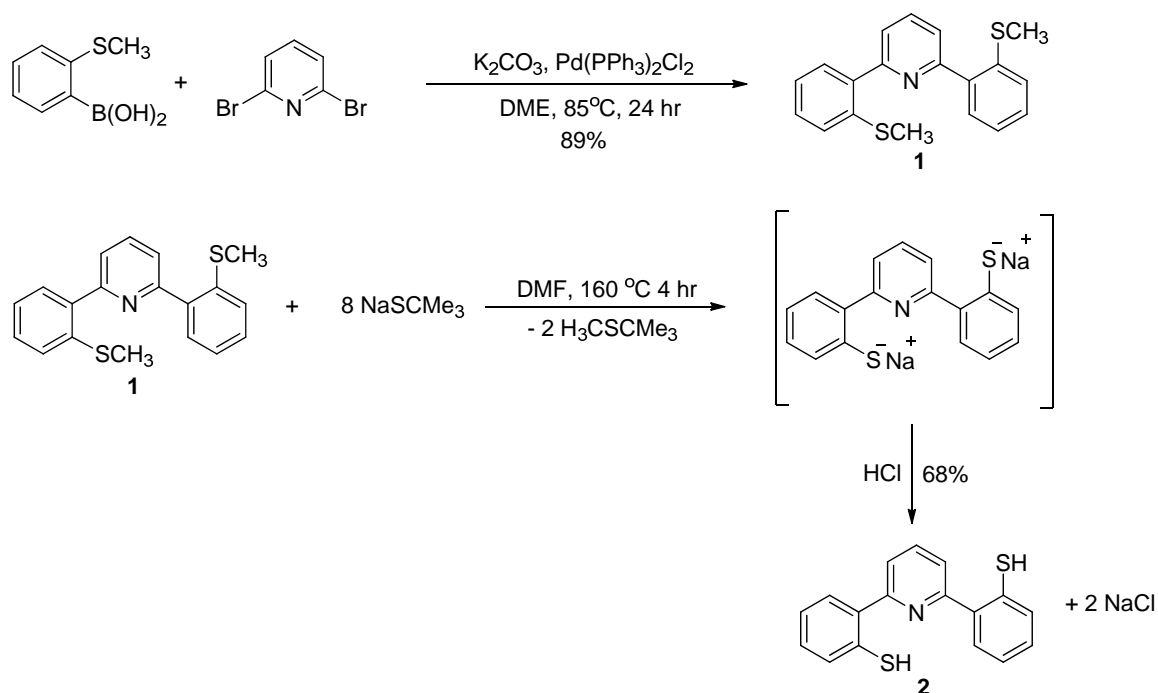
reported thus far.<sup>10</sup> Eliminating the propensity for  $\pi$  bonding with the metal should also lessen the tendency to form a  $C_s$  structure.<sup>7</sup>

Although our expectations that, as compared with their (ONO)MX<sub>2</sub> (M = Ti, Zr) and (ONO)TaX<sub>3</sub> analogs, the (SNS)MX<sub>2</sub> and (SNS)TaX<sub>3</sub> complexes do indeed strongly favor twisted,  $C_2$  geometries, the Ti and Zr amide complexes do not prove to be effective catalysts precursors for propylene polymerization. Thus it was not possible to investigate stereocontrol in producing isotactic polypropylenes. The dynamic behavior, involving both restricted rotation about the amide Ta–N bonds and interconversion between antipodes by inversion at Ta, has, however, been examined by NMR methods.

## Results and Discussion

### *Synthesis of the (SNS)H<sub>2</sub> ligand.*

The desired ligand was synthesized in two steps from 2-(methylthio)phenylboronic acid and 2,6-dibromopyridine (Scheme 2.1). These reagents were subjected to Suzuki coupling conditions which generated the protected (SNS)Me<sub>2</sub> **1** in 89% yield. Treatment of **1** with sodium 2-methyl-2-propanethiolate (Me<sub>3</sub>CSNa) at 160 °C for four hours removed the protecting methyl group.<sup>11</sup> Acid workup afforded the moderately air-sensitive ligand **2** (SNS)H<sub>2</sub> in 68% yield. A distinctive broad peak observed in <sup>1</sup>H NMR spectrum at  $\delta$  4.66 corresponds to the thiol protons.



Scheme 2.1

Palladium-catalyzed cross couplings, used previously to prepare related  $\text{LX}_2$  pincer ligands, are not generally suited to the direct synthesis of *bis*(thiophenol)pyridine due to poisoning of the Pd by sulfur. Moreover, common allyl or benzyl thioether protecting groups are easily cleaved by palladium, again leading to catalyst poisoning. A preliminary attempt to protect the thiophenol with an alkylmercaptopropionate group, which had been reported to tolerate Suzuki coupling conditions, failed.<sup>12</sup> Fortunately, a methyl protected phenyl sulfide proved stable to palladium-catalyzed Suzuki coupling conditions.

Initially methyl thioether was avoided as a protecting group because of the harsh conditions needed for the deprotection reaction. Preferential formation of the aromatic thiolate is supported by the relative pKa of benzenethiol (10.3) vs. *tert*-butylthiol (17.0) in DMSO, however, the effect of a second thiolate in the same molecule is unknown. Small amounts of moisture inhibit the deprotection reaction. To avoid this, DMF was degassed

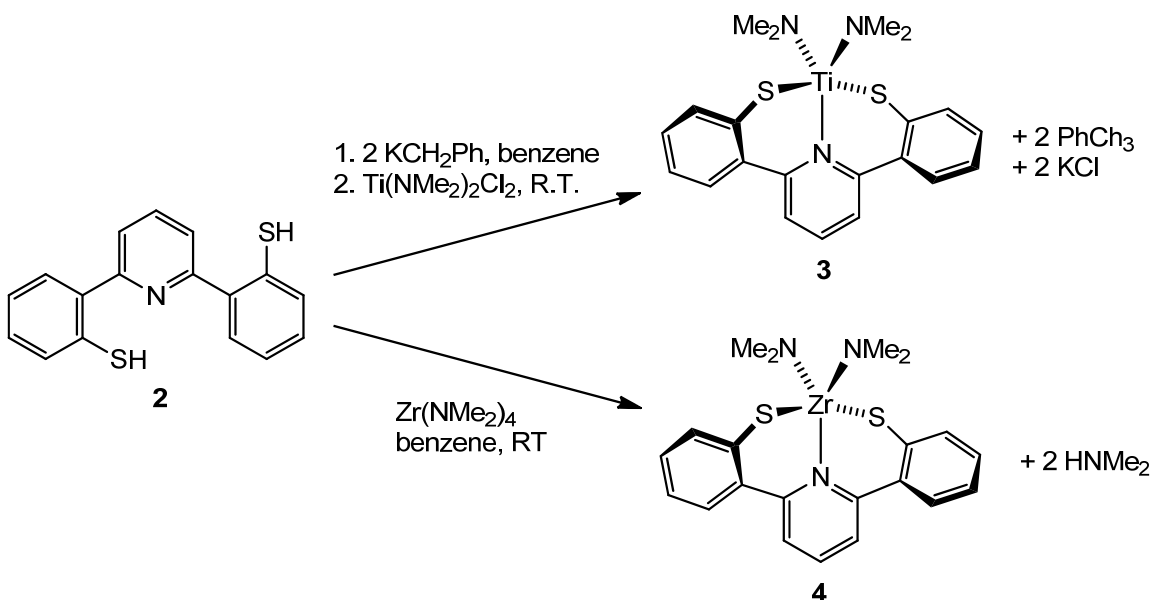
and dried sequentially over two batches of freshly activated molecular sieves for 36 hours each. Solid sodium *tert*-butyl thiolate was dried under vacuum overnight as was the protected ligand (**1**). Even under rigorously dry conditions, the reaction proved unreliable and incomplete deprotection was often observed. Reaction completion is imperative as **1** cannot be easily separated from the bis(thiolate) ligand (**2**) by crystallization, sublimation, or column chromatography.

Several other reagents were investigated as nucleophiles including sodium thiomethoxide, potassium *tert*-butoxide and potassium iodide, but none of the reactions were ever observed to go to completion. Reductive cleavage using sodium in liquid ammonia was also attempted. Generation of solvated electrons was indicated by the deep blue color of the resulting solution, however, only starting material was recovered upon workup. To date, deprotection of **1** with *tert*-butyl thiolate in dry DMF is the most efficient way to generate **2**.

Once formed, the ligand decomposes upon exposure to air and water, likely due to oxidative intermolecular disulfide formation. Although the protected ligand **1** can be synthesized on a gram scale, low reliability in the deprotection step prevented scale-up beyond a 100 mg. On small scales, however, the desired ligand was obtained in up to 68% yield after acidification and drying.

### Preparation of Titanium and Zirconium Complexes

Titanium and zirconium dimethylamido complexes were prepared by salt metathesis and aminolysis, respectively (Scheme 2.2). Although  $^1\text{H}$  and  $^{13}\text{C}$  NMR spectroscopy support clean formation of  $(\text{SNS})\text{Ti}(\text{NMe}_2)_2$  (**3**), **3** decomposes in solution over 12 hr to an insoluble red-brown solid as an intractable mixture of products. The zirconium complex  $(\text{SNS})\text{Zr}(\text{NMe}_2)_2$  (**4**) proved more stable, and X ray quality crystals were obtained by slow evaporation of pentane into a concentrated benzene solution of **4** at room temperature (Figure 2.2).



**Scheme 2.2**

Structure determination of these crystals revealed the molecule crystalizes with the  $\text{C}_2$  symmetry. The relatively long Zr–S bond lengths of 2.67 Å and 2.56 Å confirm that sulfur is binding as an X-type ligand in **4** with little S lone pair-to-Zr  $\pi$  donation.<sup>8,10</sup>

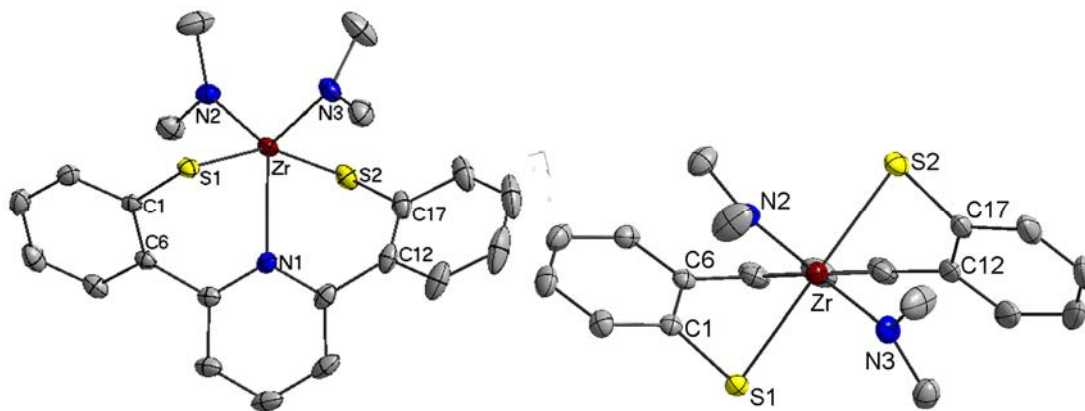


**Figure 2.2** Front (left) and top (down Zr-N1 bond, right) views of the structure of **4** with thermal ellipsoids at the 50% probability level. Hydrogen atoms omitted for clarity. Selected bond lengths (Å) and angles (deg): Zr-S1, 2.5723(3); Zr-S2, 2.5528(3); Zr-N1, 2.3499(7) Zr-N2, 1.9995(8); Zr-N3, 2.0041(8); S1-C1, 1.7743(9); S2-C17, 1.7743(11); Zr-S1-C1, 88.40(3); Zr-S2-C17, 86.12(3); S1-Zr-S2, 156.934(9); N2-Zr-N3, 113.06(3); C1-C6-C12-C17, 71.993(81).

Previous work with 5-coordinate (ONO)TiX<sub>2</sub> and (ONO)ZrX<sub>2</sub> complexes demonstrated a preference for C<sub>s</sub> binding modes when the ancillary X type ligands π donate to the metal center better than phenolate. Although C<sub>s</sub> binding increases ring strain in the complex, the ONO ligand framework is sufficiently flexible to adopt this geometry which allows increased π orbital overlap between the metal and ancillary ligand. Accordingly, (ONO)Ti(CH<sub>2</sub>Ph)<sub>2</sub> has C<sub>2</sub> symmetry while (ONO)Ti(NMe<sub>2</sub>)<sub>2</sub> has C<sub>s</sub> symmetry.<sup>4,7b</sup>

Thus, a C<sub>s</sub> geometry would be expected for 5-coordinate **4** based on the strongly π donating dimethylamido ancillary ligands. Instead, steric preferences appear to override any electronic preferences arising from nitrogen π donation to zirconium, resulting in distinctly C<sub>2</sub> twisting of the SNS ligand for **4**. This is likely a result of the long Zr-S and S-C bonds that force the 6-membered chelate to adopt a severely nonplanar ring and possible steric preferences for the two dimethylamido groups to be roughly trans. Indeed,

the 72.65° dihedral angle (C1–C6–C12–C17) between the two thiophenolate planes is larger than the corresponding dihedral angle for any  $C_2$  symmetric ONO complex synthesized to date (52.70° to 69.24°).<sup>4-5, 7</sup> The dihedral angle for **4** is smaller, however, than those for related  $C_2$ -symmetric bis(anilide)pyridine and bis(phosphide)pyridine complexes (79.20° to 94.13°). These NNN and PNP ligands have aryl groups on the secondary pnictogens that further increase the steric bulk of the ligand and force an even greater dihedral twist.<sup>13</sup>

Attempts to prepare group 4 metal complexes with ancillary ligands other than dimethylamide were unsuccessful. Toluene elimination from tetrabenzyltitanium, -zirconium, and -hafnium in order to generate dibenzyl complexes resulted in the immediate precipitation of insoluble brown solids. Efforts to generate halogen-ligated complexes by treating (SNS)K<sub>2</sub> with group 4 metal chlorides or (SNS)H<sub>2</sub> with mixed chloro-amido compounds were also ineffective, as were reactions of **3** and **4** with one or more equivalents of trimethylsilylchloride. We hypothesize that the combination of weak sulfur-to-metal  $\pi$  donation and less bulky, weaker  $\pi$  donor ancillary ligands encourage oligomerization of these alkyl- and chloro-complexes through sulfur and/or chlorine bridges, ultimately leading to oligomerization to insoluble materials.

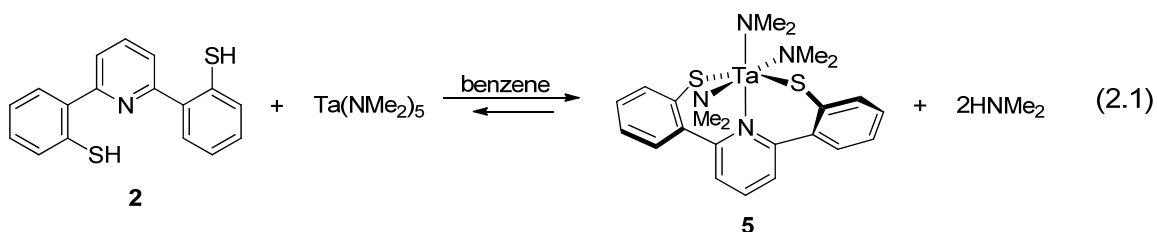
#### *Reactivity with Olefins*

Neither **3** nor **4** were competent precatalysts for propylene polymerization, likely due to decomposition during the activation process. Activation by methylaluminoxane (MAO) is expected to generate methyl cations [(SNS)MCH<sub>3</sub>]<sup>+</sup> that would likely be even more unstable than the neutral dibenzyl complexes (*vide supra*).<sup>14</sup> Adding bulk to the

ortho-position of the ligand might stabilize the electron deficient complex, while simultaneously inhibiting bridging through the sulfur lone pair.

### Preparation of Tantalum Complexes

Tantalum complex (SNS)Ta(NMe<sub>2</sub>)<sub>3</sub> (**5**) was prepared by aminolysis of Ta(NMe<sub>2</sub>)<sub>5</sub> with (SNS)H<sub>2</sub> (eq. 2.1). Only a small amount of **5** is formed initially, but the reaction can be driven to completion by removing the volatile dimethylamine.



X-ray quality crystals were obtained by diffusing pentane into a concentrated benzene solution of **5** at room temperature (Figure 2.3). The SNS fragment binds meridionally with  $C_2$  symmetry, which, for a 6-coordinate complex maximizes ancillary  $\pi$  bonding in addition to being sterically preferred (as previously established in (ONO)Ta(NMe<sub>2</sub>)<sub>3</sub> and related complexes).<sup>7a</sup> The molecule displays an average Ta–S bond length of 2.49 Å and a dihedral angle of 79.9° (C1–C6–C12–C17). Both metrics are larger than the corresponding ones observed in (ONO)Ta(NMe<sub>2</sub>)<sub>3</sub> (Ta–O bond length: 1.98 Å; dihedral angle: 59.7°) with longer S–Ta and C–S bond lengths forcing the six membered chelate rings significantly nonplanar.

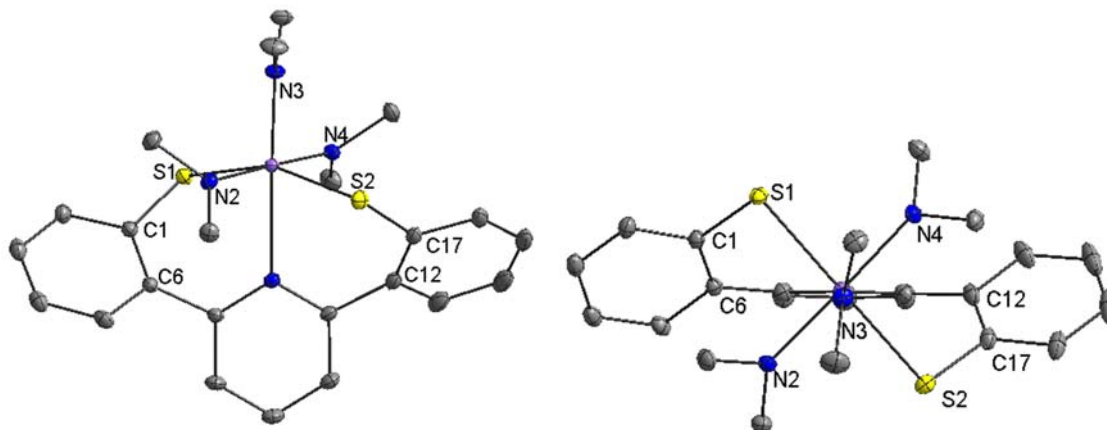
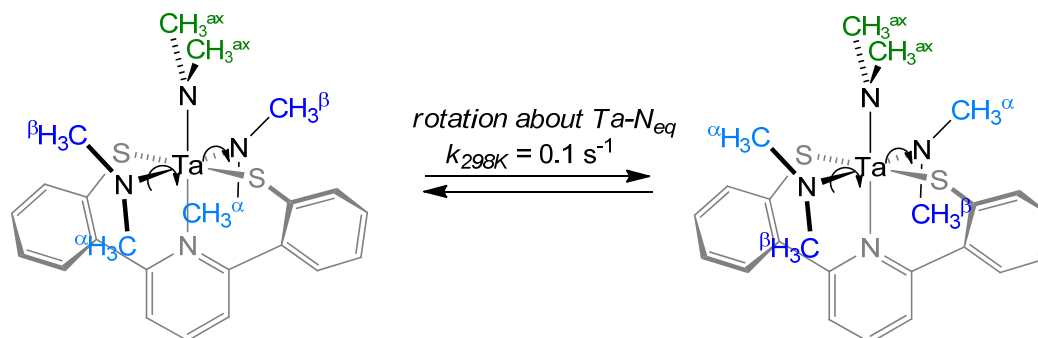


**Figure 2.3.** Front (left) and top (down Ta–N1 bond, right) views of the structure of **5** with thermal ellipsoids at the 50% probability level. Hydrogen atoms omitted for clarity. Selected bond lengths (Å) and angles (deg): Ta–S1, 2.4887(3); Ta–S2, 2.4823(3); Ta–N1, 2.3927(11); Ta–N2, 2.0264(11); Ta–N3, 1.9868 (11); Ta–N4, 2.0352(11); S1–C1, 1.7537(12); S2–C17, 1.7555(15); Ta–S1–C1, 101.79(4); Ta–S2–C17, 100.13(5); S1–Ta–S2, 158.011(11); N2–Ta–N4, 177.16(5); C1–C6–C12–C17, 79.853(112).

The dimethylamide groups of  $(\text{ONO})\text{Ta}(\text{NMe}_2)_3$  exhibit two sharp peaks by  $^1\text{H}$  NMR with a 12:6 ratio as expected for the solid state structure at room temperature.<sup>7</sup> In contrast, **5** shows three distinct amide methyl peaks in the  $^1\text{H}$  NMR spectrum at  $\delta$  2.83 ( $\text{CH}_3^\alpha$ ), 3.22 ( $\text{CH}_3^\beta$ ), and 3.65 ( $\text{CH}_3^{\text{ax}}$ ) that integrate in a 6:6:6 ratio (Figure 2.6). Restricted rotation about the equatorial Ta–N(amide) bonds leads to an inequivalence between the 'top' and 'bottom' methyl groups of the equatorial amides (Scheme 2.3). A series of through-space and through-bond  $^1\text{H}$ ,  $^{13}\text{C}$ , and  $^{15}\text{N}$  2D NMR experiments confirmed the assignment of  $\text{CH}_3^\beta$  as top and  $\text{CH}_3^\alpha$  as bottom.



**Scheme 2.3**

Furthermore, 1D-NOE  $^1\text{H}$  NMR spectroscopy revealed a process exchanging the methyl groups in sites  $\alpha$  and  $\beta$ , likely involving simple rotation of the equatorial Ta–N bond, as selectively exciting the protons of  $\text{CH}_3^\beta$  (2.83 ppm) resulted in magnetization resonance transfer to  $\text{CH}_3^\alpha$  (3.22 ppm) and vice versa (Figure 2.4). Cooling the sample to  $-10^\circ\text{C}$  slows this rotation, allowing estimation of the NOE contribution between  $\text{CH}_3^\alpha$  and  $\text{CH}_3^\beta$  (Figure 2.5). These data combined with a series of presaturation delay 1D-NOE experiments provided an exchange rate for equatorial amide methyls of  $0.11(2) \text{ s}^{-1}$  at 298 K.

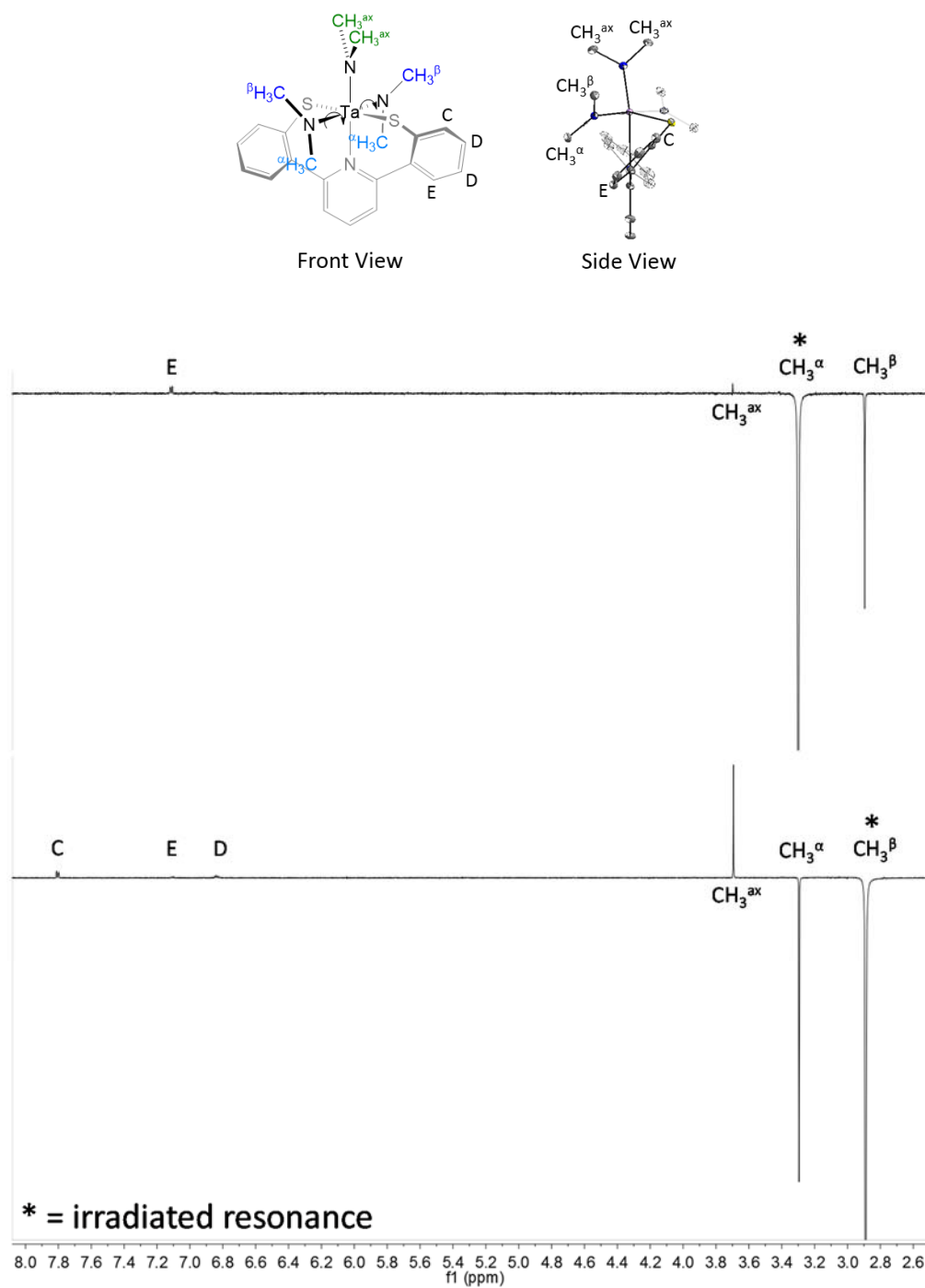


**Figure 2.4** Top: Selective band center  $\delta 3.22$  ( $\text{CH}_3^\alpha$ ). Magnetic resonance transfer to position  $\text{CH}_3^\beta$  results in a negative peak at  $\delta 2.83$  ( $\text{CH}_3^\beta$ ). Bottom: Selective band center  $\delta 2.83$  ( $\text{CH}_3^\beta$ ). Magnetic resonance transfer to position  $\text{CH}_3^\alpha$  results in a negative peak at  $\delta 3.22$  ( $\text{CH}_3^\alpha$ ).

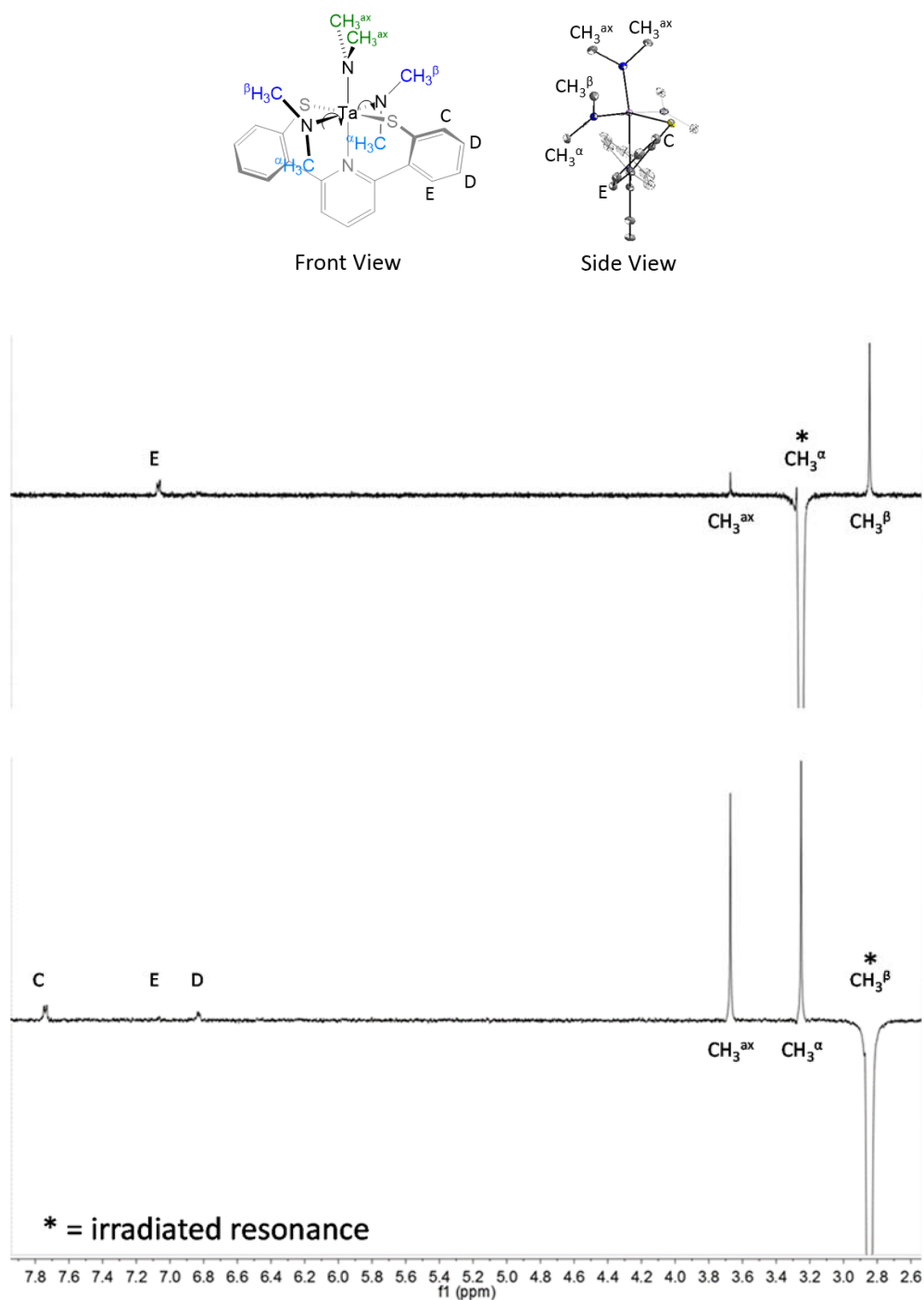


**Figure 2.5.** 1D  $^1\text{H-NMR}$  of **5** in  $d_8$ -toluene at  $-10\text{ }^\circ\text{C}$ . The solution has been cooled to stop rotation between  $\text{CH}_3^{\beta}$  and  $\text{CH}_3^{\alpha}$  on the NMR time scale. Top: Selective band center at  $\delta 3.25$  ( $\text{CH}_3^{\alpha}$ ) shows through space interactions with positions  $\text{CH}_3^{\beta}$  and  $\text{CH}_3^{\text{ax}}$ . Bottom: Selective band center  $\delta 2.85$  ( $\text{CH}_3^{\beta}$ ) shows through space interactions with protons at positions  $\text{CH}_3^{\alpha}$  and  $\text{CH}_3^{\text{ax}}$ , implicating it as the 'upper' methyl of **5**.

Heating an NMR sample of **5** from 25 to 115 °C leads to broadening of peaks attributable to  $CH_3^\alpha$  and  $CH_3^\beta$  (Figure 2.6). At the highest temperature these two peaks have coalesced and a notable broadening of the peak for  $CH_3^{ax}$  occurs, possibly an indication that relatively slow positional exchange between axial and equatorial amides occurs.

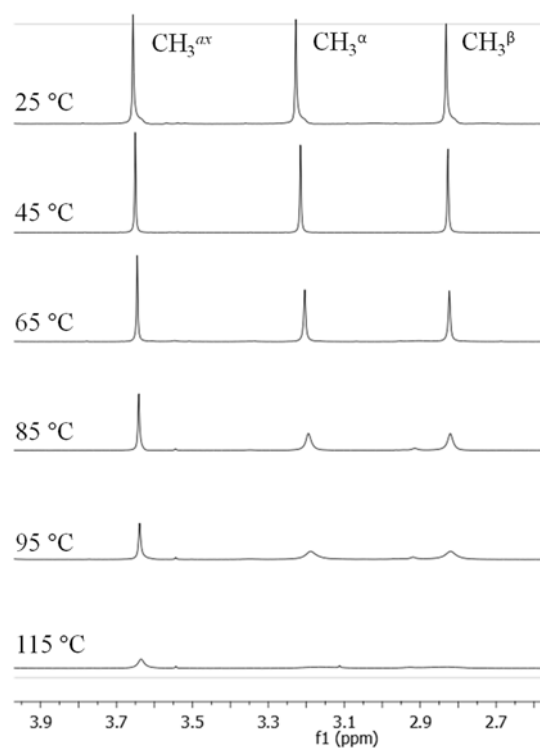
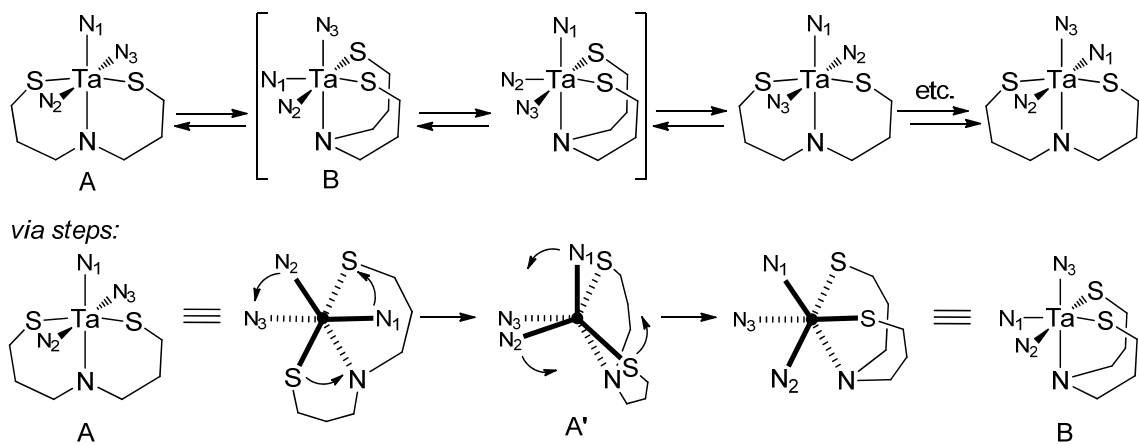


**Figure 2.6** Variable temperature  $^1\text{H}$  NMR of the alkyl region of **5** showing peak exchange between  $CH_3^\alpha$ ,  $CH_3^\beta$ , and  $CH_3^{ax}$ .

Exchange of  $CH_3^\alpha$ ,  $CH_3^\beta$ , and  $CH_3^{ax}$  might be achieved through conversion of the meridionally bound ligand to a facial binding mode followed by rotation about the  $C_3$  (N1–N2–N3) axis (Scheme 2.4). This meridional to facial rearrangement would require substantial strain on the SNS fragment but is not without precedence: a similar explanation was proposed in the exchange of axial and equatorial groups at room temperature for

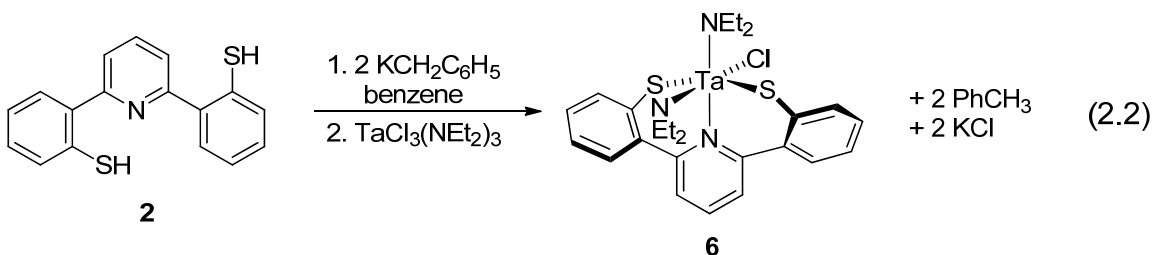
(ONO)TaMe<sub>3</sub>. Additionally the solid state structure of dimer [(ONO)Ta(OH)]<sub>2</sub>(μ<sub>2</sub>-O)<sub>2</sub> has facially bound ONO fragments.<sup>7,16</sup> Alternatively, dissociation of the pyridine of SNS and rearrangement via a five-coordinate species might be occurring.<sup>15</sup>



**Scheme 2.4**

#### *Preparation of (SNS)TaX<sub>3</sub> Complex Containing Diastereotopic Protons*

To further assess the conformational flexibility of the SNS framework, a new complex, (SNS)TaCl(NEt<sub>2</sub>)<sub>2</sub> **6**, was synthesized by salt metathesis of (SNS)K<sub>2</sub> with TaCl<sub>3</sub>(NEt<sub>2</sub>)<sub>2</sub> (equation 2.2). Our interest in this compound stems from the fact that the diastereotopic methylene protons of the diethyl amide co-ligands of **6** exchange only if the molecule can undergo interconversion between C<sub>2</sub> antipodes. Crystallization by diffusion of pentane into benzene gave crystals suitable for X-ray structural analysis (Figure 2.7).



Metrics of **6** are nearly identical to **5**, despite having a chloride in place of an amide and a more acute C1–C6–C12–C17 dihedral angle of 71.42 ° (vs. 79.9° in **5**). Here again the strained 6-member chelate rings dominate the geometric preference for  $C_2$  coordination in **6**, contrasting the ONO ligand system which assumes  $C_s$  symmetry in (ONO)TaCl(NMe<sub>2</sub>)<sub>2</sub> to maximize phenolate  $\pi$ -bonding to Ta.<sup>7</sup>

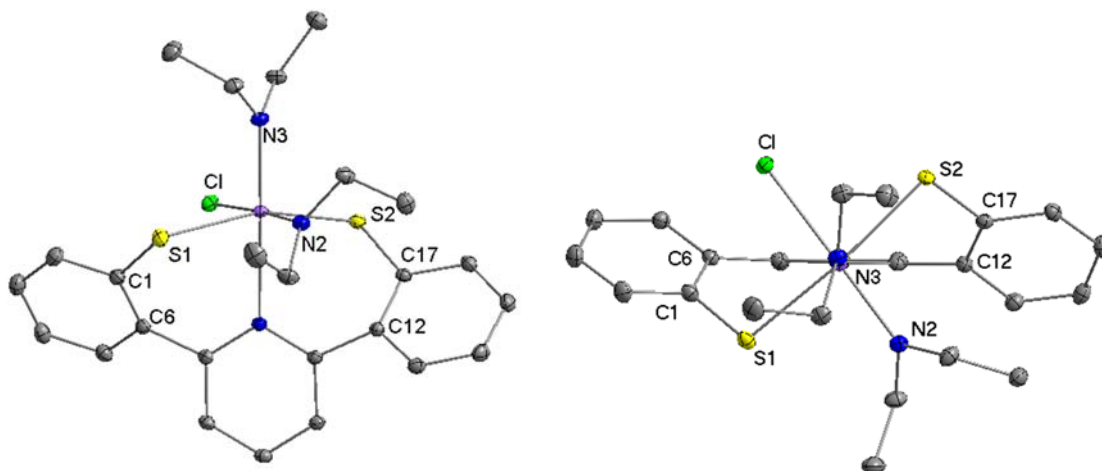


**Figure 2.7** Structure of **6** with thermal ellipsoids at the 50% probability level. The left image is a front view and the right image is a top view down the N3–Ta–N1 bond. Hydrogen atoms omitted for clarity. Selected bond lengths (Å) and angles(deg): Ta–S1, 2.42715(19); Ta–S2, 2.47717(19); Ta–N1, 2.3911(2); Ta–N2, 1.9873(6); Ta–N3, 1.9538(6); Ta–Cl, 2.45843(19); S1–C1, 1.7615(8); S2–C17, 1.7550(7); Ta–S1–C1, 103.88(2); Ta–S2–C17, 102.814(2); S1–Ta–S2, 160.364(6); N2–Ta–Cl, 176.970(18); C1–C6–C12–C17, 71.415(59).

Variable temperature <sup>1</sup>H NMR spectra reveal that antipode interconversion occurs rapidly at high temperatures but slows relative to the NMR time scale as the temperature is lowered (Figure 2.8, Scheme 2.5). The room temperature <sup>1</sup>H NMR spectrum of **6** is composed of several nondescript broad peaks. At 100 °C a simple <sup>1</sup>H NMR spectrum emerges that consists of two quartets (equatorial and axial amide methylenes) and two

triplets (equatorial and axial amide methyls) with relative intensities of 4:4:6:6. This simple splitting pattern is only possible if the diastereotopic methylene protons of the equatorial diethyl amides are averaged out due to antipode interconversion.

On cooling to  $-50\text{ }^{\circ}\text{C}$  a more complicated  $^1\text{H}$  NMR spectrum emerges revealing separate signals for some of the geminal protons of the methylene groups of the diethylamide ligands, appearing as multiplets (due to apparently comparable geminal and methyl coupling) for the methylene protons with relative intensities of 2:1:[1:2(overlapping)]:1:1. Assignments as shown in Figure 2.8 were further established by 2D NMR experiments. The four multiplet pattern of methylene protons  $\text{H}^{\text{B}1}$ ,  $\text{H}^{\text{B}2}$ ,  $\text{H}^{\text{B}3}$ , and  $\text{H}^{\text{B}4}$  further indicate both slow rotation of the equatorial Ta–N(amide) bond (as observed for **5**), and slow inversion at Ta. On the other hand, equivalencing of  $\text{H}^{\text{A}1}/\text{H}^{\text{A}1'}$  and  $\text{H}^{\text{A}2}/\text{H}^{\text{A}2'}$  leads to only two broad peaks of relative intensity 2 implies relatively rapid axial Ta–N(amide) bond rotation occurs at  $-50\text{ }^{\circ}\text{C}$ .

At  $-75\text{ }^{\circ}\text{C}$  these two broad peaks split further, and although we were not able to obtain satisfactory spectra at lower temperatures, we anticipate that these signals would continue to sharpen into four multiplets of intensities 1:1:1:1 (analogous to those for the equatorial amide methylenes) as rotation of the axial amide Ta–N bond becomes slow on the NMR time scale. Further upfield at the lower temperatures are separate triplets for the two methyl groups ( $\text{CH}_3^{\alpha}$ ) and ( $\text{CH}_3^{\beta}$ ) of the equatorial diethylamide ligand and two overlapping triplets for the less well resolved ( $\text{CH}_3^{\text{ax}}$ ) methyl groups of the axial diethylamide.

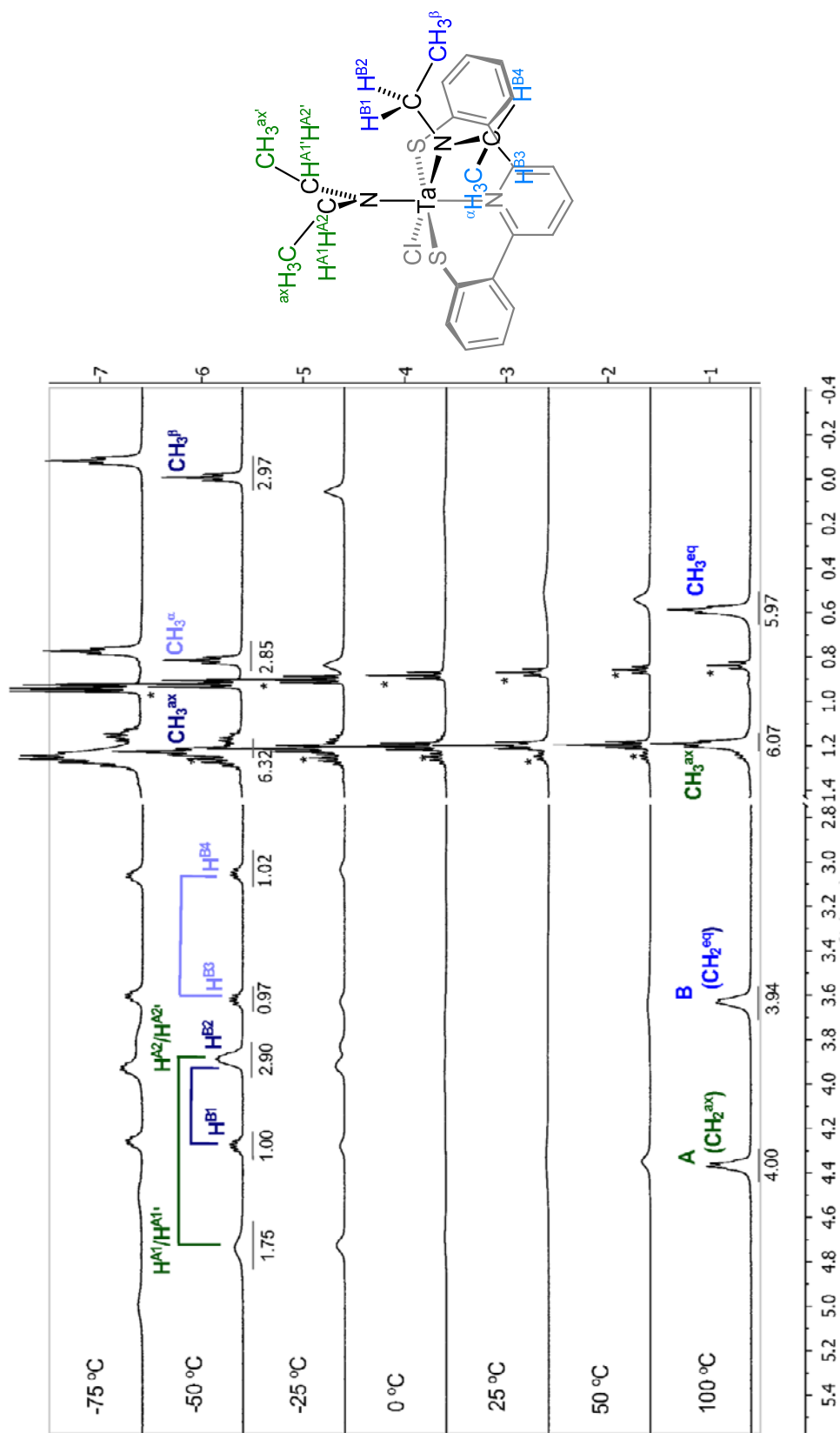


**Figure 2.8.**  $^1\text{H}$  NMR of **6** from  $-75\text{ }^\circ\text{C}$  to  $100\text{ }^\circ\text{C}$  in  $d_8$ -toluene. Integrals are shown beneath the spectra. Labeling corresponds to Scheme 2.5. Spectra are not shown on same vertical scale due to low solubility of **6** at colder temperatures. \*Impurity observed at  $0.84$  and  $1.24$  ppm (attributable to residual  $\text{Ta}(\text{NEt}_2)_2\text{Cl}_3$ ) retains solubility at lower temperatures leading to perceived signal amplification.

The  $^1\text{H}$ - $^1\text{H}$  ROESY of **6** at  $-50\text{ }^\circ\text{C}$  reveals exchange *does* occur between  $\text{H}^{\text{B1}}$  and  $\text{H}^{\text{B3}}$  and between  $\text{H}^{\text{B2}}$  and  $\text{H}^{\text{B4}}$ , indicative of relative fast equatorial amide Ta-N rotation, but importantly there is no significant exchange between  $\text{H}^{\text{B1}}$  and  $\text{H}^{\text{B2}}$  or between  $\text{H}^{\text{B3}}$  and  $\text{H}^{\text{B4}}$ , indicating that inversion at Ta is not occurring on the ROESY time scale at this temperature. Thus, at least at  $-50\text{ }^\circ\text{C}$ , equatorial amide rotation is faster than inversion at Ta.

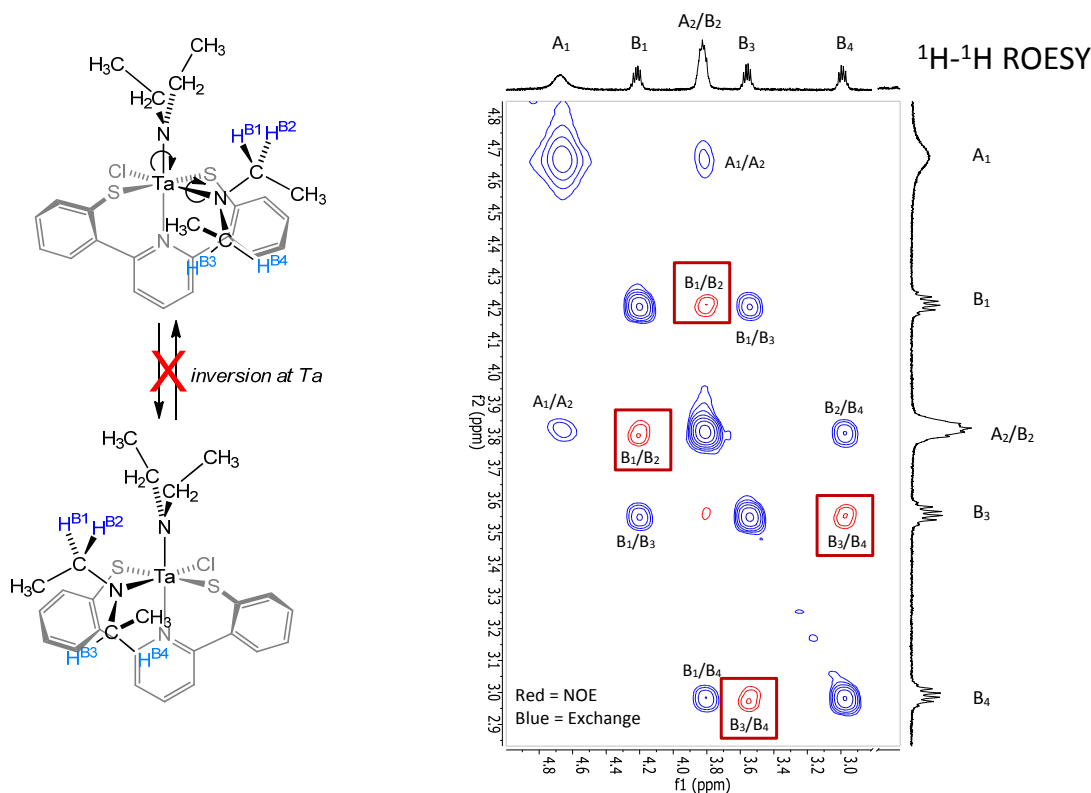
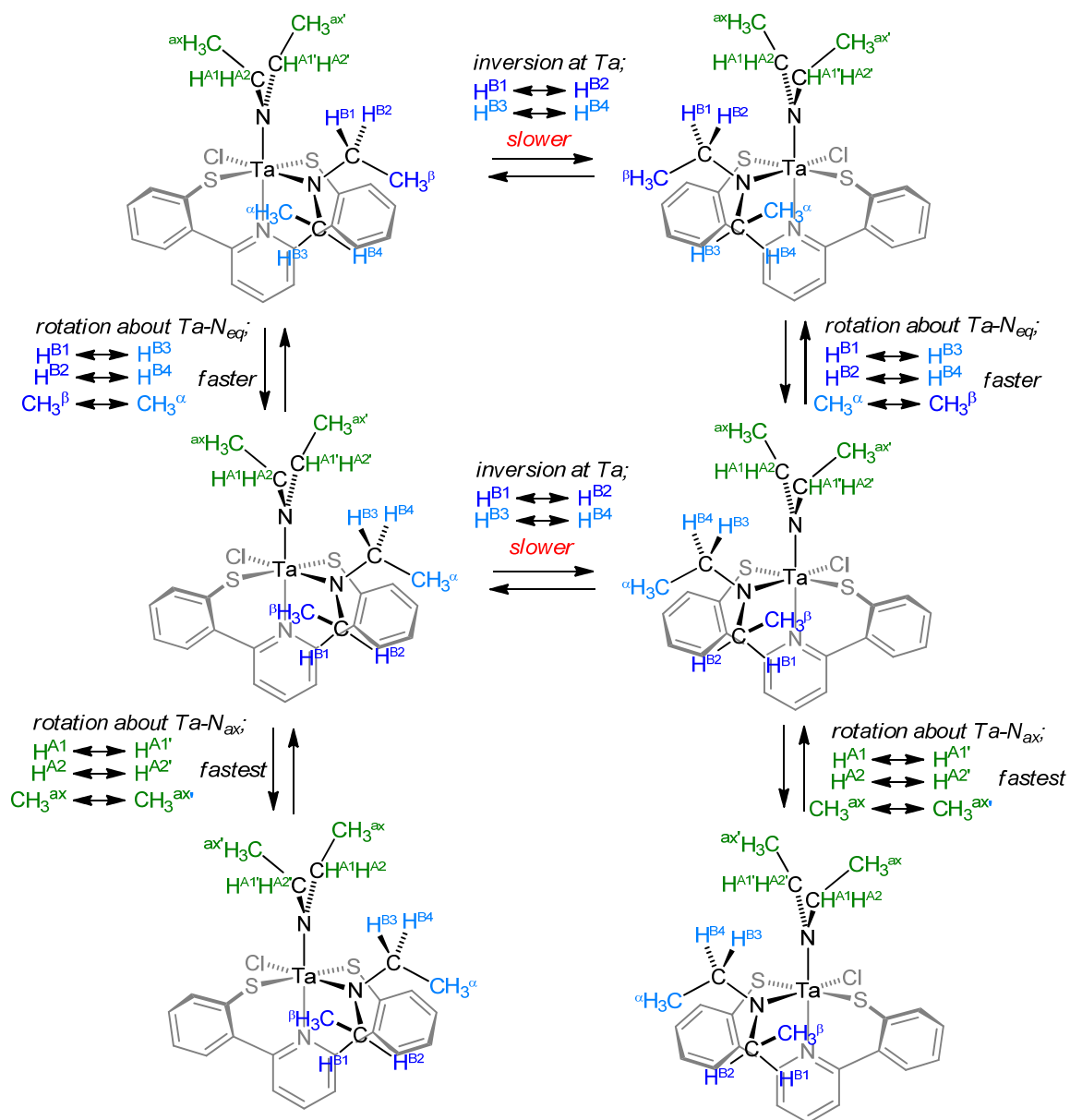


**Figure 2.9**  $^1\text{H}$ - $^1\text{H}$  ROESY NMR spectrum of **6** at  $-50\text{ }^\circ\text{C}$  in  $d_8$ -toluene.

At intermediate temperatures the spectra are not readily interpreted, however. From the spectrum at  $25\text{ }^\circ\text{C}$  we can estimate from the coalescence of the two methyl groups ( $\text{CH}_3^\alpha$ ) and ( $\text{CH}_3^\beta$ ) of the equatorial diethylamide ligand that the Ta-N rotational barrier is approximately  $13.4(1)\text{ kcal/mol}$  at  $298\text{ K}$ , corresponding to a rate of  $900\text{ s}^{-1}$ .<sup>17</sup> An

approximate fit for exchange of  $H^{A1}$  with  $H^{A1'}$  yields an axial diethylamide ligand Ta–N rotational barrier of 9.4(1) kcal/mol (at 200 K), corresponding to a rate of  $560\text{ s}^{-1}$ . At the highest temperature both amide rotation and inversion at Ta must be relatively fast in order to make both ethyl groups of each of the diethyl amide ligands equivalent, *i.e.* both  $H^{B1}$  exchange with  $H^{B3}$  (rotation) and  $H^{B1}$  exchange with  $H^{B2}$  (inversion at Ta) must be fast; same for  $H^{B2}$  exchange with  $H^{B4}$  (rotation) and  $H^{B3}$  exchange with  $H^{B4}$  (inversion at Ta).

Unfortunately, the data are not precise enough to allow deconvolution of the separate contributions of the amide rotation and inversion at Ta to the line shape of signals for these four methylene protons at intermediate temperatures. Thus, we conservatively estimate that the barrier to inversion is comparable to that for rotation, at least at the higher temperatures, *i.e.*  $\Delta G_{inv}^\ddagger \approx 14(1)\text{ kcal/mol}^{-1}$ . Thus, these NMR data indicate that although the longer Ta–S and S–C bonds result in considerable ring strain in SNS complexes, the framework is nonetheless flexible enough to allow inversion at Ta to interconvert antipodes with a moderate barrier for **6**.



Scheme 2.5

## Conclusions

A novel bis(thiophenol)pyridine ligand has been synthesized and metalated with Ti(IV), Zr(IV) and Ta(V) precursors to form dialkylamido and trialkylamido complexes. Solid state structures of Zr(IV) complex **4** and Ta(V) complexes **5** and **6** show a meridonal coordination having a twisted  $C_2$  symmetric arrangement of the SNS ligand with the largest dihedral angles for a bis(chalcogenate)pyridine ligand system thus far. Increased ring strain of the 6-membered thiophenolate rings resulting from long Ta–S and C–S bond lengths and acute bond angles at sulfur are major factors influencing this coordination mode, overriding any alternative coordination that maximizes  $\pi$  bonding between the metal and chalcogenide, as is seen for the ONO analogs. The  $C_2$  symmetry of **5** persists in solution at room temperature with relatively rapid rotation about the amide Ta–N bonds, while at higher temperatures all three amide ligands exchange, implying that the SNS framework likely exhibits sufficient flexibility to allow access to trigonal prismatic intermediates with a facial coordination of the  $LX_2$  chelate. Variable temperature studies for **6**, which possesses diastereomeric protons for the methylene groups of the two diethylamide ligands, confirm that the complex interconverts between antipodes with a moderate barrier for inversion at Ta. Although titanium and zirconium complexes proved to be poor catalyst precursors for propylene polymerization, their structures and the fluxional behavior of the tantalum complexes has provided additional insights into the coordination preferences for this class of  $LX_2$  pincer ligands.

## Experimental

**General Considerations.** All air- and moisture-sensitive compounds were manipulated using standard high-vacuum line, Schlenk, or cannula techniques or in a glovebox under a nitrogen atmosphere. Benzyl potassium (KBn) was prepared according to literature methods.<sup>18</sup> Zr(NMe<sub>2</sub>)<sub>4</sub> and Ta(NMe<sub>2</sub>)<sub>5</sub> were purchased from Stem Chemicals and sublimed prior to use. TiCl<sub>2</sub>(NMe<sub>2</sub>)<sub>2</sub> and TaCl<sub>3</sub>(NEt<sub>2</sub>)<sub>2</sub> were prepared according to literature methods.<sup>19,20</sup> DMF was dried by the Grubbs method<sup>21</sup> and stored over 3Å molecular sieves for 36 hours prior to use. All other solvents for air- and moisture-sensitive reactions were dried over sodium benzophenone ketyl and stored over titanocene where compatible or dried by the method of Grubbs et al.<sup>21</sup> Benzene-*d*<sub>6</sub> and toluene-*d*<sub>8</sub> were purchased from Cambridge Isotopes, and dried over sodium benzophenone ketyl. Methylene chloride-*d*<sub>2</sub> was purchased from Cambridge Isotopes, distilled from calcium hydride and filtered through a plug of activated alumina. All other materials were used as received. <sup>1</sup>H and <sup>13</sup>C NMR spectra were recorded on Varian Mercury 300, Varian Inova-500 or Varian Inova-600 spectrometers at room temperature unless otherwise indicated. Chemical shifts are reported with respect to internal solvent: 7.16 and 128.38 (t) ppm (C<sub>6</sub>D<sub>6</sub>); 2.08 and 25 ppm (*d*<sub>8</sub>-tol); 5.32 and 54 (q) ppm (CD<sub>2</sub>Cl<sub>2</sub>); for <sup>1</sup>H and <sup>13</sup>C data respectively.

**Synthesis of (SNS)Me<sub>2</sub> (1).** *Trans*-dichlorobis(triphenylphosphine)palladium(II) (1.22 g, 0.0018 mol) was added to a 500 mL thick-walled glass flask fitted with a Teflon valve and dissolved in 200 mL 1,2-dimethoxyethane. To this mixture was added 2-(methylthio)phenylboronic acid (8.820 g, 0.053 mol) and 2,6-dibromopyridine (4.14 g, 0.018 mol). Potassium carbonate (7.41 g 0.70 mol) was dissolved in 50 mL of water and added to the solution. The Schlenk tube was sealed and heated to 85 °C for 12 hours.

Purification by column chromatography (98:2 hexanes-ethyl acetate) afforded **1** as an off-white solid (5.06 g, 15.6 mmol, 86.7 % yield.) <sup>1</sup>H NMR (300 MHz, CD<sub>2</sub>Cl<sub>2</sub>) δ: 7.84 (dd, J = 8.2, 7.4 Hz, 1H), 7.60 (dd, J = 4.4, 3.3 Hz, 4H), 7.46 – 7.37 (m, 4H), 7.34 – 7.23 (m, 2H) (aryl); 2.43 (s, 6H) (S(CH<sub>3</sub>)). <sup>13</sup>C NMR (75 MHz, CD<sub>2</sub>Cl<sub>2</sub>) δ: 158.01, 140.06, 137.93, 136.40, 130.53, 129.18, 126.46, 124.14, 122.89 (aryl); 16.80 (CH<sub>3</sub>).

**Synthesis of (SNS)H<sub>2</sub> (2).** To a dry 50 mL thick-walled glass flask fitted with a Teflon valve were added **1** (76 mg, 0.235 mmol) and 2-methyl-2-propanethiol (211 mg, 1.87 mmol) under argon. The tube was then evacuated overnight and refilled with argon. Dry DMF (10 mL) was added via cannula. The vessel was sealed and the reaction was allowed to stir for 4 hours at 160°C. The reaction was cooled to 0 °C for 30 min. Under an argon purge, hydrochloric acid (5 mL, 3M) was added at 0 °C. The solution was transferred to a 200 mL beaker containing hydrochloric acid (10 mL, 3 M) and CH<sub>2</sub>Cl<sub>2</sub> (100 mL). The aqueous layer was washed twice with CH<sub>2</sub>Cl<sub>2</sub> (100 mL). Organic layers were combined and the solvent was removed under reduced pressure. The solid product was taken into an inert atmosphere glove box where it was filtered through a small plug of silica with hexanes. Hexanes were removed from the filtrate to afford **2** as an off-white solid (47 mg, 0.16 mmol 67%). <sup>1</sup>H-NMR (300 MHz, CD<sub>2</sub>Cl<sub>2</sub>) δ: 7.93 (t, 1H), 7.70 – 7.50 (m, 4H), 7.47 – 7.34 (m, 2H), 7.33 – 7.19 (m, 4H) (aryl), 4.66 (bs, 2H) (SH). <sup>13</sup>C NMR (75 MHz, CD<sub>2</sub>Cl<sub>2</sub>) δ 157.97, 138.44, 138.17, 132.28, 131.50, 131.01, 129.43, 126.13, 122.72 (aryl). Calculated for C<sub>17</sub>H<sub>13</sub>NS<sub>2</sub>: C 69.12, H 4.44, N 4.74; Found: C 67.89, H 4.39, N 4.63 % This compound particularly sensitive to oxidation at sulfur. Calculated analysis for C<sub>17</sub>H<sub>13</sub>NS<sub>2</sub>O<sub>0.2</sub> (estimated based on partial oxidation at sulfur): C 67.89, H 4.36, N 4.66. HRMS (FAB+) C<sub>17</sub>H<sub>13</sub>NS<sub>2</sub>: [M+H] calcd mass 296.0568, measured mass 296.0546.

**Synthesis of (SNS)Ti(NMe<sub>2</sub>)<sub>2</sub> (3).** In an inert atmosphere glove box, **2** (9.0 mg, 0.030 mmol) was dissolved in benzene (2 mL) and benzyl potassium (7.9 mg, 0.061 mmol) was added. The solution was allowed to stir 1 hour at room temperature after which TiCl<sub>2</sub>(NMe<sub>2</sub>)<sub>2</sub> (6.2 mg, 0.030 mmol) was added to the solution and allowed to react for two hours. The solution was filtered and solvent was removed under vacuum leaving a red-brown powder. The solid was re-dissolved in C<sub>6</sub>D<sub>6</sub> showing the clean formation of **3** (5.5 mg, 0.013 mmol 42.6 %). <sup>1</sup>H NMR (500 MHz, C<sub>6</sub>D<sub>6</sub>) δ: 7.63 (dd, J = 7.8, 0.8 Hz, 2H), 7.10 (dd, J = 7.7, 1.3 Hz, 2H), 7.01 (t, 1H), 6.88 (td, J = 7.6, 1.5 Hz, 2H), 6.80 (d, J = 7.8 Hz, 2H), 6.79 (td, J = 7.6, 1.3 Hz, 2H) (aryl); 2.98 (s, 6H) (N(CH<sub>3</sub>)). <sup>13</sup>C NMR (126 MHz, C<sub>6</sub>D<sub>6</sub>) δ: 156.18, 143.27, 139.96, 138.39, 134.33, 129.88, 129.61, 124.37, 123.62 (aryl); 45.33 (N(CH<sub>3</sub>)).

**Synthesis of (SNS)Zr(NMe<sub>2</sub>)<sub>2</sub> (4).** In an inert atmosphere glove box, **2** (5.1 mg, 0.017 mmol) was dissolved in benzene (5 mL) and the solution was transferred to a vial containing Zr(NMe<sub>2</sub>)<sub>4</sub> (4.8 mg, 0.017 mmol). The solution immediately turned bright yellow with some precipitate forming. The reaction was allowed to stir for 1 hour after which solvent and formed dimethylamine were removed under vacuum. Benzene was added to the solution and the precipitate was filtered off to produce pure **4** (5.0 mg, 0.011 mmol, 62%). X-ray quality crystals were grown by slow diffusion of pentane into a benzene solution of **4**. <sup>1</sup>H NMR (300 MHz, C<sub>6</sub>D<sub>6</sub>) δ: 7.83 (dd, J = 7.7, 1.2 Hz, 2H), 7.04 – 6.97 (m, 3H), 6.93 (ddd, J = 7.9, 7.3, 1.7 Hz, 2H), 6.80 (td, 2H), 6.74 (d, J = 7.9 Hz, 2H) (aryl); 2.68 (s, 12H) (N(CH<sub>3</sub>)). <sup>13</sup>C NMR (126 MHz, C<sub>6</sub>D<sub>6</sub>) δ: 156.26, 140.78, 140.18, 137.63, 137.01, 130.33, 129.74, 123.84, 123.71 (aryl); 40.05 (N(CH<sub>3</sub>)). Calculated for C<sub>21</sub>H<sub>23</sub>N<sub>3</sub>S<sub>2</sub>Zr: C 53.35, H 4.90, N 8.89; Found: C 53.48, H 4.97, N 8.46 %

**Synthesis of (SNS)Ta(NMe<sub>2</sub>)<sub>3</sub> (5).** In an inert atmosphere glove box, **2** (15.0 mg, 0.051 mmol) was dissolved in C<sub>6</sub>D<sub>6</sub> (1 mL) and the solution was transferred to a vial containing Ta(NMe<sub>2</sub>)<sub>5</sub> (20.4 mg, 0.051 mmol). The solution immediately turned bright orange and <sup>1</sup>H NMR confirmed 50% product formation. Solvent and formed dimethylamine were removed under vacuum and the orange solid was re-dissolved in C<sub>6</sub>D<sub>6</sub> and allowed to react an additional hour, affording **5** (28.2 mg, 0.046 mmol, 91%). X-ray quality crystals were grown by slow diffusion of pentane into a concentrated benzene solution of **5**. <sup>1</sup>H NMR (300 MHz, C<sub>6</sub>D<sub>6</sub>) δ: 7.87 – 7.68 (m, 2H), 7.13 – 7.07 (m, 2H), 7.04 – 6.93 (m, 3H), 6.88 – 6.79 (m, 4H), 3.69 (s, 6H), 3.30 (s, 6H), 2.89 (s, 6H). <sup>13</sup>C NMR (126 MHz, C<sub>6</sub>D<sub>6</sub>) δ 157.96, 145.14, 142.44, 137.46, 132.81, 129.75, 127.23, 125.58, 122.79 (aryl); 50.14, 47.79, 44.43 (N(CH<sub>3</sub>)<sub>2</sub>). Calculated for C<sub>23</sub>H<sub>29</sub>N<sub>4</sub>S<sub>2</sub>Ta: C 45.54, H 4.82, N 9.24. Found: C 46.27, H 4.82, N 8.19 % This compound is air and moisture sensitive and despite repeated attempts, satisfactory combustion analysis could not be obtained.

**Synthesis of (SNS)TaCl(NEt<sub>2</sub>)<sub>2</sub> (6).** In an inert atmosphere glove box, **2** (5 mg 0.017 mmol) was dissolved in C<sub>6</sub>D<sub>6</sub> (1 mL) and benzyl potassium (4.4 mg 0.35 mmol) was added. The solution was allowed to stir 1 hour after which TaCl<sub>3</sub>(NEt<sub>2</sub>)<sub>3</sub> (7.3 mg 0.017 mmol) was added to the solution and allowed to react for two hours. <sup>1</sup>H NMR showed formation of **6** with some residual impurities from the Ta starting material (9.0 mg, 0.014, 81%). Solvent and diethylamine were removed under vacuum leaving an orange powder. The solid was re-dissolved in benzene and crystallized by slow diffusion of pentane into the solution. <sup>1</sup>H NMR (500 MHz, d<sub>8</sub>-tol, -50 °C) δ 7.48 – 7.42 (m, 2H), 6.88 – 6.80 (m, 6H), 6.78 – 6.67 (m, 3H), 4.23 (dq (broad), J = 427.2 Hz, 4H), 4.12 (dq, J = 198.8, 6.9 Hz, 2H), 3.25 (dq, J = 283.7, 6.9 Hz, 2H), 1.14 (dd, J = 6.8 Hz, 6H), 0.73 (dd, J = 6.9 Hz, 3H), -0.09 (dd, J =

7.2 Hz, 3H).  $^{13}\text{C}$  NMR (126 MHz,  $\text{d}_8\text{-tol}$ ,  $-50\text{ }^\circ\text{C}$ )  $\delta$  158.90, 157.27, 145.32, 143.96, 142.61, 142.21, 138.68, 132.42, 131.03, 130.88, 128.70, 127.69, 125.13, 124.34 (aryl); 49.23, 48.65, 48.05 ( $\text{CH}_2$ ); 23.52, 14.01, 11.45 ( $\text{CH}_3$ ). Calculated for  $\text{C}_{25}\text{H}_{31}\text{ClN}_3\text{S}_2\text{Ta}$ : C 45.91, H 4.78, N 6.42; Found: C 48.98, H 4.24, N 3.55 %. This compound is 80% pure by NMR with a 20%  $\text{TaCl}_3(\text{NEt}_2)_2$  impurity in addition to being air and moisture sensitive. Despite repeated attempts at purification, satisfactory combustion analysis could not be obtained.

**References**

1. Coates, G. W., *Chem. Rev.* **2000**, *100*, 1223.
2. (a) Resconi, L.; Cavallo, L.; Fait, A.; Piemontesi, F. *Chem. Rev.* **2000**, *100* (4), 1253; (b) Fink, G.; Steinmetz, B.; Zechlin, J.; Przybyla, C.; Tesche, B. *Chem. Rev.* **2000**, *100*, 1377; (c) Kaminsky, W.; Arndt, M. *Adv. Polym. Sci.* **1997**, *127* 143; (d) Andresen, A. C., H. G.; Herwig, J.; Kaminsky, W.; Merck, A.; Mottweiler, R.; Rein, J.; Sinn, H. V., H. J., *Angew Chem. Int. Ed. Eng.* **1976**, *15*, 630.
3. (a) Chan, M. C. W.; Tam, K.-H.; Zhu, N.; Chiu, P.; Matsui, S. *Organometallics* **2006**, *25* (3), 785; (b) Chum, P. S.; Swogger, K. W. *Progress in Polym. Sci.* **2008**, *33*, 797 (c) Gibson, V. C.; Spitzmesser, S. K. *Chem. Rev.* **2003**, *103*, 283; (d) Britovsek, G. J. P.; Gibson, V. C.; Wass, D. F. *Angew. Chem. Int. Ed.* **1999**, *38*, 428.
4. Agapie, T.; Henling, L. M.; DiPasquale, A. G.; Rheingold, A. L.; Bercaw, J. E., *Organometallics* **2008**, *27*, 6245.
5. Golisz, S. R.; Bercaw, J. E. *Macromolecules* **2009**, *42*, 8751.
6. Weinberg, D. R. Hazari, N.; Labinger, J. A.; Bercaw, J. E., *Organometallics* **2010**, *29*, 89.
7. (a) Tonks, I. A.; Henling, L. M.; Day, M. W.; Bercaw, J. E. *Inorg. Chem.* **2009**, *48*, 5096. (b) Tonks, I. A.; Bercaw, J. E., unpublished results.
8. Nakayama, Y. M., K. Uetama, N. Nakamura, A., *Chem. Lett.* **1999**, *5*.
9. Douglas W. Stephan, T. T. N., *Coord. Chem. Rev.* **1996**, *147*.
10. Douglas T. Corwin, J., James F. Corning, Stephen A. Koch, Michelle Millar, *Inorg. Chim. Acta* **1995**, *229*, 335.

11. Pinchart, A.; Dallaire, C. I.; Van Bierbeek, A.; Gingras, M., *Tetrahedron Lett.* **1999**, *40*, 5479.
12. (a) Zeysing, B.; Gosch, C.; Terfort, A. *Org. Lett.* **2000**, *2*, 1843; (b) Hsung, R. P.; Babcock, J. R.; Chidsey, C. E. D.; Sita, L. R. *Tetrahedron Lett.* **1995**, *36*, 4525.
13. (a) Tonks, I. A.; Tofan, D.; Weintrob, E. C.; Agapie, T.; Bercaw, J. E. *Organometallics*, **2012**, *31*, 1965. (b) Winston, M. S.; Bercaw, J. E. *Organometallics* **2010**, *29*, 6408.
14. Zurek, E.; Ziegler, T., *Prog. Poly. Sci.* **2004**, *29*, 107.
15. Berry, R. S., *J. Chem. Phys.* **1960**, *32*, 933.
16. Agapie, T.; Day, M. W.; Bercaw, J. E. *Organometallics* **2008**, *27*, 6123.
17. (a) Friebolin, H. *Dynamic NMR Spectroscopy Basic One- and Two-Dimensional NMR Spectroscopy* 4th Ed. Wiley-VCH: Weinheim 2005; pg 311 (b) Values for  $\Delta G^\ddagger$  were calculated at  $\pm 10$  K which is taken as the uncertainty.
18. Bailey, P. J.; Coxall, R. A.; Dick, C. M.; Fabre, S.; Henderson, L. C.; Herber, C.; Liddle, S. T.; Lorono-Gonzalez, D.; Parkin, A.; Parsons, S. *Chem. Eur. J.* **2003**, *9*, 4820.
19. Benzing, E.; Kurnicker, W. *Chem. Ber.* **1961**, *94*, 2263.
20. Chao, Y. W.; Polson, S.; Wiglen, D. E. *Polyhedron* **1990**, *9*, 2709.
21. Pangborn, A. B.; Giardello, M. A.; Grubbs, R. H.; Rosen, R. K.; Timmers, F. J., *Organometallics* **1996**, *15*, 1518.

## Chapter 3

### Formation of Trivalent Zirconocene Complexes from *ansa*-Zirconocene- Based Olefin-Polymerization Precatalysts

Adapted in part from:

Lenton, T. N.; Bercaw, J. E.; Panchenko, V. N.; Zakharov, V. A.; Babushkin, D. E.;  
Soshnikov, I. E.; Talsi, E. P.; Brintzinger, H. H. *J. Am. Chem. Soc.* **2013**, *135*, 10710

© American Chemical Society

## Chapter 3

**Abstract.** Reduction of Zr(IV) metallocenium cations with sodium amalgam (NaHg) produces EPR signals assignable to Zr(III) metallocene complexes. The chloro-bridged heterobinuclear *ansa*-zirconocenium cation  $[(\text{SBI})\text{Zr}(\mu\text{-Cl})_2\text{AlMe}_2]^+$  (SBI = *rac*-dimethylsilylbis(1-indenyl)), present in toluene solution as its  $\text{B}(\text{C}_6\text{F}_5)_4^-$  salt, thus gives rise to an EPR signal assignable to the complex  $(\text{SBI})\text{Zr}^{\text{III}}(\mu\text{-Cl})_2\text{AlMe}_2$ , while  $(\text{SBI})\text{Zr}^{\text{III}}\text{-Me}$  and  $(\text{SBI})\text{Zr}^{\text{III}}(\mu\text{-H})_2\text{Al}^i\text{Bu}_2$  are formed by reduction of  $[(\text{SBI})\text{Zr}(\mu\text{-Me})_2\text{AlMe}_2]^+ \text{B}(\text{C}_6\text{F}_5)_4^-$  and  $[(\text{SBI})\text{Zr}(\mu\text{-H})_3(\text{Al}^i\text{Bu}_2)_2]^+ \text{B}(\text{C}_6\text{F}_5)_4^-$ , respectively. These products can also be accessed, along with  $(\text{SBI})\text{Zr}^{\text{III}}\text{-}^i\text{Bu}$  and  $[(\text{SBI})\text{Zr}^{\text{III}}]^+ \text{AlR}_4^-$ , when  $(\text{SBI})\text{ZrMe}_2$  is allowed to react with  $\text{HAl}^i\text{Bu}_2$ , eliminating isobutane en route to the Zr(III) complex. Studies concerning the interconversion reactions between these and other  $(\text{SBI})\text{Zr}(\text{III})$  complexes and reaction mechanisms involved in their formation are also reported.  $(\text{SBI})\text{Zr}(\text{III})$  complexes are not active catalysts for the polymerization of  $\alpha$ -olefins but initial studies suggest they may become active in the presence of both olefin and methylaluminoxane.

## Introduction

Cationic, tetravalent group 4 metallocene complexes have been well established as active  $\alpha$ -olefin polymerization catalysts.<sup>1</sup> Frequently, metallocene precatalysts such as (SBI)ZrMe<sub>2</sub> (**1**) and (SBI)ZrCl<sub>2</sub> (**2**) (SBI = *rac*-dimethylsilylbis(1-indenyl)) are activated with methylaluminoxane (MAO), producing complex reaction mixtures.<sup>2</sup> Efforts to characterize and understand these mixtures have led to the identification of several catalytically relevant structures formed upon addition of MAO.<sup>3</sup> Subsequent reactivity studies using discrete analogs of these structures, which can be synthesized using activators such as trityl tetrakis(pentafluorophenyl)borate ([Ph<sub>3</sub>C][B(C<sub>6</sub>F<sub>5</sub>)<sub>4</sub>]), have greatly added to our overall understanding of metallocene reactivity (Figure 3.1).<sup>4</sup> Unfortunately, up to half of the initial zirconium concentration becomes unaccounted for by <sup>1</sup>H NMR after addition of olefin to these precatalysts.<sup>5,6</sup> The nature and identity of these missing species is therefore of great interest.

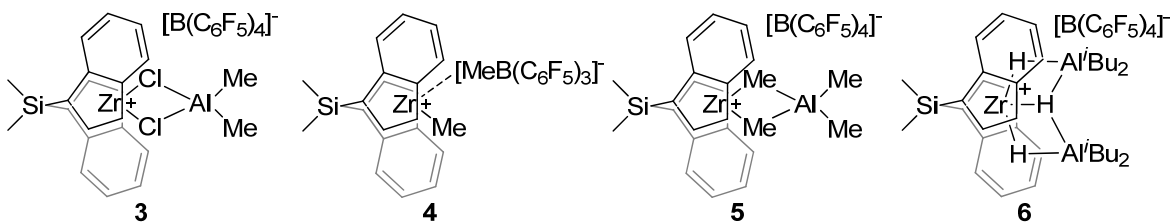


**Figure 3.1** Previously identified SBI *ansa*-zirconocene cations present under catalytic reaction conditions.

Metal species reduced by one electron to trivalent compounds have also been observed in some of these reaction systems. *In situ* formation of Ti(III) species, which are

apparently inactive, has been documented for titanocene-based polymerization catalysts<sup>7</sup> but much less attention has been directed at the formation of Zr(III) species in the course of zirconocene-catalyzed olefin-polymerizations. Despite some clear EPR-spectroscopic evidence for the occurrence of Zr(III) species in zirconocene-based polymerization catalysts,<sup>8,9</sup> and substantial previous work on trivalent zirconocene complexes in general,<sup>10</sup> information about the nature and reaction tendencies of Zr(III) complexes, which arise under polymerization conditions, is still rather limited. Identifying these reduced species and determining the mechanisms of their formation from Zr(IV) complexes present in active catalyst systems are first steps towards elucidating whether they exist as temporary resting states or are permanently removed from the catalytic cycle.

Additionally, we are interested in the role that aluminum hydrides play in polymerization systems,<sup>11</sup> as they are frequently introduced by loss of isobutene from triisobutylaluminum (TIBA), which is added to increase the overall activity of the catalytic system.<sup>12</sup> Previously it was shown that  $[(\text{SBI})\text{Zr}(\mu\text{-Me})_2\text{AlMe}_2]^+$  (**5**), a highly reactive intermediate in zirconocene-based polymerization catalysts, is converted to  $[(\text{SBI})\text{Zr}(\mu\text{-H})_3(\text{Al}^i\text{Bu}_2)_2]^+$  (**6**), itself a polymerization precatalyst,<sup>13</sup> when even small amounts of  $\text{HAl}^i\text{Bu}_2$  are present in solution.<sup>14</sup> Intriguingly, higher concentrations of paramagnetic compounds are observed by EPR-spectroscopy upon activation with MAO/TIBA mixtures than with MAO alone, which might result from Zr(III) species being formed by the introduction of aluminum hydride compounds into these reaction systems.<sup>9</sup>

In light of the above information, we have sought to generate relevant zirconocene complexes of oxidation state Zr(III) by alternative routes, in order to provide spectral and reactivity data for comparison with zirconocene reaction systems during polymerization

catalysis. Here, we present results of NMR- and EPR-spectroscopic studies on reduction reactions of several (SBI)Zr(IV) complexes with sodium amalgam and with diisobutylaluminum hydride, which give access to a variety of trivalent zirconocene species and on interconversion reactions of some of these Zr(III) complexes. This provides a more complete reference for studying Zr(III) products, that might arise under catalytic conditions, and offers first insights into possible mechanisms of their formation. Additionally, initial studies regarding the potential for Zr(III) species to be 'reactivated' to Zr(IV) precatalysts are discussed.

## **Results and Discussion**

### *Identification of (SBI)Zr(III) Species*

Due to the complex nature of these reaction systems and the limited structural information that can be obtained by EPR spectroscopy alone, a combination of data is used to identify and characterize Zr(III) species present in these reaction media. First, we consider the products that arise from the sodium amalgam reduction of various zirconocenium cations present under catalytic reaction conditions. Further studies concern the formation of Zr(III) compounds that might arise in catalytic systems upon interaction with dialkyl aluminum hydride compounds. We have also investigated the reactivity patterns of these species upon addition of aluminum-chloride, aluminum-alkyl and aluminum-hydride compounds.

### *Reduction with Sodium Amalgam.*

While sodium amalgam (NaHg) has previously been a useful reductant for various metallocene complexes,<sup>14-16</sup> no change in the NMR spectra of C<sub>6</sub>D<sub>6</sub> solutions of

(SBI)ZrMe<sub>2</sub> (**1**) was observed upon shaking with NaHg, containing 1% (wt./wt.) Na for several hours. Prolonged stirring of a C<sub>6</sub>D<sub>6</sub> solution of (SBI)ZrCl<sub>2</sub> (**2**) with NaHg for several days produced a color change to dark brown, but we were not able to isolate or identify any products from this reaction system. When AlMe<sub>3</sub> or ClAlMe<sub>2</sub> is added to a solution **2** in a 2:1 ratio before addition of NaHg, however, <sup>1</sup>H NMR signals of **2** disappear after one hour and a clear EPR signal is observed.

The same EPR spectrum is reproduced in the reduction reaction of dichloro-bridged cation [(SBI)Zr(μ-Cl)<sub>2</sub>AlMe<sub>2</sub>]<sup>+</sup> (**3**), present in solution as its B(C<sub>6</sub>F<sub>5</sub>)<sub>4</sub><sup>-</sup> salt. Reaction of NaHg with a toluene solution of **3** gives rise to an EPR spectrum with a signal at g = 1.958 (Figure 3.2). The shape of this signal – a mid-point inflection with reduced slope – indicates some unresolved hyperfine splitting. As in a similar case reported by Lyakin et al.,<sup>9</sup> a model spectrum calculated for interaction of the unpaired electron with one <sup>27</sup>Al and one <sup>91</sup>Zr nucleus is in near-perfect agreement with the observed spectrum and consistent with an assigned structure of (SBI)Zr<sup>III</sup>(μ-Cl)<sub>2</sub>AlMe<sub>2</sub> (**7**). Crystallographic data which further confirms this assignment will be discussed in a later section, as **7** was generated using alternate methods to avoid the presence of (rather insoluble) [Na][B(C<sub>6</sub>F<sub>5</sub>)<sub>4</sub>] in the reaction system.

After reduction, no signals associated with (SBI)Zr species are detected by <sup>1</sup>H NMR and the doubly-integrated intensity of the EPR signal accounts, within accuracy limits, for the total Zr content of the sample. In the absence of air, this signal is stable for days. These observations indicate that reaction of NaHg with the cation **3** furnishes the Zr(III) complex (SBI)Zr<sup>III</sup>(μ-Cl)<sub>2</sub>AlMe<sub>2</sub> (**7**) according to eq. 3.1 in practically quantitative yield.

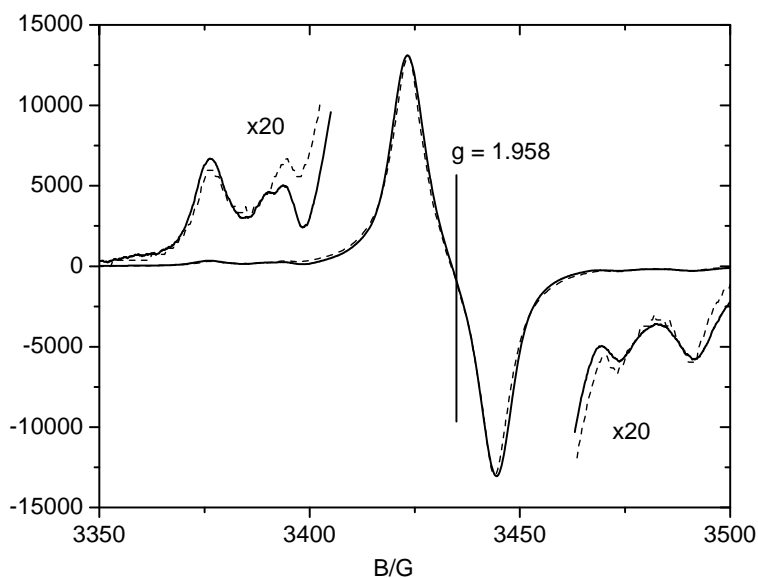
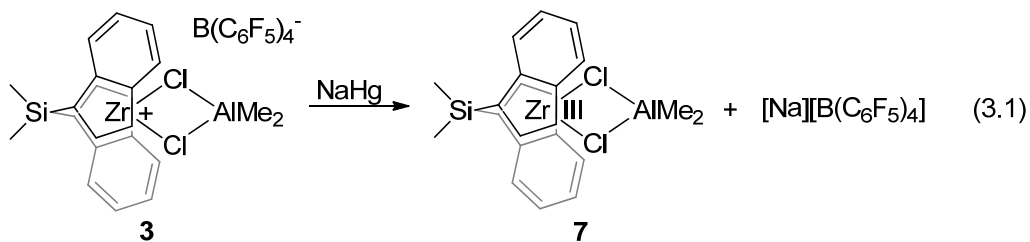


**Figure 3.2.** EPR spectrum (X-band, 25 °C) the Zr<sup>III</sup> complex **7** obtained by NaHg-induced reduction of a 3.5 mM solution of [(SBI)Zr(μ-Cl)<sub>2</sub>AlMe<sub>2</sub>]<sup>+</sup> B(C<sub>6</sub>F<sub>5</sub>)<sub>4</sub><sup>-</sup> in C<sub>6</sub>D<sub>6</sub> (solid line), and EPR spectrum calculated for interaction of the unpaired electron with one <sup>27</sup>Al and one <sup>91</sup>Zr nucleus (100% <sup>27</sup>Al, I = 5/2, a(<sup>27</sup>Al) = 3.4 G; 11% <sup>91</sup>Zr, I = 5/2, a(<sup>91</sup>Zr) = 18.6 G, line width 5 G, dashed line).



Quite different results are observed during reductions of the zirconium–methylborate ion pair [(SBI)ZrMe][Me(BC<sub>6</sub>F<sub>5</sub>)<sub>3</sub>] (**4**) or AlMe<sub>3</sub>-complexed methyl zirconocenium cation [(SBI)Zr(μ-Me)<sub>2</sub>AlMe<sub>2</sub>]<sup>+</sup> (**5**), both of which are prominent components of (SBI)Zr-based olefin-polymerization catalysts.<sup>11</sup> When a solution of **4** in benzene is mixed with NaHg for one hour, the resulting isotopic EPR spectrum contains several peaks, indicating formation of multiple reduction products (Figure 3.3).

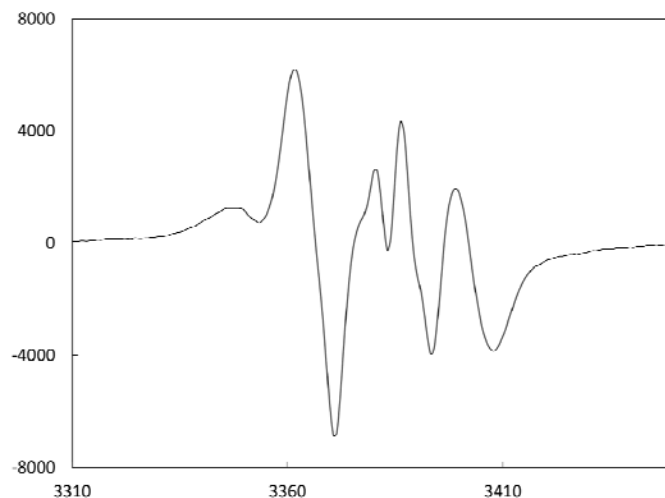


**Figure 3.3** EPR spectrum (X-band, 25 °C) obtained after reduction of a 1 mM solution of  $[(\text{SBI})\text{ZrMe}]^+[\text{MeB}(\text{C}_6\text{F}_5)_3]^-$  (**4**) in  $\text{C}_6\text{D}_6$  with 1%-NaHg.

On the other hand, when a  $\text{C}_6\text{D}_6$  solution of heterobinuclear cation **5** is shaken with sodium amalgam for ca. 1 h, it produces the much simpler EPR spectrum shown in Figure 3.4.

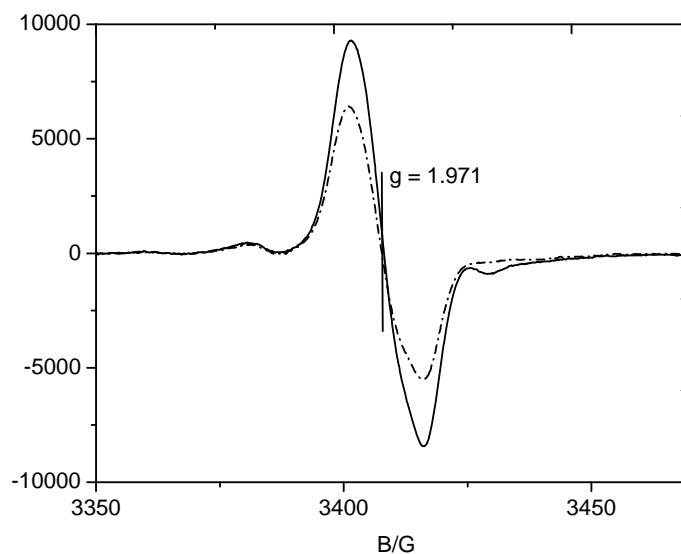
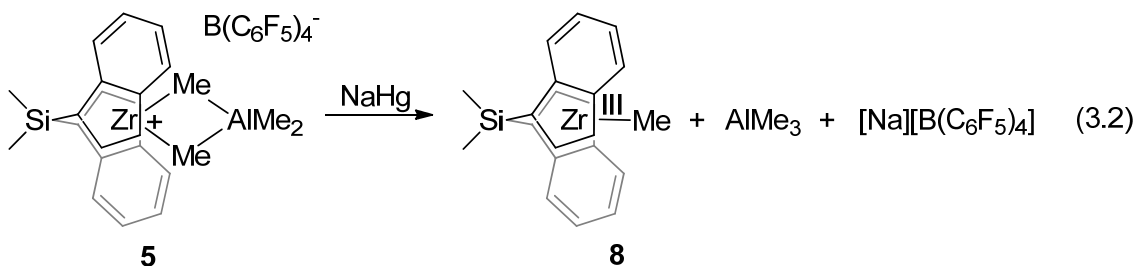


**Figure 3.4** EPR spectrum (X-band, 25 °C) obtained after reduction of a 1 mM solution of  $[(\text{SBI})\text{Zr}(\mu\text{-Me})_2\text{AlMe}_2]^+ \text{B}(\text{C}_6\text{F}_5)_4^-$  (**5**) in  $\text{C}_6\text{D}_6$  with 1%-NaHg immediately (solid line) and ca. 3 h after the end of the 1-h reaction period (broken line).

The EPR spectrum contains as its main component a signal centered at  $g = 1.971$ . Based on the absence of any  $^{27}\text{Al}$ -associated hyperfine structure from the main signal in Figure 3.4, we can tentatively assume that this signal is due to the simple methyl complex  $(\text{SBI})\text{Zr}^{\text{III}}\text{-Me}$  (**8**, eq. 3.2), rather than to the conceivable direct electron-uptake product  $(\text{SBI})\text{Zr}^{\text{III}}(\mu\text{-Me})_2\text{AlMe}_2$ . The line width of the main signal in Figure 3.4 (ca. 8 G) must obscure any hyperfine splitting by the  $\text{Zr-CH}_3$  group (usually 5 G).



The signal shown in Figure 3.4 accounts for only a small fraction (ca. 10-20%) of the total zirconocene concentration. In order to elucidate the course of the reduction reaction in more detail, we followed the EPR and  $^1\text{H}$  NMR spectra of the reaction mixture in parallel. The  $^1\text{H}$  NMR signals of the cation  $[(\text{SBI})\text{Zr}(\mu\text{-Me})_2\text{AlMe}_2]^+$  (**5**), initially the only signals discernible, completely disappear during the one-hour reduction period. Concomitant appearance of the characteristic  $^1\text{H}$  NMR signals of the dimethyl complex  $(\text{SBI})\text{ZrMe}_2$  (**1**) shows that this complex is formed in substantial concentration – about one half of the initial concentration of the cation **5** – during the reduction reaction (Figure 3.5). Reactions which might lead to the rather unexpected formation of **1** – itself not a reduction product – in the course of the reduction reaction will be discussed in a later section.

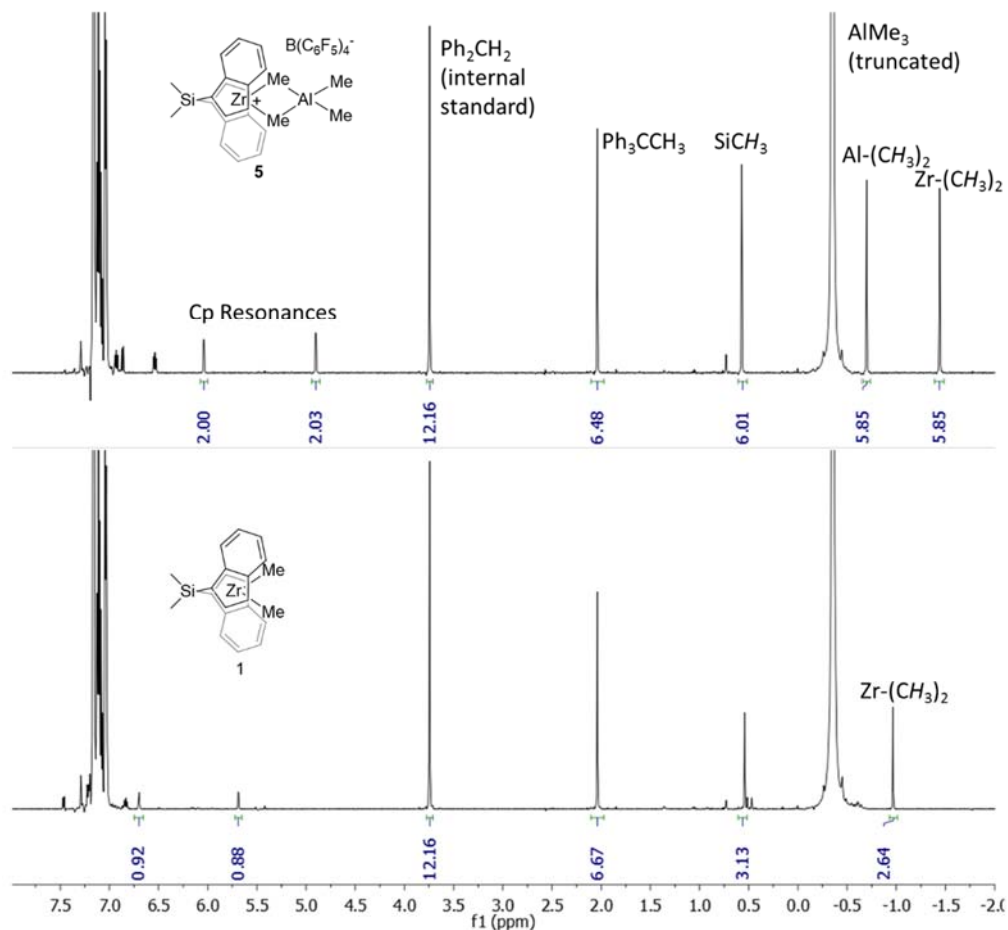


**Figure 3.5** Top: <sup>1</sup>H NMR spectra of a 3.5 mM solution of **5** in C<sub>6</sub>D<sub>6</sub>, prepared by reaction of (SBI)ZrMe<sub>2</sub> (**1**) with 1 equiv. of [Ph<sub>3</sub>C][B(C<sub>6</sub>F<sub>5</sub>)<sub>4</sub>] in the presence of excess AlMe<sub>3</sub>. Bottom: The same solution after shaking with ca. 100 mg of 1%-NaHg for 1 hr. Diphenylmethane (Ph<sub>2</sub>CH<sub>2</sub>; 3.7 ppm) was used as internal standard for quantitation of the amounts of **1** formed in relation to that of **5** reduced.

Finally, we have also studied the NaHg-induced reduction of the hydride-bridged cation [(SBI)Zr(μ-H)<sub>3</sub>(AlR<sub>2</sub>)<sub>2</sub>]<sup>+</sup> (**6**, R = Me or *i*Bu), another possible component of (SBI)Zr-based catalyst systems.<sup>10</sup> When a C<sub>6</sub>D<sub>6</sub> solution of this cation is shaken for 1 hr with sodium amalgam, it gives rise to the EPR spectrum shown in Figure 3.6. Apart from a minor, as yet not assignable component in its central part, the spectrum shows a main signal at *g* = 1.970. The shape of the main signal is indicative of a hyperfine splitting by a <sup>27</sup>Al nucleus,

which is about twice as strong as that discussed above for the Cl-bridged species **4** and the intensity of the signal indicates a yield of ca 30%.



**Figure 3.6.** EPR spectrum (X-band, 25 °C) obtained from a 1 mM C<sub>6</sub>D<sub>6</sub> solution of [(SBI)Zr(μ-H)<sub>3</sub>(AlR<sub>2</sub>)<sub>2</sub>]<sup>+</sup> (**6**) after reduction with 1%-NaHg.

Model spectra calculated with a hyperfine interaction constant of  $a(^{27}\text{Al}) = 7.5$  G closely approach the main signal shown in Figure 3.6, provided that the hyperfine splitting in its central part is not resolved, either due to an unusually large line width of 10-12 G, or alternatively, by further unresolved hyperfine interaction with two <sup>1</sup>H nuclei, each with  $a(^1\text{H}) \approx 4$  G and a more reasonable line width of 7-8 G (Figure 3.7). The EPR signal shown in Figure 3.6 is not, however, compatible with a hyperfine splitting due to two <sup>27</sup>Al nuclei, e.g. in a complex (SBI)Zr(μ-H)<sub>3</sub>(AlR<sub>2</sub>)<sub>2</sub>. We can thus tentatively assume that the main signal shown in Figure 3.6 is due to a dihydride-bridged complex (SBI)Zr<sup>III</sup>(μ-H)<sub>2</sub>AlR<sub>2</sub> (**9** eq. 3.3). Hyperfine splitting due to the minor isotope <sup>91</sup>Zr (I = 5/2, 11%) is not observed in this case, probably due to overlap with multiple splitting by <sup>27</sup>Al and <sup>1</sup>H nuclei.

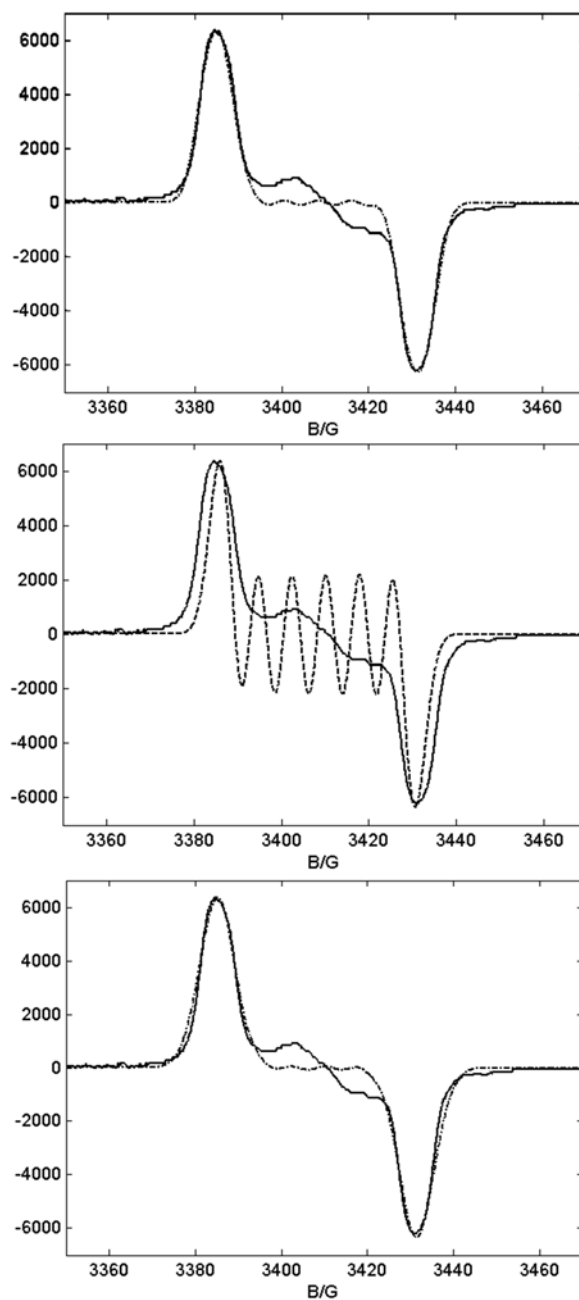
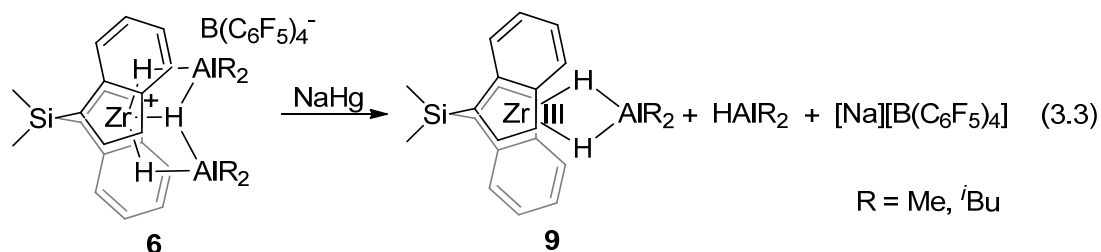


**Figure 3.7.** Solid Lines: EPR spectrum (X-band, 25 °C) obtained from a 1 mM C<sub>6</sub>D<sub>6</sub> solution of **6** after reduction with 1%-NaHg. Broken Lines: EPR spectrum calculated for interaction of the unpaired electron with Top: <sup>27</sup>Al nucleus (100% <sup>27</sup>Al, I = 5/2, a(<sup>27</sup>Al) = 7.6 G) and two <sup>1</sup>H nuclei (100% <sup>1</sup>H, I = 1/2, a(<sup>1</sup>H) = 4 G), line width 7 G; consistent with the assignment of (SBI)Zr<sup>III</sup>(μ-H)<sub>2</sub>AlR<sub>2</sub> (**9**). Middle: <sup>27</sup>Al nucleus (100% <sup>27</sup>Al, I = 5/2, a(<sup>27</sup>Al) = 7.6 G) line width 7 G. Bottom: <sup>27</sup>Al nucleus (100% <sup>27</sup>Al, I = 5/2, a(<sup>27</sup>Al) = 7.6 G), line width 11 G.



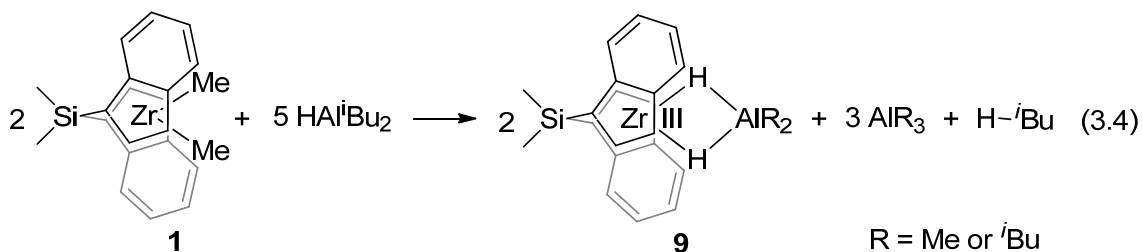
At first glance, the value of  $a(^1\text{H}) \approx 4$  G in **9** might appear rather small for hydride ligands in direct contact with a Zr(III) center, which are normally observed around 6-7 G for hydride complexes with terminal Zr<sup>III</sup>-H units.<sup>18</sup> Higher values of 7-9 have been found for anionic hydride complexes<sup>19</sup> while values as low as 3-4 G have been observed for zirconocene phosphine hydride complexes.<sup>20</sup> This assignment has further precedence in the dihydride-bridged complex  $(\text{C}_5\text{H}_5)_2\text{Zr}^{\text{III}}(\mu\text{-H})_2\text{Al}(\text{Me})(\text{C}_6\text{H}_2\text{-}2,4,6\text{-}i\text{Bu})$ , for which an EPR signal with  $a(^{27}\text{Al}) = 8.7$  G and  $a(^1\text{H}) = 3.9$  G has been reported by Wehmschulte and Power.<sup>21</sup> Substantially diminished  $a(^1\text{H})$  values of 3 and 5 G – rather than  $a(^1\text{H})$  values of 7-10 G typical for titanocene complexes with terminal Ti<sup>III</sup>-H units – have also been observed in the dihydride-bridged titanocene complexes  $(\text{C}_5\text{H}_5)_2\text{Ti}^{\text{III}}(\mu\text{-H})_2\text{AlCl}_2$  and  $(\text{C}_5\text{H}_5)_2\text{Ti}^{\text{III}}(\mu\text{-H})_2\text{AlH}_2$ , respectively.<sup>22</sup>

It must be taken into account that the Zr<sup>III</sup>( $\mu\text{-H}$ )<sub>2</sub>Al bonding situation differs distinctly from that of a terminal Zr<sup>III</sup>-H unit. Since Al(III) is likely to have a higher electronegativity than Zr(III), the complex (SBI)Zr<sup>III</sup>( $\mu\text{-H}$ )<sub>2</sub>AlR<sub>2</sub> is likely to display some character of an inner-sphere ion pair (SBI)Zr<sup>III+</sup>...H<sub>2</sub>AlR<sub>2</sub><sup>-</sup>. The diminished Zr-H covalency can thus be expected to result in reduced values of  $a(^1\text{H})$ ; hence, a value of  $a(^1\text{H}) \approx 4$  G would appear compatible with this assignment.

*Reduction of (SBI)ZrMe<sub>2</sub> by HAl<sup>i</sup>Bu<sub>2</sub>.*

While searching for causes for the incomplete progress of the reduction to **9**, described above, we noticed that EPR signals similar to that shown in Figure 3.6 are observed in solutions containing the dimethyl complex (SBI)ZrMe<sub>2</sub> (**1**) and HAl<sup>i</sup>Bu<sub>2</sub> even before the addition of [Ph<sub>3</sub>C][B(C<sub>6</sub>F<sub>5</sub>)<sub>4</sub>] and/or NaHg. More detailed studies on this reaction are described below, along with subsequent reactivity studies aimed at further characterization.

A 3.5 mM solution of **1** in C<sub>6</sub>D<sub>6</sub>, containing 10-fold excess HAl<sup>i</sup>Bu<sub>2</sub>, slowly develops the EPR spectra shown in Figure 3.8. The spectrum obtained after about one day is practically identical to that produced by reduction of the cation [(SBI)Zr(μ-H)<sub>3</sub>(AlR<sub>2</sub>)<sub>2</sub>]<sup>+</sup> (**6**) with NaHg (Figure 3.6) and is assigned as the same hydride-bridged complex (SBI)Zr<sup>III</sup>(μ-H)<sub>2</sub>AlR<sub>2</sub> (**9**). The intensity of this signal indicates that species **9** amounts to ca. 20 % of the total Zr concentration at this time and does not grow any further at longer reaction times. Parallel <sup>1</sup>H NMR measurements reveal that the reaction is accompanied by formation of isobutane along with traces of methane (Figure 3.9). Under these conditions, **9** thus appears to arise mainly by reductive elimination of isobutane (eq. 3.4).



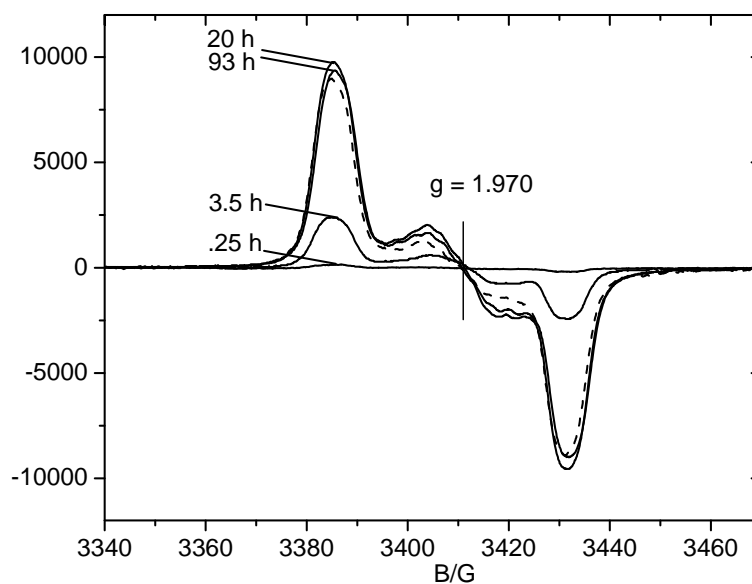


**Figure 3.8.** EPR spectrum (X-band, 25 °C) of a 3.5 mM solution of (SBI)ZrMe<sub>2</sub> (**1**) in C<sub>6</sub>D<sub>6</sub>, which contains a 10-fold excess of HA<sup>*i*</sup>Bu<sub>2</sub> at various reaction times (solid lines) and, for comparison, the spectrum assigned to **9**, taken from Figure 3.6 (broken line).

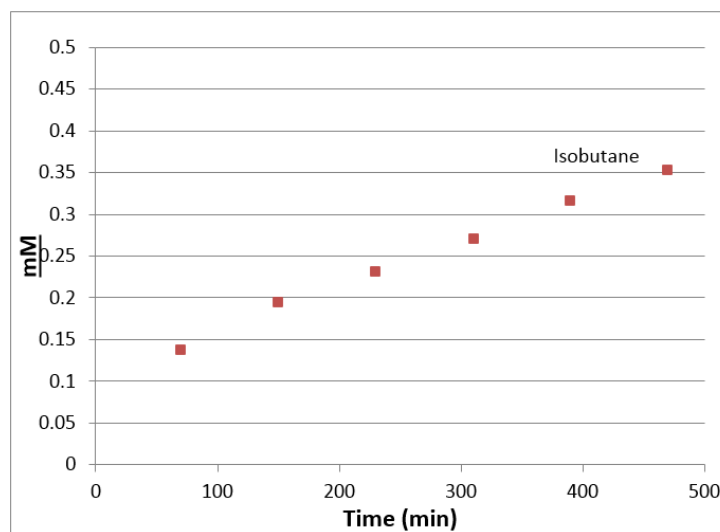


**Figure 3.9.** Isobutane concentrations derived from <sup>1</sup>H NMR spectra of a 3.5 mM solution of **1** in C<sub>6</sub>D<sub>6</sub>, before and at increasing times after addition of 10 equiv. of HA<sup>*i*</sup>Bu<sub>2</sub>.

In a related experiment, a  $C_6D_6$  solution of **1** containing only 2 equiv. of  $HAi^tBu_2$ , i.e. an amount less than that required by the stoichiometry of eq. 3.4, developed the EPR spectra shown in Figure 3.10. The spectra still show the signal of **9** but are now dominated by a central signal, also at  $g = 1.970$ . This signal shows a partly resolved hyperfine splitting due to interaction of the unpaired electron with two  $^1H$  nuclei, each with  $a(^1H) = 5.7$  G. Based on its  $g$  value, which is similar to that of the species  $(SBI)Zr^{III}-Me$  discussed above, and on its  $a(^1H)$  value, which is within the range of values previously reported for alkyl zirconocene complexes of oxidation stage  $Zr(III)$ ,<sup>9,23</sup> we assign this signal to the isobutyl complex  $(SBI)Zr^{III}-iBu$  (**10**).

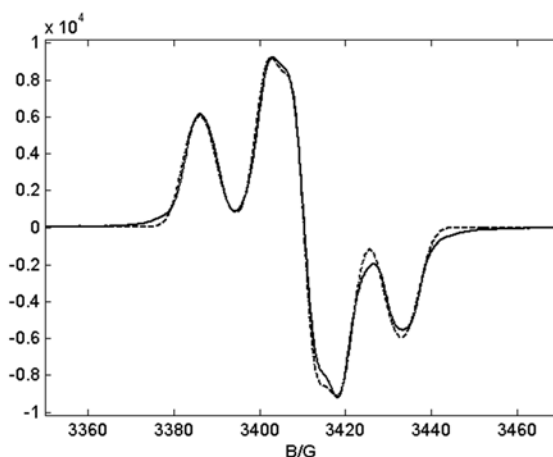


**Figure 3.10** Solid Line: EPR spectra (X-band, 25 °C) of a 3.5 mM solution of  $(SBI)ZrMe_2$  in  $C_6D_6$ , which contains 2 equiv. of  $HAi^tBu_2$  Dashed Line: The “inner” signal is reproduced through hyperfine splitting by two  $^1H$  nuclei with  $a(^1H) = 5.7$  G (16 MHz) at a line width of 7.6 G, as expected for  $(SBI)Zr^{III}-CH_2CH(CH_3)_2$  (**10**, component 1, weight 33% of total intensity). The superimposed “outer-wings” signal due to  $(SBI)Zr^{III}(\mu-H)_2AlR_2$  (**9**) is modeled using the same parameters as described in Figure 3.7 above.

After a reaction period of several hours, **9** and **10** account together for about 90% of the total zirconocene concentration in this reaction mixture. Parallel  $^1H$  NMR measurements of the reaction mixture reveal that the appearance of the EPR signals shown

in Figure 3.11 is accompanied again by substantial evolution of isobutane along with appreciable amounts of methane (Figure 3.12).

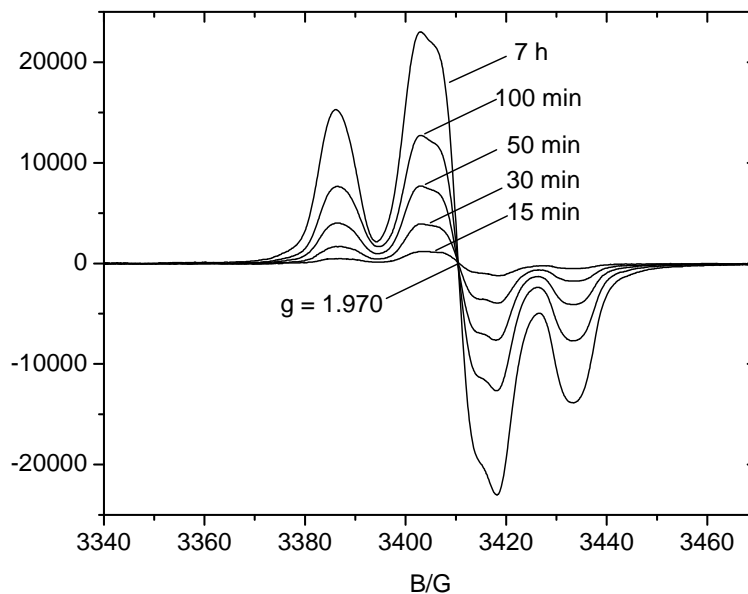


**Figure 3.11.** EPR spectra (X-band, 25 °C) of a 3.5 mM solution of (SBI)ZrMe<sub>2</sub> in C<sub>6</sub>D<sub>6</sub>, which contains 2 equiv. of HAl<sup>i</sup>Bu<sub>2</sub>, at various reaction times.

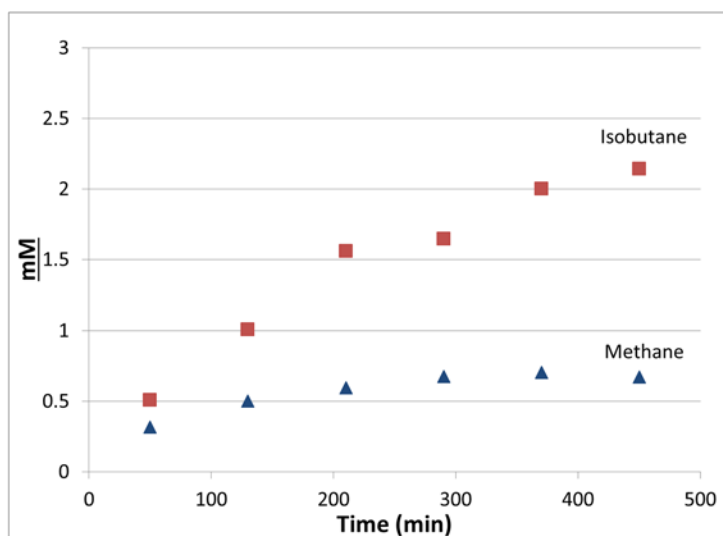
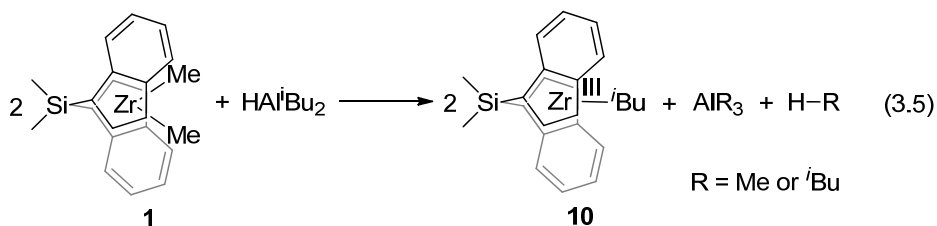


**Figure 3.12.** Isobutane and methane concentration derived from <sup>1</sup>H NMR spectra of a 3.5 mM solution of (SBI)ZrMe<sub>2</sub> in C<sub>6</sub>D<sub>6</sub>, at increasing times after addition of 2 equiv. of HAl<sup>i</sup>Bu<sub>2</sub>.

Formation of isobutyl complex **10** by reductive alkane elimination might be described by eq. 3.5. This mechanism, however, would produce only one half of an equivalent of R-H. Formation of close to 1 equiv. of alkane per unit of **1** indicates the simultaneous operation of some additional, as yet unidentified reaction(s).



Formation of **10** as the reduction product is further supported by the observation that addition of dimethylphenylphosphine to the product mixture generates, at the expense of the signals shown in Figure 3.10, a somewhat broadened EPR doublet with a hyperfine splitting of 10.6 G (Figure 3.13), as would be expected for a phosphine complex of composition (SBI)Zr(<sup>i</sup>Bu)PMe<sub>2</sub>Ph, formed according to eq. 3.6. An EPR doublet with  $a(^{31}\text{P}) = 20.6$  has been reported by Dioumaev and Harrod for the related complex (C<sub>5</sub>H<sub>5</sub>)<sub>2</sub>Zr(<sup>n</sup>Bu)PMe<sub>3</sub>.<sup>18d</sup>

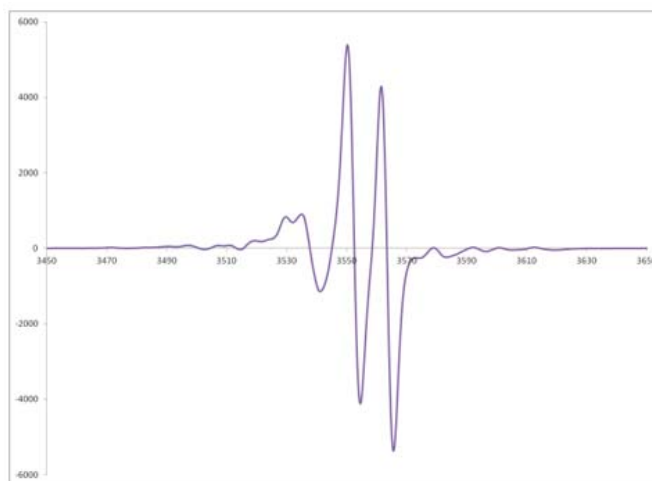
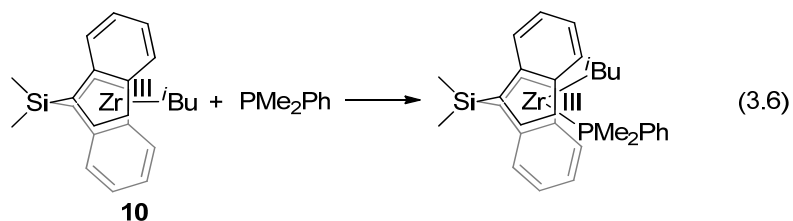
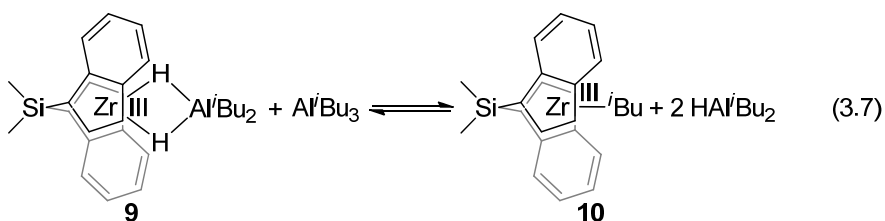


**Figure 3.13** EPR spectra (X band, 25°C) of a 3.5 mM solution of (SBI)ZrMe<sub>2</sub>, which had reacted with 2 equiv. of HAl<sup>i</sup>Bu<sub>2</sub> for one day, after addition of excess PMe<sub>2</sub>Ph.



While we were not able to corroborate the structures of complexes **9** and **10** by crystal structure determinations, our assignment of the “outer-wings” signal shown in Figure 3.10 to (SBI)Zr<sup>III</sup>(μ-H)<sub>2</sub>Al<sup>i</sup>Bu<sub>2</sub> (**9**) and of the central signal to (SBI)Zr<sup>III</sup>-<sup>i</sup>Bu (**10**) is supported by the following observation: addition of HAl<sup>i</sup>Bu<sub>2</sub> to a mixture of the two causes the signal assigned to **9** to increase relative to that of **10**, while the opposite is observed upon addition of Al<sup>i</sup>Bu<sub>3</sub>, i.e. an equilibrium reaction as in eq. 3.7 appears to interconvert **9** and **10**.



Formation of the dichloro-bridged complex **7** from **9** and **10** was studied by reacting a solution containing both of these species with increasing amounts of ClAlMe<sub>2</sub>. The EPR spectra obtained in this manner (Figure 3.14) clearly reveal a two-step reaction: addition of only 1 equiv. of ClAlMe<sub>2</sub> causes the practically complete conversion of all (SBI)Zr(III) species to a new complex with  $g = 1.968$ . Subsequent additions of ClAlMe<sub>2</sub> gradually convert this new complex to **7**. “Isosbestic” points at fields of 3416 and 3436 G indicate that only two (SBI)Zr(III) species are present under these conditions.

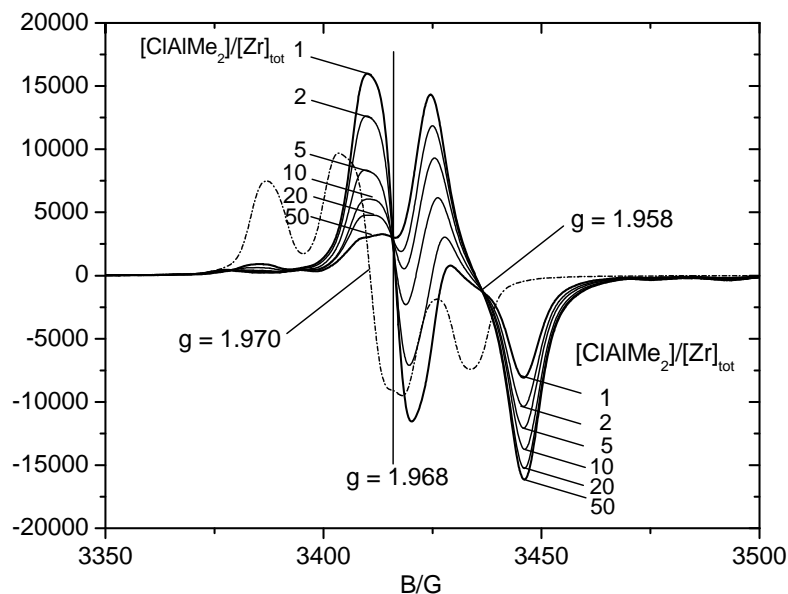
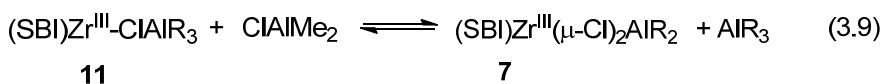


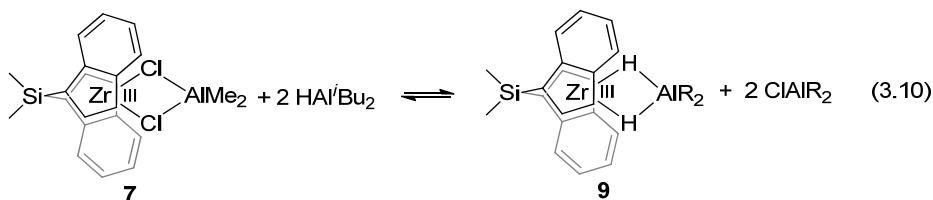
**Figure 3.14.** EPR spectra (X-band, 25 °C) of a 3.5 mM solution of (SBI)ZrMe<sub>2</sub> (**1**) in C<sub>6</sub>D<sub>6</sub>, which had reacted with 2 equiv. of HAl<sup>*i*</sup>Bu<sub>2</sub> for 16 h (broken line), after stepwise addition of 1-50 equiv. of ClAl<sup>*i*</sup>Bu<sub>2</sub> (solid lines, corrected for dilution).

Based on these observations and on the lack of obvious hyperfine interaction, the new signal at  $g = 1.968$  might *prima facie* be assigned to the monochloro complex (SBI)Zr<sup>III</sup>-Cl. Since this presumably Lewis-basic species would arise, however, in the presence of highly Lewis-acidic trialkyl aluminum compounds, it should most probably be designated as its AlR<sub>3</sub> adduct (SBI)Zr<sup>III</sup>-ClAlR<sub>3</sub> (**11**). This complex appears to be formed in practically quantitative yield under these conditions (eq. 3.8), and is then converted to **7** by excess ClAl<sup>*i*</sup>Bu<sub>2</sub> in an equilibrium reaction (eq. 3.9).



In accord with eq. 3.9, addition of excess  $\text{AlMe}_3$  to a solution of species **7** decreases its EPR signal at  $g = 1.958$  with concomitant appearance of the signal of Al-stabilized Cl species **11** at  $g = 1.968$ . The observation that excess trialkyl aluminum causes conversion of **7** to the monochloride complex supports our tentative proposal that the latter is present in form of a trialkyl aluminum adduct.

Addition of increasing proportions of  $\text{HAl}^i\text{Bu}_2$ , on the other hand, to a solution containing **7** converts most of the latter to **9**, but superimposed on the signal of this species at  $g = 1.970$  remains the signal of **11** at  $g = 1.968$ . While the equilibrium represented in eq. 3.10 thus appears to be movable to either side, the Cl ligand in  $(\text{SBI})\text{Zr}^{\text{III}}\text{-ClAlR}_3$  obviously resists exchange with an Al-bound  $^i\text{Bu}$  group.



*Crystal and molecular structure of  $(\text{SBI})\text{Zr}^{\text{III}}(\mu\text{-Cl})_2\text{AlR}_2$  (**7**)*

Taking advantage of these equilibria (eqs. 3.9 and 3.10), **7** can be obtained as a solution in pentane by first allowing  $(\text{SBI})\text{ZrMe}_2$  (**1**) to react overnight with 2 equiv. of  $\text{HAl}^i\text{Bu}_2$ , and then treating the resulting mixture of **9** and **10** with excess  $\text{ClAlMe}_2$ . When such a solution was cooled slowly to  $-20^\circ\text{C}$ , it produced crystals of X-ray quality. Structure determination of these crystals revealed a  $P2_1/c$  space group and a unit cell with  $\beta = 92.126(2)$  and four molecules of **7** with both enantiomers in equal proportions (Figure 3.15). The final anisotropic full-matrix least-squares refinement on  $F^2$  yielded a molecular structure for **7** in agreement with the spectral data discussed above (Figure 3.2).

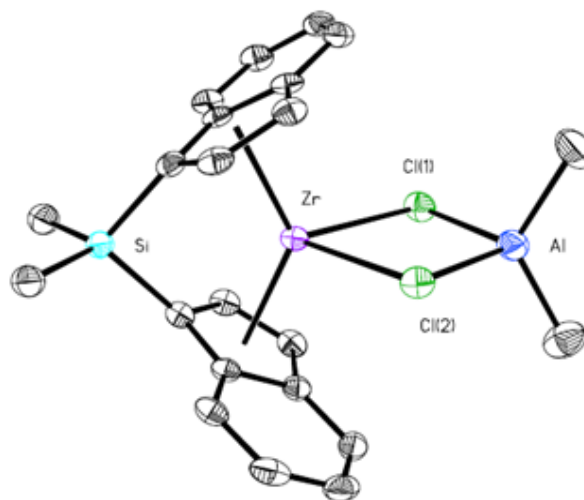


**Figure 3.15.** Molecular structure of  $(\text{SBI})\text{Zr}^{\text{III}}(\mu\text{-Cl})_2\text{Al}(\text{CH}_3)_2$  (**7**) with thermal ellipsoids at the 50% probability level. H atoms omitted for clarity. For selected bond lengths and angles see Table 1.

The coordination geometry of the Zr center of **7** can be compared to that of  $(\text{SBI})\text{ZrCl}_2$  (**2**),<sup>24</sup> as well as to those of several other zirconocene chloride complexes of oxidation state Zr(III) (Table 1).<sup>25-27</sup> The distance of the C<sub>5</sub>-ring centroid (CT) from the Zr center is found – somewhat unexpectedly – to be smaller by ca. 0.1 Å for the Zr(III) complex **7** than for its Zr(IV) congener **2**. This observation and the substantially longer Zr–Cl distances in **7** than in **2** conform with the notion that the extra electron resides in a molecular orbital of **7** which is anti-bonding with regard to the Cl ligands but mainly non-bonding with respect to the ring ligands.<sup>28</sup>

Additionally, Zr<sup>III</sup>–Cl distances are found to be significantly longer for **7** than for the dimeric Zr(III) chloride compounds listed in Table 3.1. The Al–Cl distances, on the other hand are shorter in **7** than those reported for a number of dimeric  $[\text{R}_2\text{Al}(\mu\text{-Cl})_2]$  compounds (2.32 - 2.35 Å) and close to those in the electron-poor perfluorinated compound

$[(C_6F_5)_2AlCl]_2$  (Table 3.2).<sup>29-32</sup> These deviations of Zr–Cl and Al–Cl bond distances in the heterobinuclear species **7** from values reported for related homobinuclear species – as well as its conspicuously diminished Cl–Zr–Cl and widened Cl–Al–Cl angles – can all be considered to suggest that  $(SBI)Zr^{III}(\mu-Cl)_2Al(CH_3)_2$  is indeed approaching the bonding situation of a contact ion pair  $(SBI)Zr^{III+}\cdots Cl_2Al(CH_3)_2^-$ .

	Zr-Cl	Cl-Zr-Cl	Zr-CT	CT-Zr-CT	ref.
$(SBI)Zr^{III}(\mu-Cl)_2AlMe_2$ ( <b>4</b> )	2.650(1) 2.624(1)	77.07(3)	2.1908 2.1836	130.70	this work
$(SBI)ZrCl_2$ ( <b>2</b> )	2.431(<1)	98.76(1)	2.293	119.04	24
$[(Me_3Si-C_5H_4)_2Zr^{III}(\mu-Cl)]_2$	2.560±4 <sup>a</sup>	93.34±0.10 <sup>b</sup>			25
$[(1,3-(Me_3Si)_2-C_5H_3)_2Zr^{III}(\mu-Cl)]_2$	2.602±6 <sup>a</sup>	82.77±1.10 <sup>b</sup>			26
$[(C_5H_5)Zr^{III}(\mu-Cl)]_2-(\mu-C_5H_4-C_5H_4)$	2.578	100			27

**Table 3.1.** Selected bond lengths (Å) and angles (deg) for a series of zirconocene compounds; <sup>a</sup>Averages of multiple Zr-Cl bond lengths; <sup>b</sup>Averages of multiple Cl-Zr-Cl bond angles.

	Al-Cl	Cl-Al-Cl	Al - R	Ref.
$(SBI)Zr(\mu-Cl)_2AlMe_2$ ( <b>4</b> )	2.253(1) 2.263(1)	93.37(5)	1.941(4) 1.946(4)	this work
$[tBu_2Al(\mu-Cl)]_2$	2.316(3) 2.324(3)	87.2(1)	1.966(6) 1.982(9)	29
$[Mes_2Al(\mu-Cl)]_2$	2.346(2) 2.315(2)	85.2(1)	1.972(4) 1.966(5)	30
$[AlMe(CSiR_3)(\mu-Cl)]_2$	2.3216(12)	86.53(4)	1.938(4)	31
$[(C_6F_5)_2AlCl]_2$	2.244(1) 2.273(1)	90.60 90.75	1.953(3) 1.944(3)	32

**Table 3.2.** Selected bond lengths (Å) and angles (deg) for a series of aluminum compounds.

*Formation of a Cationic Zirconium(III) complex*

The Zr(III) compounds discussed above seem to be relatively stable, but isobutyl compound **10** undergoes a slow further transformation to give a signal centered at  $g = 1.983$ . When the reaction between **1** and 2 equiv. of  $\text{HAl}^i\text{Bu}_2$  (Figure 3.11), is observed for longer reaction times, it yields the spectral changes shown in Figure 3.16. Over the course of several days, the signals of **9** and **10** both diminish to ca. 10 percent of their previous size, while a new signal grows in which is centered at  $g = 1.983$ . After about one week, little if any further changes occur. Some loss of overall signal intensity appears to occur over this period of time.

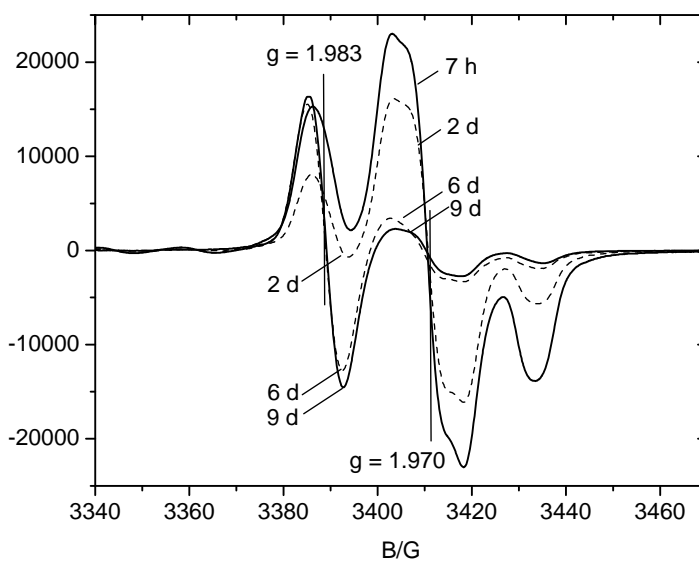


**Figure 3.16.** EPR spectra (X-band, 25 °C) of a 3.5 mM solution of  $(\text{SBI})\text{ZrMe}_2$  in  $\text{C}_6\text{D}_6$ , which contains 2 equiv. of  $\text{HAl}^i\text{Bu}_2$  (cf. Figure 3.11), measured after increasing reaction times.

Spectral changes of the same kind occur to a more complete extent, if a 3.5 mM solution of **1** is allowed to react with only 1 equiv. of  $\text{HAl}^i\text{Bu}_2$ . In this case, we observe,

after ca. 6 days, only the signal centered at  $g = 1.983$  (Figure 3.17). This rather narrow signal shows a hyperfine splitting due to the  $^{91}\text{Zr}$  nucleus with  $a(^{91}\text{Zr}) = 17$  G, but no signs of other hyperfine interactions. Based on the stoichiometry described in eq. 3.4, there is not enough  $\text{HAl}^i\text{Bu}_2$  to fully reduce **1**. Therefore, signals of **1** remain observable by  $^1\text{H}$ -NMR even after long reaction times.

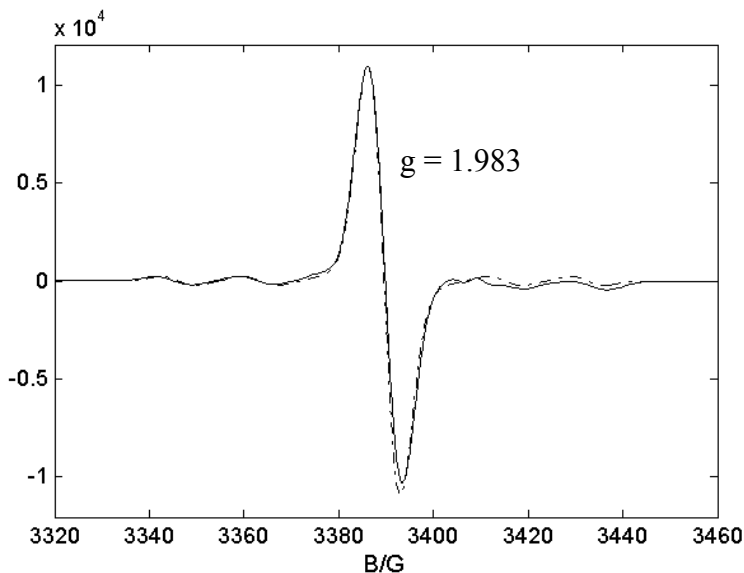
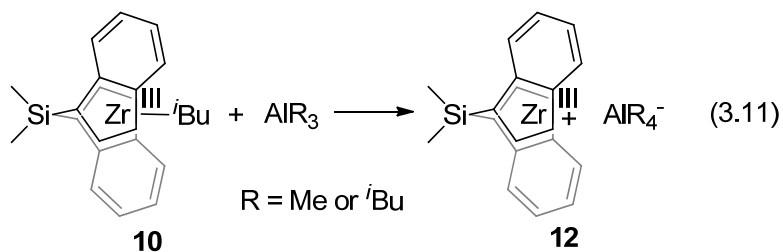


**Figure 3.17.** EPR spectrum (X-band, 25 °C) of **12**, generated from a 3.5 mM solution of **1** in  $\text{C}_6\text{D}_6$ , which contains 1 equiv. of  $\text{HAl}^i\text{Bu}_2$ , after a reaction time of ca. 6 days (solid line) and spectrum calculated for a hyperfine splitting due to a  $^{91}\text{Zr}$  nucleus (11%  $^{91}\text{Zr}$ ,  $I = 5/2$ ,  $a(^{91}\text{Zr}) = 17$  G).

Signals with similar  $g$ -values and hyperfine splitting, previously observed after reduction of  $(\text{C}_5\text{H}_5)_2\text{ZrCl}_2$  with  $\text{BuLi}$  and in MAO-activated toluene solutions of  $(2\text{-Ph-ind})_2\text{ZrCl}_2$  and  $(\text{SBI})\text{ZrCl}_2$ , were assigned to the cations  $[\text{Cp}_2\text{Zr}^{\text{III}}]^+$ ,  $[(2\text{-Ph-ind})_2\text{Zr}^{\text{III}}]^+$  and  $[(\text{SBI})\text{Zr}^{\text{III}}]^+$ , respectively, based on their lack of ligand hyperfine structure and their low-field position.<sup>7,43</sup> We follow this proposal in tentatively assigning the signal at  $g = 1.983$ , shown in Figure 3.17, to the “free” cation  $[(\text{SBI})\text{Zr}^{\text{III}}]^+$  (**12**, eq. 3.11).



This assignment raises the question of how such a cationic species could arise in a reaction system free of any of the typical cationization reagents, such as MAO or trityl cation, and which kind of anion would be associated with it. Inspection of eq. 3.11 suggests that the “spontaneous ionization” represented there is likely to be exergonic, since an aluminum trialkyl is most likely a stronger Lewis acid than the  $[(\text{SBI})\text{Zr}^{\text{III}}]^+$  cation and thus prone to abstract an  $i\text{Bu}^-$  ligand from the latter. The resulting ion pair  $[(\text{SBI})\text{Zr}^{\text{III}}]^+ \text{AlR}_4^-$  would then differ from inner-sphere ion pairs such as  $(\text{SBI})\text{Zr}^{\text{III}+}\cdots\text{Cl}_2\text{AlR}_2^-$  and  $(\text{SBI})\text{Zr}^{\text{III}+}\cdots\text{H}_2\text{AlR}_2^-$ , discussed above as representations of the chloride- and hydride-bridged complexes **7** and **9**. Apparently, the alkyl periphery of an anion  $\text{AlR}_4^-$  has a much lower tendency to coordinate to a Zr(III) center than the chloride or hydride units of a  $\text{Cl}_2\text{AlR}_2^-$  or an  $\text{H}_2\text{AlR}_2^-$  anion, such that the cation  $[(\text{SBI})\text{Zr}^{\text{III}}]^+$  associates with the anion  $\text{AlR}_4^-$  predominantly in an outer-sphere ion pair.

Consistent with this proposal is the observation that addition of  $\text{HAl}i\text{Bu}_2$  (50 equiv.) to a solution containing the ion pair **12** causes the signal at  $g = 1.983$  to disappear, while regenerating the signal pattern of the dihydride-bridged complex **9**. Apparently, scrambling of alkyl and hydride units between neutral and anionic aluminum alkyls leads to formation of  $\text{H}_2\text{Al}i\text{Bu}_2^-$ , which upon association with  $[(\text{SBI})\text{Zr}^{\text{III}}]^+$  gives  $(\text{SBI})\text{Zr}^{\text{III}+}\cdots\text{H}_2\text{AlR}_2^- \equiv (\text{SBI})\text{Zr}^{\text{III}}(\mu\text{-H})_2\text{AlR}_2$ .

This notion would also provide an explanation for the rather unexpected formation of (SBI)ZrMe<sub>2</sub> (**1**) – itself not a reduction product – in the course of the NaHg-induced reduction of the dimethyl-bridged cation **5**, noted in above. Formation of **1** is not explicable by a disproportionation of (SBI)Zr<sup>III</sup>-Me (**8**), one of the reduction products, to **1** and some (SBI)Zr complex of oxidation stage Zr(II), since **8** is found to be quite stable when prepared, in analogy to the reaction in eq. 3.7, by reaction of **1** with HAlMe<sub>2</sub> (instead of HAl<sup>t</sup>Bu<sub>2</sub>) followed by excess AlMe<sub>3</sub> (Figure 3.18).

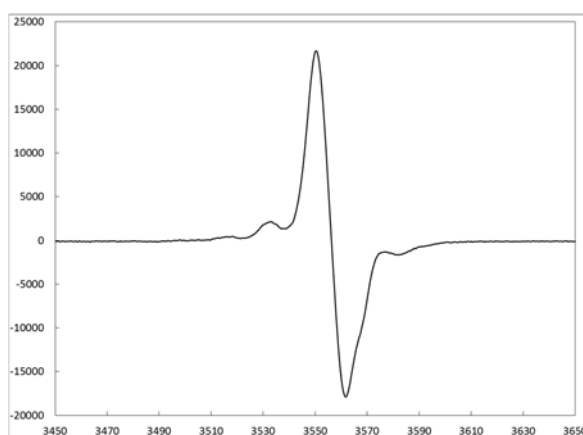
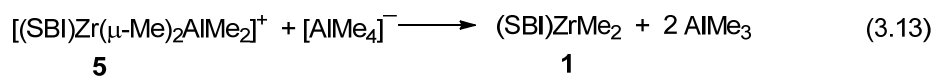
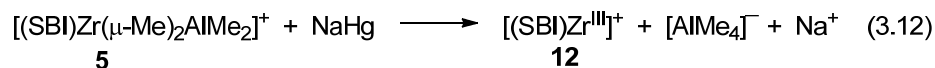
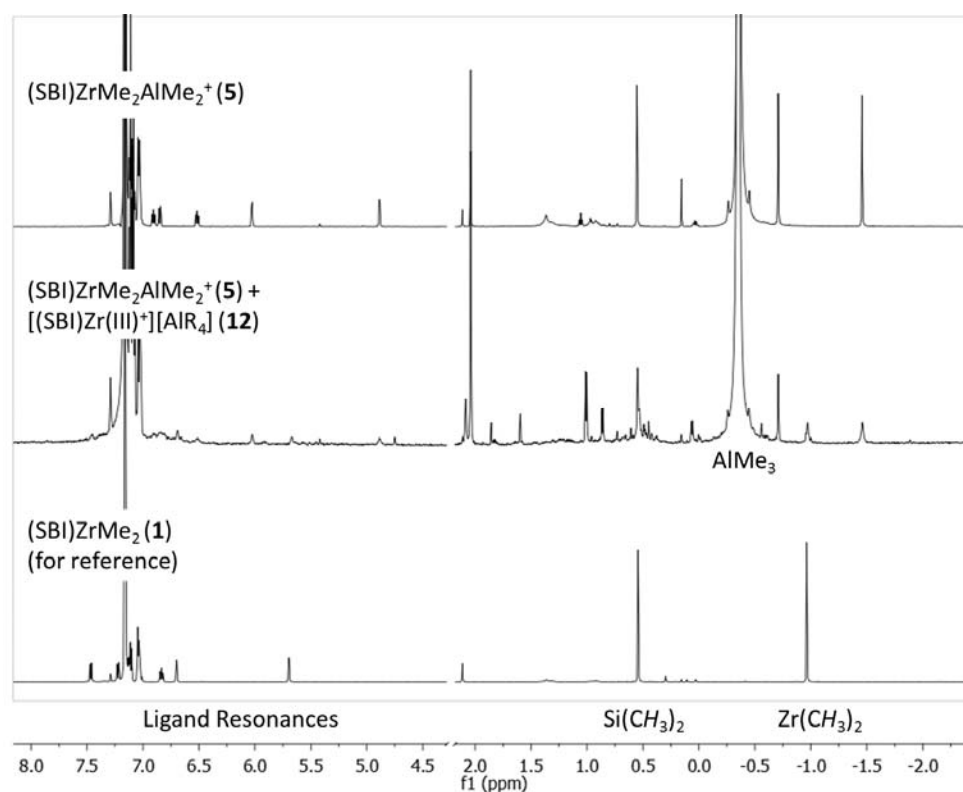


**Figure 3.18.** EPR spectra (X band, 25°C) of a 3.5 mM solution of (SBI)ZrMe<sub>2</sub> in toluene after reaction with ca. 10 equiv. of HAlMe<sub>2</sub> for ca. 22 hr followed by the addition of 10 equiv. of AlMe<sub>3</sub>.

If, however, the cation [(SBI)Zr(μ-Me)<sub>2</sub>AlMe<sub>2</sub>]<sup>+</sup> (**5**) would be initially reduced directly to (SBI)Zr<sup>III</sup>(μ-Me)<sub>2</sub>AlMe<sub>2</sub>, this species with its unfavorable alkyl bridges might arise only as a short-lived intermediate and rapidly dissociate to [(SBI)Zr<sup>III</sup>]<sup>+</sup> and AlMe<sub>4</sub><sup>-</sup> (eq. 3.12). The rather basic anion AlMe<sub>4</sub><sup>-</sup> would then most likely react with the highly Lewis-acidic Zr(IV) cation **5** so as to release **1** (eq. 3.13). This reaction sequence would generate, in accord with our experimental results (Figure 3.5) 0.5 equiv. of **1** for each cation [(SBI)Zr(μ-Me)<sub>2</sub>AlMe<sub>2</sub>]<sup>+</sup> reduced.



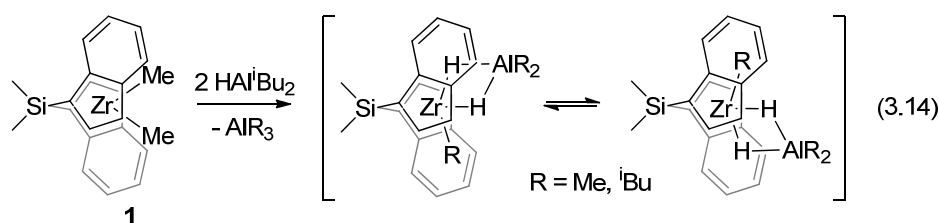
Support for this proposal comes from the following observation: when a  $d_8$ -toluene solution of **5** is added to **12**, signals from **5** diminish and new resonances that might correspond to **1** appear in the baseline (Figure 3.19). Additionally, the EPR spectrum of **12** is replaced by that of **8**, which was previously observed during the NaHg reduction of **5** (Figure 3.4). How the coordinatively unsaturated cation **12** reacts to form the simple methyl complex  $(\text{SBI})\text{Zr}^{\text{III}}\text{-Me}$  (**8**), as well as the overall fate of **8** remains unknown.



**Figure 3.19.** Top:  $^1\text{H}$  NMR spectra of a 3.5 mM solution of **5** in  $d_8$ -toluene, prepared by reaction of  $(\text{SBI})\text{ZrMe}_2$  (**1**) with 1 equiv. of  $[\text{Ph}_3\text{C}][\text{B}(\text{C}_6\text{F}_5)_4]$  in the presence of excess  $\text{AlMe}_3$ . Middle: The same solution after addition of  $\sim 3.5$  mM solution of **12** in  $d_8$ -toluene. Bottom:  $^1\text{H}$  NMR spectra of a 3.5 mM solution of **1** in  $d_8$ -toluene.

*Mechanisms of Zr(III) Formation*

The dihydride-bridged complex (SBI)Zr<sup>III</sup>(μ-H)<sub>2</sub>AlR<sub>2</sub> (**9**) and the isobutyl complex (SBI)Zr<sup>III</sup>-*i*Bu (**10**) are formed, according to equations 3.4 and 3.5, when (SBI)ZrMe<sub>2</sub> (**1**) is treated with varying amounts of HAl<sup>*i*</sup>Bu<sub>2</sub>. Under these conditions, the Zr(III) products thus appear to arise mainly by reductive elimination of the alkanes isobutane and methane. Conceivable mechanisms for a reduction of Zr(IV) to Zr(III) centers by alkane elimination might be gleaned from the following observations: Immediately upon addition of HAl<sup>*i*</sup>Bu<sub>2</sub> to solutions of **1**, the HAl and ZrMe <sup>1</sup>H-NMR signals of the reagents disappear and are replaced by broad signals, the intensities and positions of which depend on the [HAl<sup>*i*</sup>Bu<sub>2</sub>]<sub>init</sub>/[Zr]<sub>tot</sub> ratios used (Figure 3.20). These changes indicate the formation of H/Me exchange products and/or adducts between HAl<sup>*i*</sup>Bu<sub>2</sub> and **1**. While our data do not allow an unequivocal identification of these intermediary reaction products, we assume that they are analogs, with Me in place of Cl, of those formed from (SBI)ZrCl<sub>2</sub> and HAl<sup>*i*</sup>Bu<sub>2</sub>,<sup>11c</sup> i.e. heterobinuclear dihydride-bridged Zr(IV) species of the type shown in eq. 3.14.



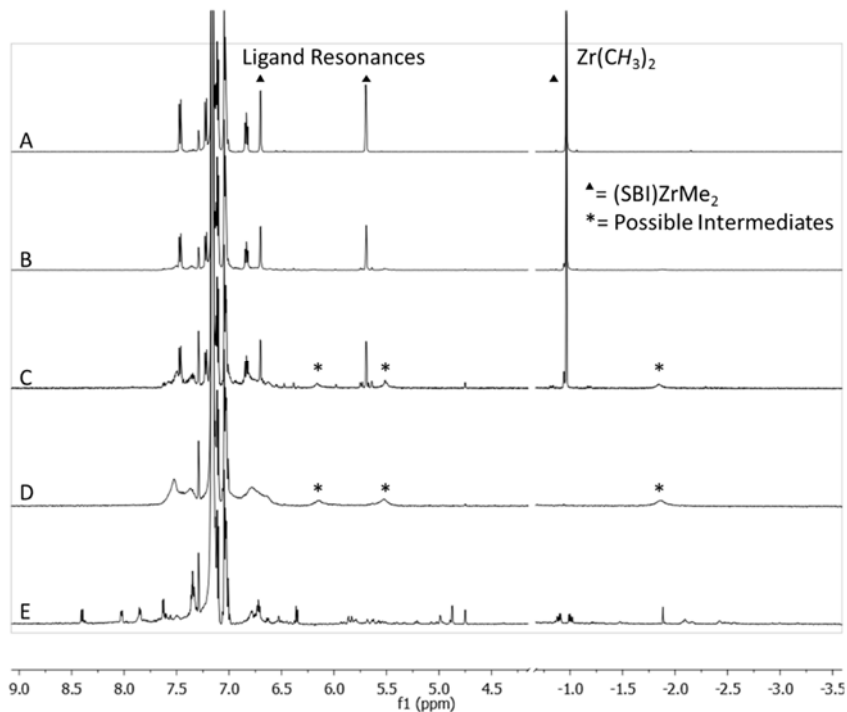
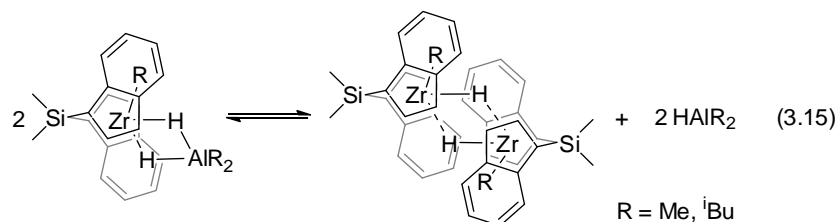
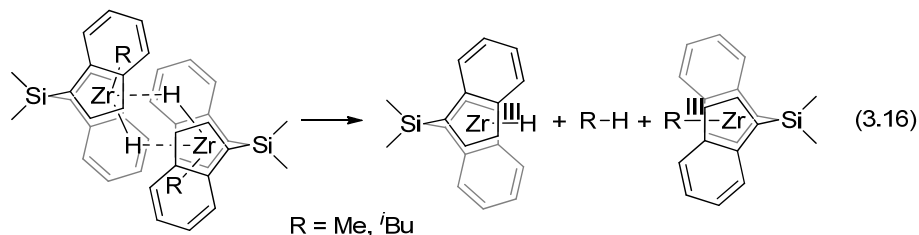


**Figure 3.20.**  $^1\text{H}$  NMR spectra (600 MHz,  $25^\circ\text{C}$ ) of 3.5 mM solutions in benzene- $d_6$  of A:  $(\text{SBI})\text{ZrMe}_2$  (**1**) B:  $(\text{SBI})\text{ZrMe}_2$  10 min after addition of 1 equiv. of  $\text{HAl}^i\text{Bu}_2$  C:  $(\text{SBI})\text{ZrMe}_2$  10 min after addition of 2 equiv. of  $\text{HAl}^i\text{Bu}_2$  D:  $(\text{SBI})\text{ZrMe}_2$  10 min after addition of 4 equiv. of  $\text{HAl}^i\text{Bu}_2$  E: the same solution as seen in spectrum D after 12 hours.

While these species would fulfill the formal requirement for reductive alkane elimination, *viz.* cis-positioned hydride and alkyl ligands, alternative and possibly more facile reaction paths might start from homobinuclear complexes which should be accessible from these heterobinuclear species *via* equilibria of the type represented in eq. 3.15.



Rather than leading to Zr(II) products, which would arise by alkane elimination from heterobinuclear Zr(IV) species of the type shown in eq. 3.14, alkane elimination from homobinuclear species, as in eq. 3.15, would lead directly to Zr(III) reduction products (eq. 16), which could then yield the final products,  $(\text{SBI})\text{Zr}^{\text{III}}(\mu\text{-H})_2\text{AlR}_2$  and  $(\text{SBI})\text{Zr}^{\text{III}}\text{-}i\text{Bu}$ , by subsequent association or ligand exchange with  $\text{HAL}^i\text{Bu}_2$ .



Our proposal, that homobinuclear complexes might be involved in the reduction process, is supported by the following observation: At a ratio of  $[\text{HAL}^i\text{Bu}_2]_{\text{init}}/[\text{Zr}]_{\text{tot}} = 2$ , formation of Zr(III) products from  $(\text{SBI})\text{ZrMe}_2$  and  $\text{HAL}^i\text{Bu}_2$  occurs with a half-life of about 1.5 h. The half-life of this reaction increases unexpectedly to ca. 5.5 h when – under otherwise identical conditions –  $\text{HAL}^i\text{Bu}_2$  is used at a higher ratio of  $[\text{HAL}^i\text{Bu}_2]_{\text{init}}/[\text{Zr}]_{\text{tot}} = 10$ . This counter-intuitive observation would be explained by the involvement of  $\text{HAL}^i\text{Bu}_2$  in the equilibrium represented in eq. 3.15: An excess of  $\text{HAL}^i\text{Bu}_2$  would favor formation of heterobinuclear species at the expense of homobinuclear complexes and would thus be expected to decrease the rate of Zr(III) formation, if homobinuclear complexes are indeed required for efficient reductive alkane elimination.

### *Reactivity Zr(III) compounds with olefins and MAO*

In order to investigate the ability of these Zr(III) complexes to polymerize olefins and, assuming they are not active, to re-enter the catalytic cycle through some reoxidation step, several reactions were performed. As expected, the Zr(III) complexes described above

are not active precatalysts and no olefin is consumed upon addition of propylene or 1-hexene to solutions of **7** in toluene.

On the other hand, when the compound is 'reactivated' by addition of MAO immediately following introduction of 1-hexene to a solution of **7** in  $d_8$ -toluene,  $^1\text{H}$  NMR signals from 1-hexene are rapidly replaced by those of poly(1-hexene) with nearly complete consumption after 45 minutes. It appears that the presence of olefin is required for this reactivation process as no  $^1\text{H}$  NMR signals attributable to Zr(IV) products are observed when MAO is added directly to **7**. Subsequent addition of 1-hexene to this solution does lead to polymerization but at a slower rate (i.e. over one hour).

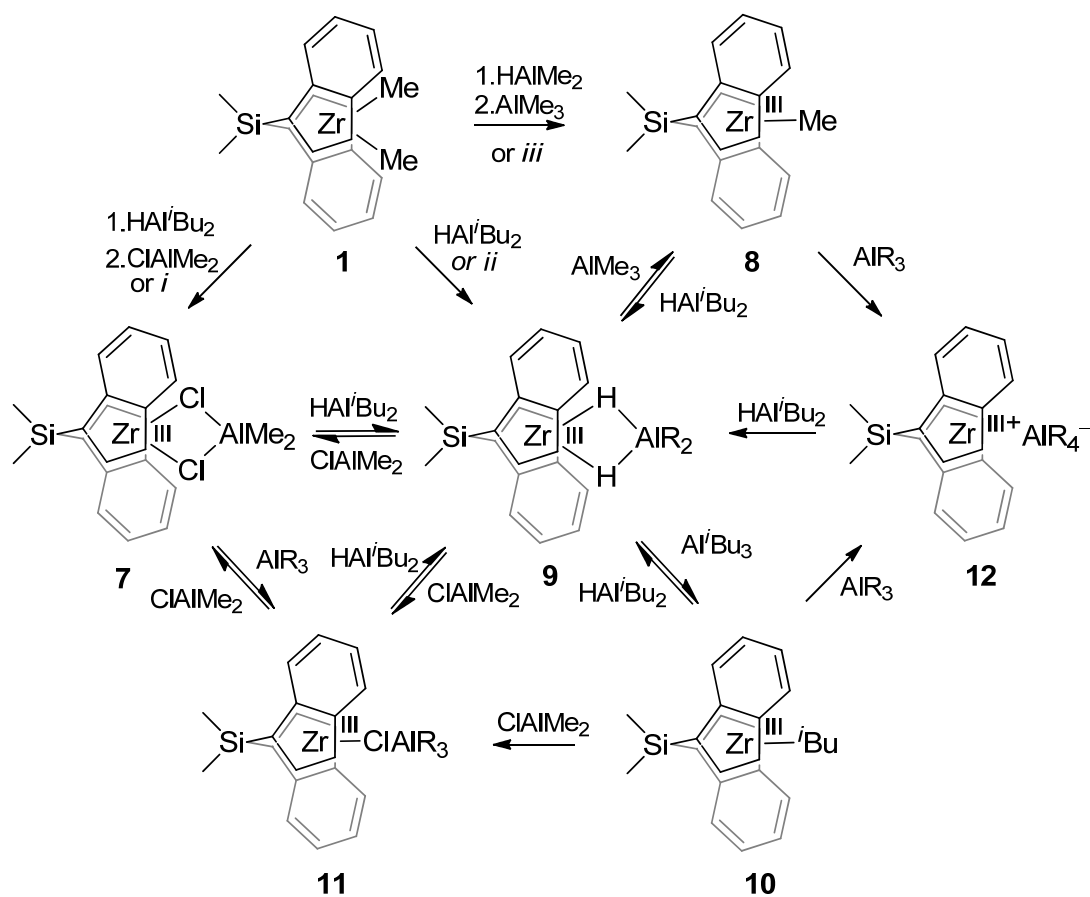
To help rule out the possibility that trace Zr(IV) compounds were responsible for the observed polymerization activity, several batch polymerizations were run under high pressures of propylene (Table 3.3). Again, no reaction was observed in the presence of **7** alone. Reactivation of **7** with MAO led to substantial polymerization activity. This system is  $\sim 1/3$  as active as the (SBI)ZrCl<sub>2</sub> (**2**) control. Furthermore, the isotactic nature of the polymer produced suggests that any reactivated Zr(III) retains the SBI ligand environment needed to exert stereocontrol during the reaction.

System	Activity
(SBI)Zr <sup>III</sup> ( $\mu$ -Cl) <sub>2</sub> AlR <sub>2</sub>	-
(SBI)Zr <sup>III</sup> ( $\mu$ -Cl) <sub>2</sub> AlR <sub>2</sub> + MAO <sup>a</sup>	$3.9 \times 10^6$
(SBI)ZrCl <sub>2</sub> + MAO <sup>a</sup>	$1.1 \times 10^7$

**Table 3.3.** Polymerization activities (g polymer/mol Zr · hr) of several complexes at 0 °C in high-pressure glass reactor. <sup>a</sup> Reactions carried out in the presence of 5000 equiv MAO.

## Conclusions

Based on the evidence described above, six (SBI)Zr(III) species appear to be accessible by reduction processes starting from (SBI)ZrMe<sub>2</sub> (**1**) in the presence of Lewis-acidic organoaluminum compounds. These are two complexes with  $\eta^2$ -bound aluminate ligands, (SBI)Zr<sup>III</sup>( $\mu$ -Cl)<sub>2</sub>AlR<sub>2</sub> (**7**) and (SBI)Zr<sup>III</sup>( $\mu$ -H)<sub>2</sub>AlR<sub>2</sub> (**9**), three complexes with simple  $\eta^1$ -bound ligands, (SBI)Zr<sup>III</sup>-Me (**8**), (SBI)Zr<sup>III</sup>-*i*Bu (**10**), and (SBI)Zr<sup>III</sup>-ClAlR<sub>3</sub> (**11**), and the cation [(SBI)Zr<sup>III</sup>]<sup>+</sup> (**12**). Our EPR results indicate that these species are related to one another and/or to **1**, by the reactions summarily represented in Scheme 3.1.



- i.* ClAlMe<sub>2</sub>, [Ph<sub>3</sub>C][B(C<sub>6</sub>F<sub>5</sub>)<sub>4</sub>], NaHg  
*ii.* HAi'Bu<sub>2</sub>, [Ph<sub>3</sub>C][B(C<sub>6</sub>F<sub>5</sub>)<sub>4</sub>], NaHg  
*iii.* AlMe<sub>3</sub>, [Ph<sub>3</sub>C][B(C<sub>6</sub>F<sub>5</sub>)<sub>4</sub>], NaHg

R = Me or *i*Bu

Scheme 3.1

Most of these complexes appear to be coordinatively unsaturated, with valence-electron counts of 13 for [(SBI)Zr<sup>III</sup>]<sup>+</sup>, and 15 for SBZr<sup>III</sup>-X (with X = ClAlR<sub>3</sub>, Me or *i*Bu). Even for (SBI)Zr<sup>III</sup>(μ-X)<sub>2</sub>AlR<sub>2</sub>, (with X = H or Cl), the effective electron density at the metal center is probably lower than suggested by their formal 17-electron count, due to the polar character of their Zr-ligand bonding, which might be written as (SBI)Zr<sup>III+</sup>...X<sub>2</sub>AlR<sub>2</sub><sup>-</sup> (with X = H or Cl). The trivalent entities encountered in this study appear to have metal centers of lower electronegativity than the Zr(IV) centers of their tetravalent precursors, and hence an increased tendency to transfer their ligands to Lewis-acidic aluminum compounds present in the reaction medium.

In the course of these studies, we have not been able to obtain any clear indication of stable homobinuclear dimers of the type (SBI)Zr<sup>III</sup>(μ-X)<sub>2</sub>Zr<sup>III</sup>(SBI), with X = Cl, H or alkyl. Monomeric and dimeric forms of trivalent zirconocene chlorides have both been reported with complexes [(Me<sub>3</sub>Si-C<sub>5</sub>H<sub>4</sub>)<sub>2</sub>Zr<sup>III</sup>(μ-Cl)]<sub>2</sub>,<sup>34</sup> and [(1,3-(Me<sub>3</sub>Si)<sub>2</sub>-C<sub>5</sub>H<sub>3</sub>)<sub>2</sub>Zr<sup>III</sup>(μ-Cl)]<sub>2</sub>,<sup>35</sup> existing as diamagnetically coupled dimers in the solid state, whereas (1,3-(Me<sub>3</sub>C)<sub>2</sub>-C<sub>5</sub>H<sub>3</sub>)<sub>2</sub>Zr<sup>III</sup>Cl, with doubly Me<sub>3</sub>C-substituted rings, is monomeric.<sup>34</sup> The propensity of a trivalent zirconocene chloride to associate to a Cl-bridged dimer thus appears to be determined by rather subtle changes in the steric load of its ring ligands. While we cannot assess how a “free” (SBI)Zr<sup>III</sup>Cl species would range in this regard, its monomeric form is apparently stabilized by formation of the AlR<sub>3</sub> adduct (SBI)Zr<sup>III</sup>ClAlR<sub>3</sub> (**11**).

Similar considerations are likely to apply also to (SBI)Zr<sup>III</sup>-hydride species, where adduct formation with a dialkylaluminum hydride is evident from the EPR spectra of **9**. For (SBI)Zr<sup>III</sup>-alkyl species, on the other hand, no tendency to form any stable alkyl-

bridged heterobinuclear adducts with alkylaluminum compounds is apparent from our data. Here, we can assume that a similarly low propensity of alkyl ligands to occupy a bridging position would also thwart any tendency of (SBI)Zr<sup>III</sup>-alkyl species to form alkyl-bridged dimers.

At any rate, the EPR signal of (SBI)Zr<sup>III</sup>( $\mu$ -Cl)AlR<sub>3</sub> (**11**) at  $g = 1.968$  accounts for practically the entire zirconocene concentration, as does that of (SBI)Zr<sup>III</sup>( $\mu$ -Cl)<sub>2</sub>AlMe<sub>2</sub> (**7**), with which it is in equilibrium according to eq. 3.9 (cf. Figure 3.14), and the Zr(III) complexes **9** and **10**, produced by reaction of **1** with 2 equiv. of HAl<sup>*i*</sup>Bu<sub>2</sub>. Any EPR-silent dimers of the type [(SBI)Zr<sup>III</sup>( $\mu$ -X)]<sub>2</sub>, with X = Cl, H or alkyl, could thus represent only insignificant fractions of the zirconocene concentration in these reaction systems.

For some reaction systems, however, such as those where **1** reacts with 10 equiv. of HAl<sup>*i*</sup>Bu<sub>2</sub>, the resulting EPR signals account only for rather small fractions (20-30%) of the total zirconocene content. In these as in some of the other reaction systems, the appearance of new <sup>1</sup>H NMR signals indicates the formation of some diamagnetic products, which we have not been able to identify so far (Figure 3.19). It must thus remain open, to which degree e.g. diamagnetically coupled Zr(III) dimers or products of the (SBI)Zr(II) oxidation stage might accumulate in the course of these reactions.

In our present study we have obtained first evidence concerning some relevant structures and reaction patterns of trivalent *ansa*-zirconocene complexes occurring in catalysis-related reaction media. Preliminary results indicate that (SBI)Zr<sup>III</sup>( $\mu$ -Cl)<sub>2</sub>AlMe<sub>2</sub> is activated by methylalumoxane to polymerize propene at a rate about one third of that with which propene is polymerized by (SBI)ZrCl<sub>2</sub> after activation with methylalumoxane

under comparable conditions. Further studies will be aimed at elucidating the role which these Zr(III) species play in zirconocene-based olefin-polymerization catalysis.

## Experimental

**General Considerations.** All operations were carried out under a protective dinitrogen atmosphere, either in a glovebox or on a vacuum manifold. Solvents (benzene, toluene, benzene- $d_6$ , toluene- $d_8$ ) were degassed and dried over 3-Å molecular sieves for 12 hours or filtered through a plug of activated alumina. (SBI)ZrMe<sub>2</sub> was obtained from Dr. M. Ringwald, MCAT, Konstanz. Trimethylaluminum, diisobutylaluminum hydride, aluminum chloride, triisobutylaluminum (1 M in toluene), and dimethylphenylphosphine were used as obtained from Aldrich Chemical Co., Milwaukee. Dimethylaluminum hydride was synthesized as previously reported.<sup>11</sup> Stock solutions of diisobutylaluminum hydride, dimethylphenylphosphine, and dimethylaluminum chloride were made at two concentrations (280 mM and 28 mM) in toluene and benzene- $d_6$ . Solutions of [(SBI)Zr( $\mu$ -Cl)<sub>2</sub>AlMe<sub>2</sub>][B(C<sub>6</sub>F<sub>5</sub>)<sub>4</sub>],<sup>13,17</sup> [(SBI)Zr( $\mu$ -H)<sub>3</sub>(Al<sup>*i*</sup>Bu<sub>2</sub>)<sub>2</sub>][B(C<sub>6</sub>F<sub>5</sub>)<sub>4</sub>]<sup>13</sup> and [(SBI)Zr( $\mu$ -Me)<sub>2</sub>AlMe<sub>2</sub>][B(C<sub>6</sub>F<sub>5</sub>)<sub>4</sub>]<sup>11</sup> were prepared in analogy to previous reports.

Samples for NMR and EPR spectra were prepared in the glove box by transferring 0.8 mL of prepared sample solutions into 5-mm OD glass NMR tubes. These were closed with rubber stoppers which had been washed with pentane and dried extensively *in vacuo*. For each measurement, these sample tubes were taken from the glovebox to the respective spectrometer and immediately transferred back to the glovebox for storage.

EPR spectra were measured using a Magnettech Miniscope MS400 spectrometer at an X-band frequency of 9.41 GHz. Hyperfine interaction parameters and *g* values were

analyzed by model calculations using the software EASYSPIN.<sup>35</sup> Concentration of Zr(III) species were obtained by double integration of the EPR signal, compared to reference samples of TEMPO. NMR spectra were measured using Varian Inova 500, 600, or Mercury 300 spectrometers. Chemical shifts are referenced to residual solvents peaks, 7.16 ppm for benzene and 2.08 ppm for CD<sub>2</sub>H proton resonances of toluene.

**CAUTION:** alkylaluminum compounds are pyrophoric and must be handled with special precautions (see, e.g., Shriver, D.F. *The Manipulation of Air-sensitive Compounds*; Robert E. Krieger Publishing Company; Malabar, Florida, 1982).

**Solutions of AlMe<sub>2</sub>Cl.** Solutions of ClAlMe<sub>2</sub> were prepared at 280 mM and 28 mM concentrations by dissolving 0.2 mL (0.934 mmol) of trimethyl aluminum in 4.8 mL of toluene, adding 62.3 mg (0.467 mmol) of aluminum chloride to the solution and stirring until the solid had dissolved. From this 280 mM solution, a 28 mM toluene solution of ClAlMe<sub>2</sub> was formed by adding 0.2 mL to 1.8 mL of toluene. These solutions were used as stock ClAlMe<sub>2</sub> solutions in the experiments described below.

**Solutions of [(SBI)Zr(μ-Cl)<sub>2</sub>AlMe<sub>2</sub>]<sup>+</sup>.** To a solution of 2.3 mg (5.6 μmol) (SBI)ZrMe<sub>2</sub> in 0.8 mL toluene was added 0.1 mL of the 280 mM ClAlMe<sub>2</sub> solution prepared above. The solution was diluted with toluene to a total volume of 1.6 mL and transferred to a vial containing 5.16 mg (5.6 μmol) of solid [Ph<sub>3</sub>C][B(C<sub>6</sub>F<sub>5</sub>)<sub>4</sub>]. Complete dissolution of the trityl salt yielded a dark blue, 3.5 mM solution of [(SBI)Zr(μ-Cl)<sub>2</sub>AlMe<sub>2</sub>][B(C<sub>6</sub>F<sub>5</sub>)<sub>4</sub>] in toluene. Analogously prepared benzene-d<sub>6</sub> and toluene-d<sub>8</sub> solution of [(SBI)Zr(μ-Cl)<sub>2</sub>AlMe<sub>2</sub>][B(C<sub>6</sub>F<sub>5</sub>)<sub>4</sub>] gave rise to <sup>1</sup>H NMR signals at 6.26, 5.23 and 0.68 ppm (25 °C, 600 MHz) and to a characteristic UV/vis absorbance band at 614 nm, in close agreement to values of 6.26, 5.17 and 0.71 ppm and 614 nm, reported for the

homologous cation  $[(\text{SBI})\text{Zr}(\mu\text{-Cl})_2\text{Al}^i\text{Bu}_2]^+$  in  $\text{C}_6\text{D}_6$  solution (Baldwin, S. M.; Bercaw, J. E.; Henling, L. M.; Day, M. W.; Brintzinger, H. H. *J. Am. Chem. Soc.* **2011**, *133*, 1805-1813).

**Solutions of  $[(\text{SBI})\text{Zr}(\mu\text{-Me})_2\text{AlMe}_2]^+$ .** To a solution of 4.0 mg (9.8  $\mu\text{mol}$ ) of  $(\text{SBI})\text{ZrMe}_2$  in 2.8 mL of either toluene or benzene- $\text{d}_6$  was added 3 drops (22.5 mg, 0.3 mmol) of trimethylaluminum. The solution was transferred to a vial containing 9.0 mg (9.8  $\mu\text{mol}$ ) of solid  $[\text{Ph}_3\text{C}][\text{B}(\text{C}_6\text{F}_5)_4]$ . Complete dissolution of the trityl salt yielded an orange-red, 3.5 mM solution of  $[(\text{SBI})\text{Zr}(\mu\text{-Me})_2\text{AlMe}_2][\text{B}(\text{C}_6\text{F}_5)_4]$ .

**Solutions of  $[(\text{SBI})\text{Zr}(\mu\text{-H})_3\text{AlR}_2]^+$ .** To a solution of 4.0 mg (9.8  $\mu\text{mol}$ ) of  $(\text{SBI})\text{ZrMe}_2$  in 1.4 mL of toluene or benzene- $\text{d}_6$  was added 1.4 mL (28 mM, 39.2  $\mu\text{mol}$ ) of diisobutylaluminum hydride in toluene or benzene- $\text{d}_6$  via microliter syringe. The solution was transferred to a vial containing 9.0 mg (9.8  $\mu\text{mol}$ ) of  $[\text{Ph}_3\text{C}][\text{B}(\text{C}_6\text{F}_5)_4]$ . Complete dissolution of the trityl salt yielded a yellow, 3.5 mM solution of  $[(\text{SBI})\text{Zr}(\mu\text{-H})_3\text{AlR}_2][\text{B}(\text{C}_6\text{F}_5)_4]$  in toluene.

**Reductions with sodium amalgam.** A 1-mL syringe with 16-gauge needle was used to add three drops (ca. 50 mg) of sodium amalgam (1% wt/wt) to a vial containing 0.8 mL of a 3.5 mM solution of the respective Zr(IV) compound. The vial was capped and placed in a wrist-action shaker for one hour. Excess sodium amalgam was allowed to settle to the bottom of the vial and the solution was transferred with a pipette into a 5 mm OD glass tube for EPR and NMR spectroscopy.

**Reduction of  $(\text{SBI})\text{ZrMe}_2$  with 10 equivalents of  $\text{HAl}^i\text{Bu}_2$ .** To a solution of 4.0 mg (9.8  $\mu\text{mol}$ ) of  $(\text{SBI})\text{ZrMe}_2$  in 1.4 mL of toluene or benzene- $\text{d}_6$  was added 0.35 mL (280 mM, 98.0  $\mu\text{mol}$ ) of diisobutylaluminum hydride in toluene or benzene- $\text{d}_6$  via microliter

syringe. The solution was diluted with toluene or benzene-d<sub>6</sub> to a total volume of 2.8 mL (3.5 mM Zr). From this solution, 0.8 mL was transferred to a 5 mm OD glass tube to monitor the reaction by EPR and/or NMR spectroscopy.

**Reduction of (SBI)ZrMe<sub>2</sub> with 4 equivalents of HAl<sup>i</sup>Bu<sub>2</sub>.** To a solution of 4.0 mg (9.8 μmol) of (SBI)ZrMe<sub>2</sub> in 1.4 mL of toluene or benzene-d<sub>6</sub> was added 1.4 mL (28 mM, 19.6 μmol) of diisobutylaluminum hydride in toluene or benzene-d<sub>6</sub> via microliter syringe.

Addition of Al<sup>i</sup>Bu<sub>3</sub>. To an NMR tube containing 0.8 mL of the zirconium solution described above, was added 0.01 mL of a 1 M solution of triisobutylaluminum in toluene.

**Reduction of (SBI)ZrMe<sub>2</sub> with 2 equivalents of HAl<sup>i</sup>Bu<sub>2</sub>.** To a solution of 4.0 mg (9.8 μmol) of (SBI)ZrMe<sub>2</sub> in 1.4 mL of toluene or benzene-d<sub>6</sub> was added 0.7 mL (28 mM, 19.6 μmol) of diisobutylaluminum hydride in toluene or benzene-d<sub>6</sub> via microliter syringe. The solution was diluted with toluene or benzene-d<sub>6</sub> to a total volume of 2.8 mL and allowed to sit overnight before further use.

Addition of HAl<sup>i</sup>Bu<sub>2</sub>. To an NMR tube containing 0.8 mL of the zirconocene solution described above, was added 0.1 mL of diisobutylaluminum hydride (280 mM in benzene-d<sub>6</sub>, 2 equiv)

Addition of Dimethylphenylphosphine. From the zirconocene solution described above, 0.2 mL (3.5 mM, 7 μmol) was transferred to a 4 mm OD quartz EPR tube and 10 μL of dimethylphenylphosphine (0.35 μmol, 0.5 equiv.) was added. After obtaining an EPR spectrum, the tube was returned to the glove box, where an additional 10 μL dimethylphenylphosphine (0.35 μmol, 1 equiv.) was added. After obtaining EPR spectra

and returning the tube to the glove box, 1 drop of neat dimethylphenylphosphine was added before obtaining a final spectrum.

Conversion to (SBI)Zr( $\mu$ -Cl)<sub>2</sub>AlR<sub>2</sub>. Two NMR tubes were prepared with 0.8 mL each of the (SBI)ZrMe<sub>2</sub>/diisobutylaluminum reaction mixture described above. To the first tube, one equivalent of ClAlMe<sub>2</sub> in toluene (0.1 mL, 28 mM) was added via syringe. After obtaining an EPR spectrum, the tube was returned to the box and a second equivalent of ClAlMe<sub>2</sub> was added in the same manner. This was continued sequentially until 9 equivalents had been added. Similarly, ClAlMe<sub>2</sub> was added in 10-equivalent steps to the second tube by adding 0.1 mL aliquots of a 280 mM solution of ClAlMe<sub>2</sub> in toluene, EPR spectra being obtained before and after each addition.

**Reduction of (SBI)ZrMe<sub>2</sub> with 1 equivalent of HAl<sup>i</sup>Bu<sub>2</sub>,** To a solution of 4.0 mg (9.8  $\mu$ mol) of (SBI)ZrMe<sub>2</sub> in 1.4 mL of benzene-d<sub>6</sub> was added (0.35 mL) (28 mM, 9.8  $\mu$ mol) of diisobutylaluminum hydride in benzene-d<sub>6</sub> via microliter syringe. The solution was diluted with toluene or benzene-d<sub>6</sub> to a total volume of 2.8 mL. A portion of this solution (0.8 mL, 3.5 mM) was transferred to a 5 mm OD NMR tube and monitored by EPR and NMR spectroscopy for 6 days, after which full formation of the EPR signal assigned to [(SBI)Zr<sup>III</sup>]<sup>+</sup> was observed.

Reaction with HAl<sup>i</sup>Bu<sub>2</sub>. To an NMR tube containing 0.8 mL of the zirconocene solution described above was added 0.1 mL (280 mM, 2 equiv) of diisobutylaluminum hydride in benzene-d<sub>6</sub>.

**Preparation of crystalline (SBI)Zr<sup>III</sup>( $\mu$ -Cl)<sub>2</sub>AlR<sub>2</sub> and structure determination.**

To 8 mg (0.020 mmol) of (SBI)ZrMe<sub>2</sub> was added 1.4 mL HAl<sup>i</sup>Bu<sub>2</sub> (28 mM) in pentane, (0.04 mmol). The mixture was allowed to sit overnight after which it was filtered and 1 mL

ClAlMe<sub>2</sub> was added (~1 M in pentane, 1 mmol). The solution was cooled to -10 °C overnight in a glass vial and then further to -25 °C after which several crystals formed directly above the solvent line. Crystals were removed from the cooled glass vial to a microscope slide coated with Fluorolube®. Samples were selected and mounted using a cryoloop that was also coated with Fluorolube®. Data collection was carried out on a BrukerKAPPA APEXII diffractometer with a 0.71073 Å MoKR source.

**1-Hexene Polymerization Procedure.** A solution of [(SBI)Zr(μ-Cl)<sub>2</sub>AlMe<sub>2</sub>] [B(C<sub>6</sub>F<sub>5</sub>)<sub>4</sub>] (3.5 mM in toluene) was prepared as described above. Three samples were prepared in Teflon-sealed NMR tubes, each with a volume of 500 μL. Neat 1-hexene (0.1 mL) was added to each NMR tube before or after the addition of MAO.

**Batch Propylene Polymerization Procedure.** A high-pressure glass reactor was charged with solid MAO (780 mg, 2000 equiv), and toluene (3 mL, distilled from Na/Ph<sub>2</sub>CO) was added inside an inert atmosphere glove box. The vessel was sealed, removed from the glove box, and attached to a propylene tank and purged. The glass reactor was cooled to 0 °C after which propylene (20-30 mL) was condensed in. **2** or **7** (0.02 mmol) were added via syringe through a rubber septa at the top of the vessel, as a toluene solution (0.7 mL). The reaction mixture was stirred vigorously at 0 °C for 5 min. Excess propylene was vented and a MeOH/HCl solution (10:1, 50 mL) was added slowly to quench the reaction. The resulting mixture was transferred to an Erlenmeyer flask, additional MeOH/HCl solution was added (50 mL), and the mixture was allowed to stir at room temperature overnight. The methanol solution was decanted and the polymer was rinsed with methanol. The polymer was transferred to a vial, and volatile materials were removed by placing the vial under high vacuum overnight.

**References**

1. Reviews: a) Resconi, L.; Cavallo, L.; Fait, A.; Piemontesi, F. *Chem. Rev.* **2000**, *100*, 1253-1345. b) Resconi, L.; Chadwick, J. C.; Cavallo, L., In *Comprehensive Organometallic Chemistry III*, Crabtree, R. H.; Mingos, D. M. P., Eds. Elsevier: Oxford, **2007**; Vol. 4, Bochmann, M., Ed., Chapter 4.09, p. 1005-1166.
2. Reviews: a) Chen, E. Y. X.; Marks, T. J. *Chem. Rev.* **2000**, *100*, 1391-1434. b) Bochmann, M. *J. Organomet. Chem.* **2004**, *689*, 3982-3998. c) Bochmann, M. *Organometallics* **2010**, *29*, 4711-4740.
3. a.) Tritto, I.; Donetti, R.; Sacchi, M. C.; Locatelli, P. Zannoni, G. *Macromolecules*, **1999**, *32*, 264 b.) Babushkin, D. E.; Naundorf, C. Brintzinger, H. H. *Dalton Trans.*, **2006**, 4539. c.) Bryliakov, K. P.; Semikolenova, N. V.; Panchenko, V. N.; Aakharov, V. A.; Brintzinger, H. H.; Talsi, E. P. *Macromol. Chem. Phys.*, **2006**, *207*, 327.
4. a.) Bochmann, M.; Lancaster, S. J. *Angew. Chem. Int. Ed. Engl.* **1994**, *33*, 1634-1637. Yang, X. M.; Stern, C. L.; Marks, T. J. *J. Am. Chem. Soc.* **1994**, *116*, 10015. c.) Baldwin, S. M.; Bercaw, J. E.; Henling, L. M.; Day, M. W.; Brintzinger, H. H. *J. Am. Chem. Soc.* **2011**, *133*, 1805-1813.
5. Babushkin, D. E.; Brintzinger, H. H., *J. Am. Chem. Soc.* **2010**, *132*, 452.
6. Novstrup, K. A.; Travia, N. E.; Medvedev, G. A.; Stanciu, C.; Switzer, J. M.; Thomson, K. T.; Delgass, W. N.; Abu-Omar, M. M.; Caruthers, J. M.; *J. Am. Chem. Soc.* **2010**, *132*, 558.
7. a) Huang, Y. H.; Yu, Q.; Zhu, S.; Rempel, G. L.; Li, L. *J. Polym. Sci. A, Polym. Chem.* **1999**, *37*, 1465-1472. b) Bryliakov, K. P.; Babushkin, D. E.; Talsi, E. P.;

- Voskoboynikov, A. Z.; Gritzko, H.; Schröder, L.; Damrau, H.-R. H.; Wieser, U.; Schaper, F.; Brintzinger, H. H. *Organometallics* **2005**, *24*, 894-904.
8. Cram, D.; Sartori, F.; Maldotti, A. *Macromol. Chem. Phys.* **1994**, *195*, 2817-2826.
9. Lyakin, O. Y.; Bryliakov, K. P.; Panchenko, V. N.; Semikolenova, N. V.; Zakharov, V. A.; Talsi, E. P. *Macromol. Chem. Phys.* **2007**, *208*, 1168-1175.
10. Review: Lancaster, S. J.; In *Comprehensive Organometallic Chemistry III*, Crabtree, R. H.; Mingos, D. M. P., Eds.; Elsevier, Oxford, **2007**, Vol. 4, Bochmann, M., Ed., Chapter 4.07, p. 741-757.
11. a) Babushkin, D. E.; Brintzinger, H. H. *Chem. Eur. J.* **2007**, *13*, 5294-5299. b) Babushkin, D. E.; Panchenko, V. N.; Timofeeva, M. N.; Zakharov, V. A.; Brintzinger, H. H. *Macromol. Chem. Phys.* **2008**, *209*, 1210-1219. c) Baldwin, S. M.; Bercaw, J. E.; Brintzinger, H. H. *J. Am. Chem. Soc.* **2008**, *130*, 17423-17433.
12. Kleinschmidt, R.; van der Leek, Y.; Reffke, M.; Fink, G. *J. Mol. Catal. A-Chem.* **1999**, *148*, 29-41.
13. Baldwin, S. M.; Bercaw, J. E.; Brintzinger, H. H. *J. Am. Chem. Soc.* **2010**, *132*, 13969-13971.
14. Baldwin, S. M.; Bercaw, J. E.; Henling, L. M.; Day, M. W.; Brintzinger, H. H. *J. Am. Chem. Soc.* **2011**, *133*, 1805-1813.
15. Wailes, P. C.; Weigold, H. *J. Organomet. Chem.* **1971**, *28*, 91-95.
16. Cuenca, T.; Royo, P. *J. Organomet. Chem.* **1985**, *293*, 61-67.
17. Review: Connelly, N. G.; Geiger, W. E. *Chem. Rev.* **1996**, *96*, 877-910.
18. a) Samuel, E.; Maillard, P.; Gianotti, C. *J. Organomet. Chem.* **1977**, *142*, 289-298. b) Hudson, A.; Lappert, M. F.; Pichon, R. *J. Chem. Soc., Chem. Comm.* **1983**, 374.

- c) Bajgur, C. S.; Jones, S. B., Petersen, J. L. *Organometallics* **1985**, *4*, 1929-1936. d) Dioumaev, V.K.; Harrod, J. F. *Organometallics* **1997**, *16*, 1452-1464.
19. Choukroun, R.; Gervais, D. *J. Chem. Soc., Chem. Comm.* **1985**, 224-225.
20. Larsonneur, A.-M.; Choukroun, R.; Jaud, J. *Organometallics* **1993**, *12*, 3216-3224.
21. Wehmschulte, R. J.; Power, P. P. *Polyhedron* **1999**, *18*, 1885-1888.
22. a) Brintzinger, H. H. *J. Am. Chem. Soc.* **1967**, *89*, 6871-6876. b) Lukens, W. W.; Matsunaga, P. T.; Andersen, R. A. *Organometallics* **1998**, *17*, 5240-5247. c) Henrici-Olive, G.; Olive, S. *J. Organomet. Chem.* **1970**, *23*, 155-157).
23. a) Lappert, M. F.; Pickett, C. J.; Riley, P. I.; Yarrow, P. I. *J. Chem. Soc., Dalton Trans.* **1981**, 805-813. b) Lappert, M. F.; Raston, C. L.; Skelton, B. W.; White, A. H. *J. Chem. Soc., Dalton Trans.* **1997**, 2895-2902.
24. Herrmann, W. A.; Rohrmann, J.; Herdtweck, E.; Spaleck, W.; Winter, A. *Angew. Chem. Int. Ed. Engl.* **1989**, *28*, 1511-1512.
25. Pool, J. A.; Chirik, P. J. *Can. J. Chem.* **2005**, *83*, 286-295.
26. Hitchcock, P. B.; Lappert, M. F.; Lawless, G. A.; Olivier, H.; Ryan, E. J. *J. Chem. Soc., Chem Comm.* **1992**, 474-476.
27. Gambarotta, S.; Chiang, M. Y. *Organometallics* **1987**, *6*, 897-899.
28. Lauher, J. W.; Hoffmann, R. *J. Am. Chem. Soc.* **1976**, *98*, 1729-1742.
29. McMahon, C. N.; Francis, J. A.; Barron, A. R. *J. Chem. Cryst.* **1997**, *27*, 191-194.
30. Lalama, M. S.; Kampf, J.; Dick, D. G.; Oliver, J. P. *Organometallics*, **1995**, *14*, 495-501.
31. Asadi, A.; Avent, A. G.; Coles, M. P.; Eaborn, C.; Hitchcock, P. B.; Smith, J. D. *J. Organomet. Chem.* **2004**, *689*, 1238-1248.

32. Chakraborty, D.; Chen, E. Y.-X. *Inorg. Chem. Commun.* **2002**, *5*, 698-701.
33. Dioumaev, V. K.; Harrod, J. F. *Organometallics* **1997**, *16*, 2798-2807.
34. Urazowski, I.F.; Ponomaryev, V. I.; Nifant'ev, I. E.; Lemenovski, D. A. *J. Organomet. Chem.* **1989**, *368*, 287-294.
35. Stoll, S.; Schweiger, A. *J. Magn. Reson.* **2006**, *178*, 42-55.

## Chapter 4

Hydroalumination versus Polymerization in Zirconocene Systems

Containing Aluminum Hydrides

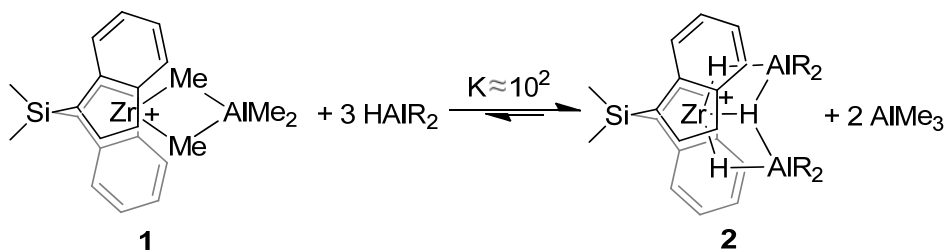
## Chapter 4

**Abstract.** The addition of  $\text{HAl}^i\text{Bu}_2$  to precatalyst  $[(\text{SBI})\text{Zr}(\mu\text{-H})_3(\text{Al}^i\text{Bu}_2)_2]^+$  significantly slows the polymerization of propylene and changes the kinetics of polymerization from 1<sup>st</sup> to 2<sup>nd</sup> order with respect to propylene. This is likely due to competitive inhibition by  $\text{HAl}^i\text{Bu}_2$ . When the same reaction is investigated using  $[(^n\text{BuCp})_2\text{Zr}(\mu\text{-H})_3(\text{Al}^i\text{Bu}_2)_2]^+$ , propylene is added across the Al–H bond of  $\text{HAl}^i\text{Bu}_2$  via hydroalumination instead of the expected polymerization reaction. A survey of cationic trihydride zirconocene complexes with several other ligand frameworks suggests that the change in reactivity correlates with ligand structure and a mechanistic proposal for the observed reactivity is described.

## Introduction

Propylene polymerization by zirconocene-based catalysts is carried out on industrial scales due to their high activity and ability to control polymer tacticity with up to 99% accuracy.<sup>1</sup> Although the most common activator for these catalyst systems is methylaluminoxane (MAO), aluminum alkyl additives such as diisobutylaluminum hydride or triisobutylaluminum (which exists in solution in equilibrium with diisobutylaluminum hydride through  $\beta$ -hydride elimination of isobutene)<sup>2</sup> are frequently added to increase overall activity.<sup>3</sup> Previously it was shown that zirconocene precatalyst, (SBI)ZrCl<sub>2</sub> (SBI = *rac*-dimethylsilylbis(1-indenyl)), activated with a mixture of MAO and HAl<sup>*i*</sup>Bu<sub>2</sub>, displays <sup>1</sup>H NMR resonances associated with zirconium hydrides in addition to the well-established cation zirconium alkyl species [(SBI)Zr( $\mu$ -Me)<sub>2</sub>AlR<sub>2</sub>]<sup>+</sup> (**1**).<sup>4</sup>

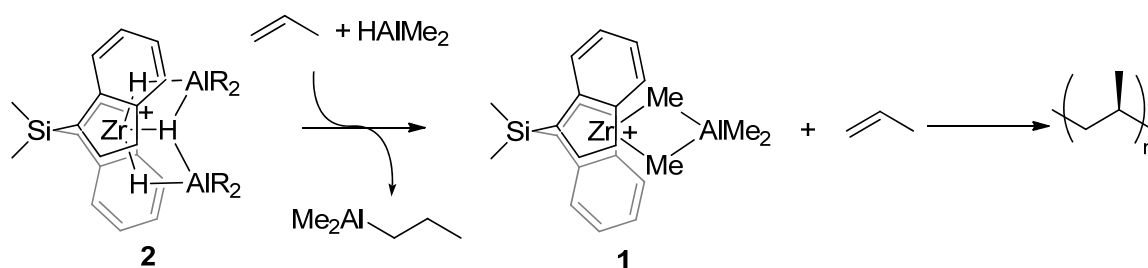
Our group has identified the structure of this zirconium hydride as [(SBI)Zr( $\mu$ -H)<sub>3</sub>(Al<sup>*i*</sup>Bu<sub>2</sub>)<sub>2</sub>]<sup>+</sup> (**2**) and shown it exists in equilibrium with the heterobinuclear cation **1** under catalytic conditions (Scheme 4.1).



**Scheme 4.1**

Compound **2** is an active polymerization precatalyst when synthesized as its B(C<sub>6</sub>F<sub>5</sub>)<sub>4</sub><sup>-</sup> salt, by reaction of (SBI)ZrCl<sub>2</sub> with 1 equiv of trityl tetrakis(pentafluorophenyl)borate ([Ph<sub>3</sub>C][B(C<sub>6</sub>F<sub>5</sub>)<sub>4</sub>]) in the presence of 5-20 equiv of HAl<sup>*i*</sup>Bu<sub>2</sub>.<sup>5</sup> Similarly, [(SBI)Zr( $\mu$ -Me)<sub>2</sub>AlR<sub>2</sub>]<sup>+</sup> (**1**, which is synthesized by reaction of

(SBI)ZrMe<sub>2</sub> with [Ph<sub>3</sub>C][B(C<sub>6</sub>F<sub>5</sub>)<sub>4</sub>] in the presence of AlMe<sub>3</sub>) is a highly active precatalyst for polymerization.<sup>4</sup> When MAO/HAl<sup>*i*</sup>Bu<sub>2</sub> activation conditions are simulated by combining solutions of **1** and **2**, however, comproportionation between HAl<sup>*i*</sup>Bu<sub>2</sub> and AlMe<sub>3</sub> leads to HAlR<sub>2</sub> (R = <sup>*i*</sup>Bu, Me).<sup>5</sup> This undergoes hydroalumination with propylene until all hydride equivalents have been consumed, at which point polymerization ensues (Scheme 4.2). Simultaneous conversion of **2** to **1** suggests that **2** catalyzes hydroalumination of propene during the course of this transformation.



**Scheme 4.2**

Hydroalumination, the addition of Al–H across double or triple bonds of unsaturated organic compounds, generates highly reactive alkyl and vinyl aluminum intermediates which are used synthetically to form alcohols, alkyl acetates, or halogenated compounds with anti-Markovnikov regioselectivity.<sup>6</sup> Neutral zirconocene complexes have been observed to catalyze the hydroalumination of alkenes and alkynes with high yields under mild conditions although the exact mechanism is still debated.<sup>7</sup> On the other hand, cationic *ansa*-zirconocenes such as [(EBI)Zr(μ-Me)<sub>2</sub>AlR<sub>2</sub>]<sup>+</sup> (EBI = *rac*-ethylenebis(1-indenyl)) have been observed to catalyze a closely related process, carboalumination, of propylene in the presence of AlMe<sub>3</sub>.<sup>8</sup>

With these observations in mind, we have investigated the mechanistic features of polymerization by **2** with and without excess  $\text{HAl}^i\text{Bu}_2$ . Additionally, cationic trihydride complexes synthesized with a variety of metallocene ligands were investigated under the same conditions. These results provide insight into the preference for hydroalumination of propylene in the presence of **2** and  $\text{HAlMe}_2$ .

## Results and Discussion

### *Kinetics of Propylene Polymerization by 2*

In previous studies  $[(\text{SBI})\text{Zr}(\mu\text{-H})_3(\text{Al}^i\text{Bu}_2)_2]^+$  (**2**) was generated *in situ*, by reacting  $(\text{SBI})\text{ZrCl}_2$  with  $[\text{Ph}_3\text{C}][\text{B}(\text{C}_6\text{F}_5)_4]$  in the presence of excess  $\text{HAl}^i\text{Bu}_2$ , and used without further purification.<sup>5,9,10</sup> To investigate the kinetic parameters of propylene polymerization by **2**, the compound was isolated as a solid by removing excess  $\text{HAl}^i\text{Bu}_2$  (Figure 4.1).

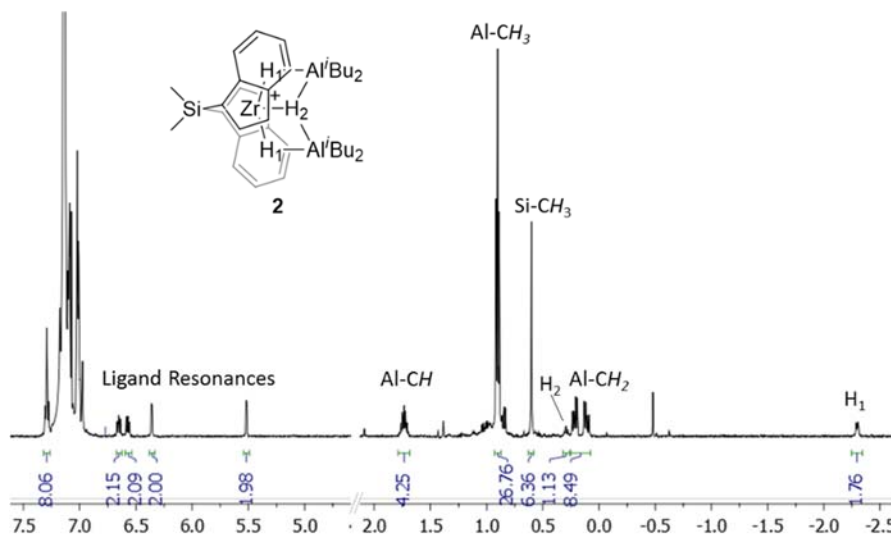


**Figure 4.1.**  $^1\text{H}$  NMR spectra (500 MHz, 25 °C) of a  $\text{C}_6\text{D}_6$  solution of  $[(\text{SBI})\text{Zr}(\mu\text{-H})_3(\text{Al}^i\text{Bu}_2)_2]^+$  (**2**), after removal of excess  $\text{HAl}^i\text{Bu}_2$ . An impurity remains at -0.5 ppm.

The rate of propylene polymerization was measured by  $^1\text{H}$  NMR under pseudo first order conditions by condensing 80 equivalents of propylene into a Teflon-sealed NMR tube containing a frozen solution of **2**. The sample was briefly thawed in a dry ice/acetone bath ( $-78\text{ }^\circ\text{C}$ ) and inserted into an NMR probe pre-cooled to  $-50\text{ }^\circ\text{C}$ .  $^1\text{H}$  NMR spectra were recorded every 5 minutes and the rate of propylene consumption was monitored as an estimate for the overall rate of polymerization. Integrating the  $^1\text{H}$  NMR signals of propylene shows first order consumption of propylene (Figure 4.2).  $^1\text{H}$  NMR signals of **2** remain constant through the reaction.

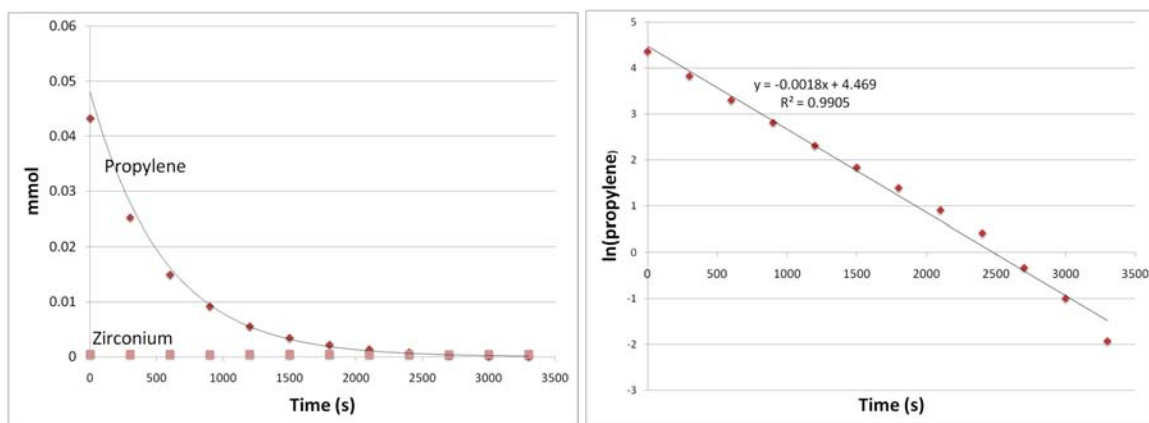


**Figure 4.2.** First order exponential fit to the disappearance of propylene during polymerization in the presence of  $[(\text{SBI})\text{Zr}(\mu\text{-H})_3(\text{Al}^i\text{Bu}_2)_2]^+$  (**2**) at  $-50\text{ }^\circ\text{C}$  in  $d_8$ -toluene (right). The same data plotted as the natural log of propylene the vs. time (left).

If, on the other hand, the same reaction is run in the presence of  $\text{HAl}^i\text{Bu}_2$ , the rate of polymerization slows considerably and we observe a second order dependence on propylene (Figure 4.3).  $^1\text{H}$  NMR signals of both  $\text{HAl}^i\text{Bu}_2$  and  $[(\text{SBI})\text{Zr}(\mu\text{-H})_3(\text{Al}^i\text{Bu}_2)_2]^+$  (**2**) remain constant throughout the reaction.

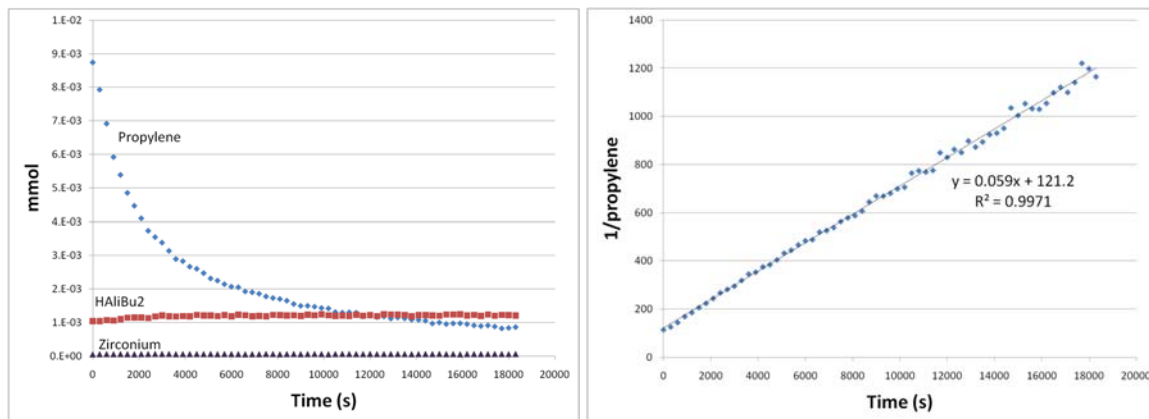


**Figure 4.3.** Disappearance of propylene during polymerization in the presence of  $[(\text{SBI})\text{Zr}(\mu\text{-H})_3(\text{Al}^i\text{Bu}_2)_2]^+$  (**2**) and 10 equiv HAl<sup>i</sup>Bu<sub>2</sub> at -50 °C in d<sub>8</sub>-toluene (right). The same data plotted as the reciprocal of propylene vs. time (left).

The change in order of propylene upon addition of HAl<sup>i</sup>Bu<sub>2</sub> was surprising as polymerization reactions generally display first order dependence on both catalyst and monomer; however, deviations from this have been observed.<sup>11</sup> We anticipated that competitive binding by HAl<sup>i</sup>Bu<sub>2</sub> was responsible for the slower rate of polymerization and possibly the change in order of propylene consumption. To further study the effect of HAl<sup>i</sup>Bu<sub>2</sub> on reaction kinetics, several reactions were performed with aluminum hydride at several concentrations (5 and 10 equivalents relative to **2**).

Qualitatively, increasing the concentration of HAl<sup>i</sup>Bu<sub>2</sub> clearly inhibits the rate of polymerization. Unfortunately, rates varied between runs and it was not possible to obtain statistically significant rate data on the order of HAl<sup>i</sup>Bu<sub>2</sub> in the reaction (Figure 4.4).

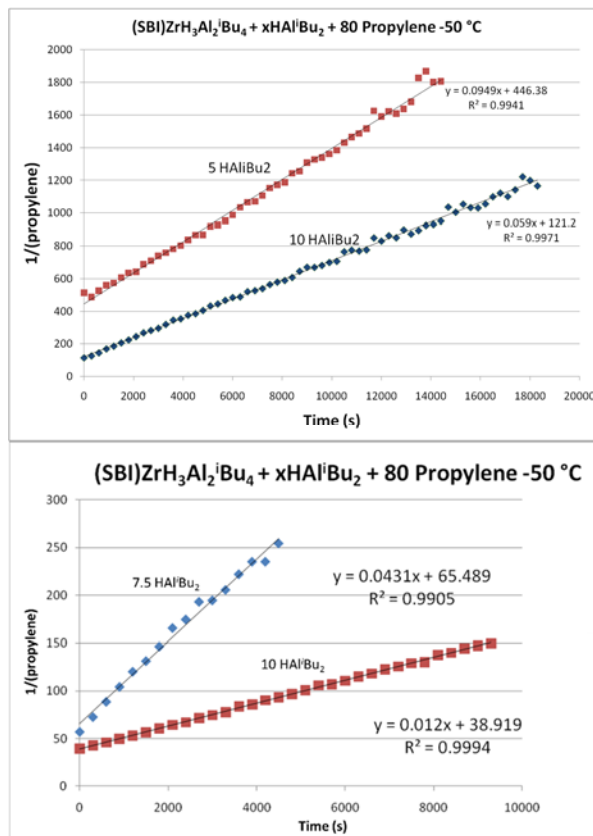
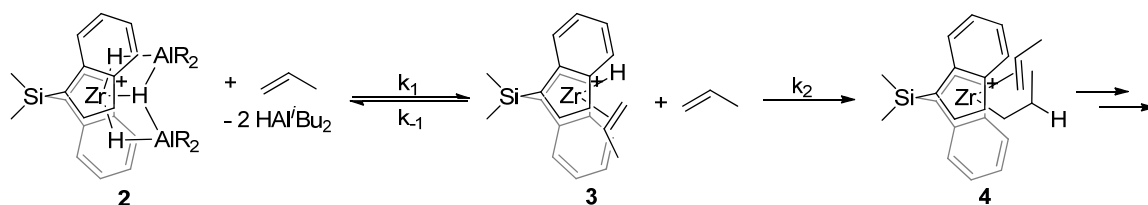


**Figure 4.4.** Top: The disappearance of propylene during polymerization (plotted as the natural log vs. time) in the presence of [(SBI)Zr( $\mu$ -H)<sub>3</sub>(Al<sup>i</sup>Bu<sub>2</sub>)<sub>2</sub>]<sup>+</sup> (**2**) and 5 or 10 equiv HAl<sup>i</sup>Bu<sub>2</sub> at -50 °C in d<sub>8</sub>-toluene. Bottom: The same reaction performed with a separately prepared sample of **2** and 7.5 equiv HAl<sup>i</sup>Bu<sub>2</sub>.

The rate inconsistencies could be a result of variable amounts of non-reactive Zr(III) species in solution which are introduced during the synthesis of [(SBI)Zr( $\mu$ -H)<sub>3</sub>(Al<sup>i</sup>Bu<sub>2</sub>)<sub>2</sub>]<sup>+</sup> (**2**).<sup>10</sup> To control for the relative concentrations of Zr(IV):Zr(III) in solution, larger quantities of **2** were synthesized at once and frozen until use but this did not improve the reliability in reaction rates. A more likely problem arises from the fact that zirconocene catalysts generally display much lower rates of initiation than propagation.<sup>12</sup> This results in a small but variable fraction of zirconium centers responsible for the polymerization

activity observed during each run.<sup>5</sup> Although the overall order in propylene is consistent during individual reactions, quantifying the effect of  $\text{HAl}^i\text{Bu}_2$ , which necessitates comparing rates across multiple reactions, is not currently possible.

Although we were not able to fully quantify the kinetic parameters of this reaction, the following model is consistent with the data above and offers a possible explanation for the observed reactivity (Scheme 4.3).



**Scheme 4.3**

If  $\text{HAl}^i\text{Bu}_2$  must dissociate from **2** before the first equivalent of propylene can bind, compound **3** might exist as a steady-state intermediate leading to the following rate law (Eqs. 4.1 to 4.3). Two equiv of  $\text{HAl}^i\text{Bu}_2$  are assumed to dissociate in Scheme 4.3, however, propylene coordination might occur after dissociation of only one  $\text{HAl}^i\text{Bu}_2$ .

$$\text{rate} = d[\mathbf{4}]/dt = k_2[\mathbf{4}][\text{prop}] \quad (4.1)$$

$$\text{s.s. treatment of } [\mathbf{3}]: \quad [\mathbf{3}] = \frac{k_1[\mathbf{2}][\text{prop}]}{k_{-1}[\text{Al}] + k_2[\text{prop}]} \quad (4.2)$$

$$\text{overall rate:} \quad \text{rate} = \frac{k_1 k_2 [\mathbf{2}] [\text{prop}]^2}{k_{-1}[\text{Al}] + k_2[\text{prop}]} \quad (4.3)$$

When no  $\text{HAl}^i\text{Bu}_2$  is added to the reaction, the concentration of Al is negligible and this rate law simplifies to the expected first order dependence on propylene (eq. 4.4).

$$\text{rate} = k_1[\mathbf{2}][\text{prop}] \quad (4.4)$$

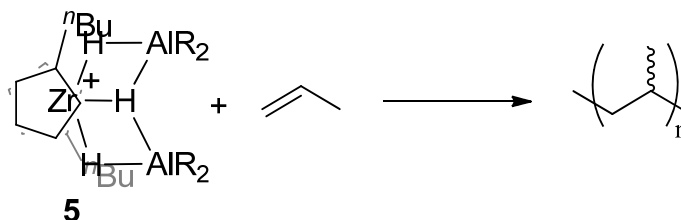
On the other hand, excess  $\text{HAl}^i\text{Bu}_2$  could result in a second order dependence on propylene if the second term of the denominator is negligible (eq. 4.5).

$$\text{rate} = \frac{k_1 k_2 [\mathbf{2}] [\text{prop}]^2}{k_{-1} [\text{Al}]} \quad (4.5)$$

In order for these conditions to hold true in the presence of 10 equiv  $\text{HAl}^i\text{Bu}_2$  and 80 equiv propylene, initial insertion of propylene into a zirconium-hydride bond ( $k_2$ ) must be much slower than coordination of  $\text{HAl}^i\text{Bu}_2$  to **3** ( $k_{-1}$ ). This is consistent with work from Landis and Abu-Omar which suggests that the first insertion of propylene is up to 2 orders of magnitude slower than related steps of polymerization.<sup>12</sup>

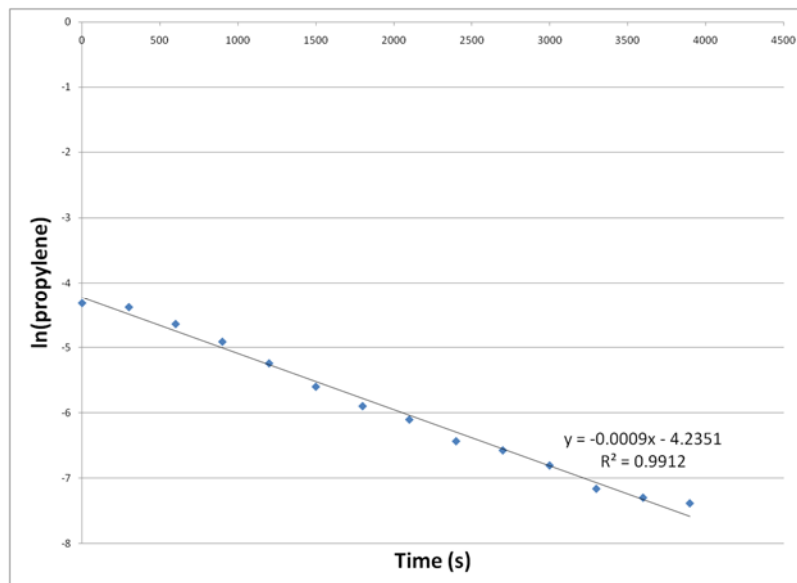
*Reactivity of  $[(^n\text{BuCp})_2\text{Zr}(\mu\text{-H})_3(\text{Al}^i\text{Bu}_2)_2]^+$  (**5**)*

Trihydride  $[(^n\text{BuCp})_2\text{Zr}(\mu\text{-H})_3(\text{Al}^i\text{Bu}_2)_2][\text{Ph}_3\text{C}][\text{B}(\text{C}_6\text{F}_5)_4]$  (**5**), synthesized and isolated in the same manner as (**2**), is also a competent precatalyst for propylene polymerization although the rate of reaction is too slow to monitor below 25 °C (Scheme 4.4).



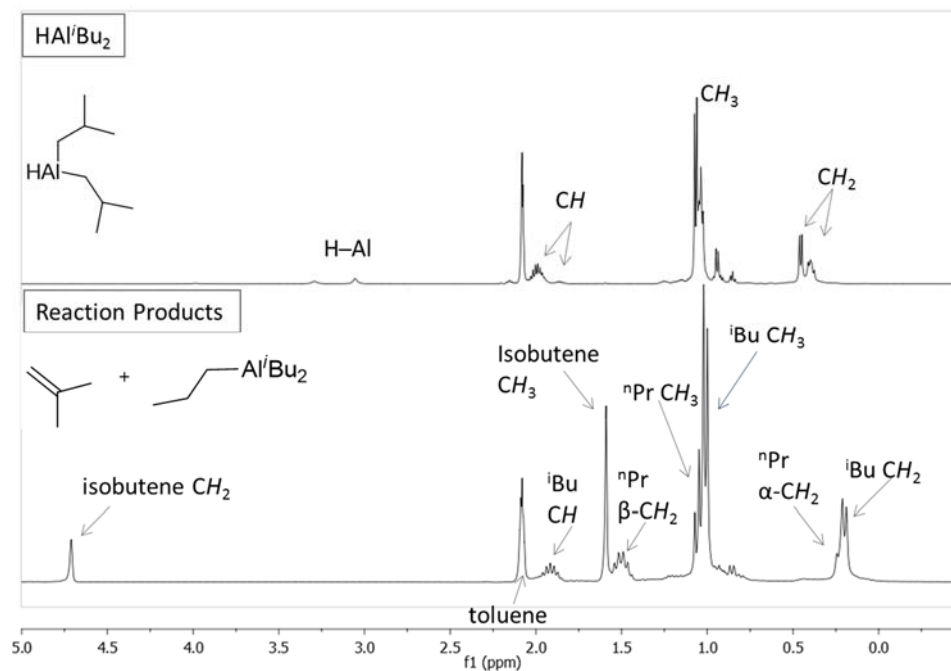
**Scheme 4.4**

Again, first order dependence on propylene is observed by monitoring the disappearance of its  $^1\text{H}$  NMR signals (Figure 4.5).



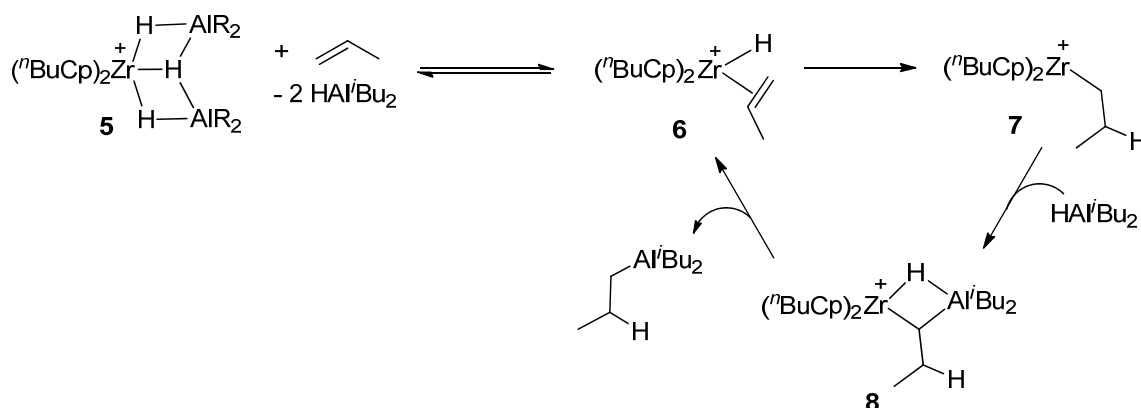
**Figure 4.5.** The disappearance of propylene during polymerization in the presence of  $[(^n\text{BuCp})_2\text{Zr}(\mu\text{-H})_3(\text{Al}^i\text{Bu}_2)_2]^+$  (**5**) at 25 °C in  $d_8$ -toluene plotted as the natural log of propylene vs. time.

Whereas adding  $\text{HAl}^i\text{Bu}_2$  to a solution of **2** changes the dependence on propylene from first to second order, addition of 10 equivalents  $\text{HAl}^i\text{Bu}_2$  to **5** changes the overall reactivity of the system. In this case, the disappearance of propylene is not associated with the formation of polypropylene, but instead the propylene is inserted into the Al–H bond of  $\text{HAl}^i\text{Bu}_2$  via hydroalumination to form  $\text{Al}(^n\text{Pr})_x(^i\text{Bu})_{2-x}$  as well as isobutene (Figure 4.6). The overall rate of this reaction is about three times slower than the comparable polymerization with **5** (Scheme 4.4).

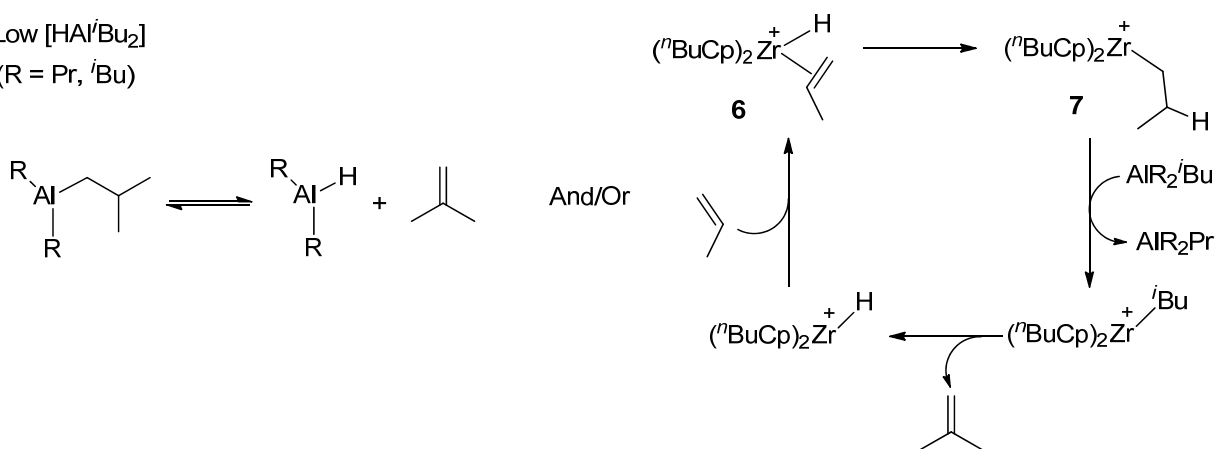


**Figure 4.6.**  $^1\text{H}$  NMR spectra of  $\text{HAl}^i\text{Bu}_2$  in  $d_8$ -toluene which exists as a mixture of monomer and dimer (top); and the solution obtained after reaction of **5** with propylene in the presence of 10  $\text{HAl}^i\text{Bu}_2$  in  $d_8$ -toluene (bottom).

In analogy to Scheme 4.3, hydroalumination most likely proceeds through dissociation of  $\text{HAl}^i\text{Bu}_2$  from the cationic trihydride (**5**), followed by propylene insertion into the  $\text{Zr-H}$  bond of **6** (Scheme 4.5). If the insertion product (**7**) is trapped by  $\text{HAl}^i\text{Bu}_2$ , the resulting complex (**8**) would be ideally suited for alkyl transfer to aluminum, a process that is rapid and facile between zirconium and aluminum centers (Scheme 4.5).<sup>13</sup> After the initial hydride has been consumed, more equivalents are likely generated through  $\beta$ -hydride elimination from  $\text{Al}^i\text{Bu}$  or  $\text{Zr}^i\text{Bu}$  with concomitant isobutene formation (Scheme 4.6).<sup>2</sup>

High  $[\text{HAl}^i\text{Bu}_2]$ 

Scheme 4.5

Low  $[\text{HAl}^i\text{Bu}_2]$   
(R = Pr,  $^i\text{Bu}$ )

Scheme 4.6

### Reactivity of Other Zirconocene Trihydrides

A survey of cationic trihydride zirconocene complexes with several other ligand frameworks suggests that reactivity correlates with ligand structure. *Ansa*-zirconocenes such as  $[(\text{SBI})\text{Zr}(\mu\text{-H})_3(\text{Al}^i\text{Bu}_2)_2]^+$  (**2**) and  $[(\text{EBI})\text{Zr}(\mu\text{-H})_3(\text{Al}^i\text{Bu}_2)_2]^+$  are capable of polymerizing propylene even in the presence of  $\text{HAl}^i\text{Bu}_2$  whereas mono- and di-substituted Cp rings react via hydroalumination (Table 4.1).

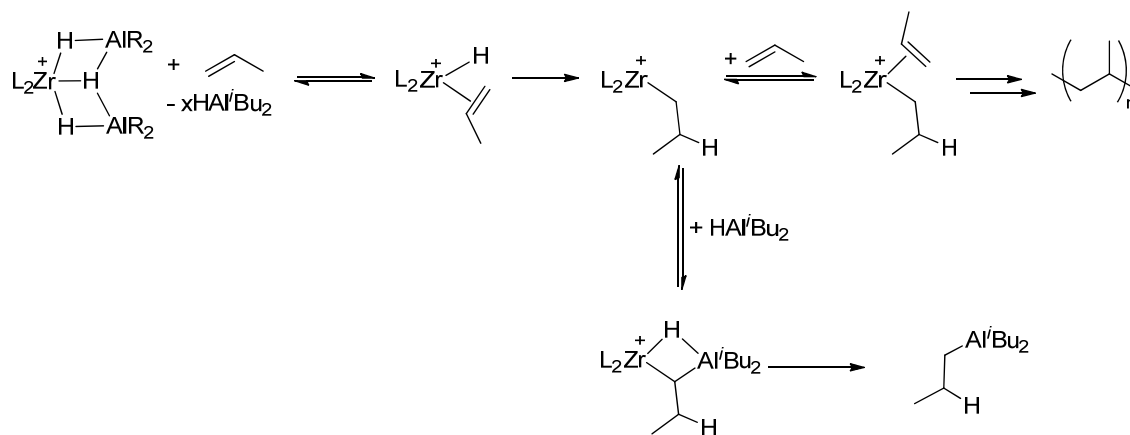
Compound #	Ligand	Reactivity	Reduction Potential <sup>a</sup>
<b>2</b>	(SBI) <sup>14</sup>	Polymer	≈102
<b>9</b>	(EBI) <sup>15</sup>	Polymer	91
<b>5</b>	<sup>n</sup> BuCp <sup>16</sup>	Hydroalumination	≈-50
<b>10</b>	Cp <sup>16</sup>	Hydroalumination	0
<b>11</b>	<sup>1,2</sup> Me <sub>2</sub> Cp <sup>17</sup>	Hydroalumination	-105
<b>12</b>	<sup>t</sup> BuCp <sup>16</sup>	Hydroalumination	-14
<b>13</b>	<sup>TMS</sup> Cp <sup>18</sup>	Hydroalumination	84

**Table 4.1.** Metallocene ligands used to form cationic trihydride complexes  $[\text{L}_2\text{Zr}(\mu\text{-H})_3(\text{Al}^i\text{Bu}_2)_2]^+$  ( $\text{L} = \text{Cp}, 1,2\text{-Me}_2\text{Cp}, {}^n\text{BuCp}, {}^t\text{BuCp}, \text{TMS Cp}$ ) from  $\text{L}_2\text{ZrCl}_2$  or  $[\text{LZr}(\mu\text{-H})_3(\text{Al}^i\text{Bu}_2)_2]^+$  ( $\text{L} = \text{EBI}, \text{SBI}$ ) from  $\text{LZrCl}_2$  and the reactivity observed upon addition of excess propylene in the presence of 10 equiv  $\text{HAL}^i\text{Bu}_2$ . <sup>a</sup>One electron reduction potential relative to  $\text{Cp}_2\text{ZrCl}_2$  (from reference 12).

The overall electronic environment at the metal center does not seem to correlate with the change in reactivity between polymerization and hydroalumination, leading us to believe this change is likely due to the overall steric profile of the ligand.<sup>19</sup> Whether this results from the linked cyclopentadienyl rings of *ansa*-zirconocenes or another aspect of the ring substituents remains unclear. Following this hypothesis, hydroalumination of propylene by  $[(\text{SBI})\text{Zr}(\mu\text{-H})_3(\text{Al}^i\text{Bu}_2)_2]^+$  (**2**) and  $\text{HAlMe}_2$ , which does not catalyze hydroalumination of propylene alone or in the presence of  $\text{HAL}^i\text{Bu}_2$ , likely results from the lower steric profile of  $\text{HAlMe}_2$  as compared to  $\text{HAL}^i\text{Bu}_2$  (Scheme 4.1).<sup>5</sup>

Surprisingly, no peaks associated with polypropylene are observed in any of the hydroalumination reactions (Figure 4.6; **5**, **10-13** Table 4.1) and no hydroalumination products  $\text{Al}({}^n\text{Pr})_x({}^i\text{Bu})_{2-x}$  are observed during polymerization reactions (Scheme 4.3),

although it is possible that  $^1\text{H}$  NMR signals from these peaks are obscured by the broad polypropylene peaks. Additionally, although aluminum species are well known chain transfer reagents, previous batch polymerizations with  $[(\text{SBI})\text{Zr}(\mu\text{-H})_3(\text{Al}^i\text{Bu}_2)_2]^+$  (**2**) in the presence of 20 equiv  $\text{HAl}^i\text{Bu}_2$  display  $M_w$  and  $M_n$  data typical for MAO catalyzed reactions. It appears, therefore that  $\text{HAl}^i\text{Bu}_2$  is not increasing the number of chain transfer events after a growing polymer chain is formed.<sup>5,20</sup> Thus, a branch point seems to exist only after initial  $\text{HAl}^i\text{Bu}_2$  dissociation, propylene coordination, and insertion (Scheme 4.7). Depending on the ligand environment, the relative rate of dialkyl aluminum hydride coordination and hydroalumination outcompetes coordination of a second equivalent of propylene. If on the other hand, this coordination is unfavored, polypropylene formation is observed.



**Scheme 4.7**

## Conclusions

The observation that cationic trihydrides, such as  $[(\text{SBI})\text{Zr}(\mu\text{-H})_3(\text{Al}^i\text{Bu}_2)_2]^+$  (**2**), exist under some polymerization conditions and are themselves polymerization precatalysts, was an important contribution to our overall knowledge of these reaction systems. Unfortunately, the presence of aluminum hydrides has unintended consequences, both in promoting the formation of Zr(III) species in solution and in competitive binding to species along the polymerization pathway. Depending on the metallocene ligand, this coordination either slows down the rate of initiation and polymerization (Figure 4.3) or promotes different reactivity entirely (Figure 4.6). Any activity gain from zirconocene systems activated with MAO and  $\text{Al}^i\text{Bu}_3$  or  $\text{HAl}^i\text{Bu}_2$  must therefore be weighed against the potential for Zr(III) and hydroalumination products to be introduced into the system.

## Experimental

**General Considerations.** All operations were carried out under a protective dinitrogen atmosphere, either in a glovebox or on a vacuum manifold. Solvents (benzene, toluene, benzene- $d_6$ , toluene- $d_8$ ) were degassed and dried over 3-Å molecular sieves for 12 hours or filtered through a plug of activated alumina. All other solvents for air- and moisture-sensitive reactions were dried over sodium benzophenone ketyl and stored over titanocene where compatible or dried by the method of Grubbs et al.<sup>21</sup> (SBI)ZrCl<sub>2</sub> was purchased from Strem Chemicals and rinsed with benzene before use or synthesized as described below. (SBI)ZrMe<sub>2</sub> was obtained from Dr. M. Ringwald, MCAT, Konstanz. All other zirconocene complexes used as starting materials were either purchased from Strem Chemicals, or prepared in our laboratories according to published procedures (see Table 4.1 of the text). Trimethylaluminum and diisobutylaluminum hydride, were used as obtained from Aldrich Chemical Co., Milwaukee. Dimethylaluminum hydride was synthesized as previously reported.<sup>11</sup> Stock solutions of diisobutylaluminum hydride were made at two concentrations (280 mM and 28 mM) in toluene and benzene- $d_6$ . <sup>1</sup>H and <sup>13</sup>C NMR spectra were recorded on Varian Mercury 300, Varian Inova-500 or Varian Inova-600 spectrometers. Chemical shifts are reported with respect to internal solvent: 7.16 ppm (C<sub>6</sub>D<sub>6</sub>) and 2.08 (*d*<sub>8</sub>-tol) for <sup>1</sup>H data.

**Synthesis of (SBI)ZrCl<sub>2</sub>.** This complex was synthesized according to the procedures outlined in ref. 14 with the following modifications: Lithium-indenyl (6.9 g, 0.057 mol) was added to a round bottom flask and fitted with a Teflon sealed 180° adapter. The flask was evacuated on the high vacuum line and Et<sub>2</sub>O was vacuum transferred into the flask at -78 °C. Dimethyldichlorosilane (3.86 mL, 0.32 mol) was quantitatively vacuum

transferred into the flask using a graduated cylinder with a ground glass adapter on the high vacuum line. The reaction was allowed to warm to room temperature to stir overnight. The reaction was quenched with H<sub>2</sub>O, the product was extracted with Et<sub>2</sub>O and dried under vacuum to give the desired ligand (SBI)H<sub>2</sub>. <sup>1</sup>H NMR (300 MHz, C<sub>6</sub>D<sub>6</sub>) δ 7.56 (m, 4H), 6.96 (m, 2H), 6.87 (dd, 2H), 6.71 (m, 2H), 6.22 (d, 2H), 2.49 (s, 12H), 0.81 (s, 6H).

The ligand (5 g, 0.2 mol) was transferred into the glove box in a Schlenk flask and Zr(NMe<sub>2</sub>)<sub>4</sub> (4.6 g, 0.2 mol) was added as a solid. The two solids were dissolved in hexanes, and flask was removed from the box. The flask was fitted with a reflux condenser and the solution was refluxed under an argon purge for 8 hours. Hexanes were removed under vacuum, and the solid was returned to the glove box where it was dissolved in minimal pentane. Crystals of *rac*-(SBI)Zr(NMe<sub>2</sub>)<sub>2</sub> were collected over several batches and treated with excess trimethylsilyl chloride to form (SBI)ZrCl<sub>2</sub>. <sup>1</sup>H NMR (300 MHz, C<sub>6</sub>D<sub>6</sub>) δ 7.40 (m, 3H), 7.23 (m, 2H), 6.86 (m, 3H), 6.81 (dd, 2H), 5.76 (d, 2H), 0.54 (s, 6H).

**Synthesis of [(SBI)Zr(μ-H)<sub>3</sub>(Al<sup>*i*</sup>Bu<sub>2</sub>)<sub>2</sub>][Ph<sub>3</sub>C][B(C<sub>6</sub>F<sub>5</sub>)<sub>4</sub>] (2).** To a 50 mL round bottom, (SBI)ZrCl<sub>2</sub> (132 mg, 0.29 mmol) and [Ph<sub>3</sub>C][B(C<sub>6</sub>F<sub>5</sub>)<sub>4</sub>] (268 mg, 0.29 mmol) were added as solids. Toluene was added (~20 mL) and HAl<sup>*i*</sup>Bu<sub>2</sub> (1.04 mL, 5.8 mmol) was added slowly to the solution while stirring. The flask was fitted with a swivel frit and moved to the high vacuum line where toluene was evaporated to leave a yellow powder ([[(SBI)Zr(μ-H)<sub>3</sub>(Al<sup>*i*</sup>Bu<sub>2</sub>)<sub>2</sub>][Ph<sub>3</sub>C][B(C<sub>6</sub>F<sub>5</sub>)<sub>4</sub>]) mixed with a clear oil (HAl<sup>*i*</sup>Bu<sub>2</sub>). Pentane was vacuum transferred into the flask and the solid was filtered through the swivel frit. The solid was washed twice more with pentane through the swivel frit side arm before drying under vacuum to produce **2** in 60% yield. <sup>1</sup>H NMR (300 MHz, C<sub>6</sub>D<sub>6</sub>) δ 7.42 (s, 2H), 6.89 (s, 2H),

6.64 (m, 4H), 6.38 (d, 2H), 5.54 (d, 2H), 1.75 (m, 4H), 0.93 (dd, 24H), 0.62 (s, 6H), 0.32 (t, 1H), 0.18 (m, 8H), -2.28 (d, 2H).

**Synthesis of [<sup>n</sup>BuCp)<sub>2</sub>Zr(μ-H)<sub>3</sub>(Al<sup>i</sup>Bu<sub>2</sub>)<sub>2</sub>][Ph<sub>3</sub>C][B(C<sub>6</sub>F<sub>5</sub>)<sub>4</sub>]** This compound was synthesized and purified as described above for **2** using (<sup>n</sup>BuCp)<sub>2</sub>ZrCl<sub>2</sub><sup>16</sup> (60.7 mg, 0.15 mmol); [Ph<sub>3</sub>C][B(C<sub>6</sub>F<sub>5</sub>)<sub>4</sub>] (138 mg, 0.15 mmol); HAl<sup>i</sup>Bu<sub>2</sub> (160 μL, 0.9 mmol). The product is a brown waxy solid. <sup>1</sup>H NMR (300 MHz, d<sub>8</sub>-toluene) δ 5.75 (d, 6H), -1.56 (t, 2H), -1.93 (q, 1H), <sup>n</sup>Bu and <sup>i</sup>Bu peaks between δ 2.23 and δ 0.42 are not well resolved.

**Synthesis of Other Cationic Trihydrides.** All remaining cationic trihydrides (**9-13**) were generated as followed and used *in situ* without further purification. To a solution of d<sub>8</sub>-toluene (0.1 mL) was added zirconocene dichloride (0.003 mmol) and 10 equiv HAl<sup>i</sup>Bu<sub>2</sub> (0.1 mL, 28 mM) and [Ph<sub>3</sub>C][B(C<sub>6</sub>F<sub>5</sub>)<sub>4</sub>] (2.6 mg, 0.003 mmol). The reagents were allowed to mix for 3-5 minutes.

**Reactions with Propylene.** Stock solutions containing the appropriate zirconocene and HAl<sup>i</sup>Bu<sub>2</sub> were added to a Teflon-sealed NMR tube to form solutions with a total zirconium concentration of 0.0005 mmol in 0.8 mL d<sub>8</sub>-toluene. The NMR tube was attached to the high vacuum line where the solution was degassed and frozen using liquid nitrogen. Propylene (80 equiv) was condensed onto the top of the frozen solution using a glass bulb with an internal volume of 2.78 mL. The NMR tube was transferred from a dewar containing LN<sub>2</sub> into a dewar containing dry ice/acetone until the solution thawed (~30 seconds) at which point it was transferred into an NMR probe pre-cooled to -50 °C. NMR spectra were recorded every 5 minutes using VnmrJ software with nt=1, d1=1 in order to obtain accurate integration of the <sup>1</sup>H NMR signals of propylene.

**References**

1. a.) Hustad, P. D. *Science* **2009**, *325*, 704-707. b.) Market Study: Polypropylene - 2nd edition overview (UC-4205) Ceresana **2012** Accessed on web Aug 15, 2013 <http://www.ceresana.com/en/market-studies/plastics/polypropylene/>
2. a.) Henderson, M. A.; Trefz, T. K.; Collins, S.; Wang, M. Y.; McIndoe, J. S. *Organometallics*, **2013**, *32*, 2079. b.) Wu, F.-J.; Simeral, L. A.; Mrse, A. A.; Eilertsen, J. L.; Negureanu, L.; Gan, Z.; Fronczek, F. R.; Hall, R. W.; Butler, L. G. *Inorg Chem.* **2007**, *46*, 44. c.) Egger, K. W. *J. Am. Chem. Soc.* **1969**, *91*, 2867.
3. a.) Kleinschmidt, R.; van der Leek, Y.; Reffke, M.; Fink, G. *J. Mol. Catal. A.* **1999**, *148*, 29. b.) Kaminaka, M.; Matsuoka, H. Jpn Patent 11240912, 1999 c.) Wang, S. U. S. Patent 20050070675, 2005 d.) Gregorius, H. Fraaije, V.; Lutringhauser, M. Ger. Patent 10258968 e.) Crapo, C, C.; Malpass, D. B. Eur. Pat. Appl. 372617, 1990.
4. Babushkin, D. E.; Panchenko, V. N.; Timofeeva, M. N.; Zakharov, V. A.; Brintzinger, H. H. *Macromol. Chem. Phys.* **2008**, *209*, 1210.
5. Baldwin, S. M.; Bercaw, J. E.; Brintzinger, H. H. *J. Am. Chem. Soc.* **2010**, *132*, 13969
6. Uhl, W. *Coord. Chem. Rev.* **2008**, *252*, 1540.
7. a.) Negishi, E.; Yoshida, T. *Tet. Lett.* **1980**, *21*, 1501 b.) Makabe, H.; Negishi, E. *Eur. J. Org. Chem.* **1999**, 969 c.) Parfenova, L. V.; Pechatkina, S. V.; Khalilov, L. M.; Dzhemilev, U. M. *Russ. Chem. Bull. Int. Ed.* **2005**, *54*, 316.
8. Shaughnessy, K. H.; Waymouth, R. M. *Organometallics*, **1998**, *17*, 5728.
9. Baldwin, S. M.; Bercaw, J. E.; Henling, L. M.; Day, M. W.; Brinzingler, H. H. *J. Am. Chem. Soc.* **2011**, *133*, 1805.

10. Lenton, T. N.; Bercaw, J. E.; Panchenko, V. N.; Zakharov, V. A.; Babushkin, D. E.; Soshnikov, I. E.; Talsi, E. P.; Brintzinger, H. H. *J. Am. Chem. Soc.* **2013**, *135*, 10710.
11. a.) Schaper, F.; Brintzinger, H.-H.; Kleinschmidt, R.; Leek, Y.; Reffke, M.; Fink, G.,  
b.) Higher-order Kinetics in Propene Polymerizations by Zirconocene Catalysts.  
Analysis of Alternative Reaction Mechanisms via a Genetic Algorithm. In  
*Organometallic Catalysts and Olefin Polymerization*, Blom, R.; Follestad, A.; Rytter, E.; Tilset, M.; Ystenes, M., Eds. Springer Berlin Heidelberg: 2001; pp 46-62.
12. a.) Liu, Z. X.; Somsook, E.; White, C. B.; Rosaaen, K. A.; Landis, C. R. *J. Am. Chem. Soc.* **2001**, *123*, 11193 b.) Novstrup, K. A.; Travia, N. E.; Medvedev, G. A.; Stanciu, C.; Switzer, J. M.; Thomson, K. T.; Delgass, W. N.; Abu-Omar, M. M.; Caruthers, J. *M. J. Am. Chem. Soc.* **2010**, *132*, 558.
13. Beck, S.; Brintzinger, H. H. *Inorg. Chim. Acta.* **1998**, *270*, 376.
14. Christopher, J. H.; Diamond, G. M.; Jordan, R. F. *Organometallics* **1996**, *15*, 4038.
15. Voskoboynikov, A. Z.; Agarkov, A. Yu.; Chernyshev, E. A.; Beletskaya, I. P.; Churakov, A. V.; Kuz'mina, L. G. *J. Organomet. Chem.* **1997**, *530*, 75.
16. Purchased from Strem Chemicals, Newburyport, MA.
17. Deck, P. A.; Beswick, C. L.; Marks, T. J. *J. Am. Chem. Soc.* **1998**, *120*, 1772.
18. Lappert, M. F.; Riley, P. I.; Yarrow, P. I. W.; Atwood, J. L.; Hunter, W. E.; Zaworotko, M. J. *J. Chem. Soc., Dalton Trans.* **1981**, 814.
19. Zachmanoglou, C. E.; Docrat, A.; Bridgewater, B. M.; Parkin, G.; Brandow, C. G.; Bercaw, J. E.; Jardine, C. N.; Lyall, M.; Green, J. C.; Keister, J. B. *J. Am. Chem. Soc.* **2002**, *124*, 9525.

20. a.) Kaminsky, W. *Cat. Today* **1994**, 20, 257. b.) Kleinschmidt, R.; van der Leek, Y.;  
Reffke, M.; Fink, G. *J. Mol. Cat. A* **1999**, 29.

## Appendix A

Synthesis of  $(\text{ONO})\text{ZrMe}_2$  and  $(\text{ONO})\text{ZrNp}_2$ : Towards Stoichiometric  
Activation and Post-Metallocene Insertion Studies

## Appendix A

### Introduction.

The mechanism of propylene polymerization by metallocene catalysts has been well-established as a site-controlled process in which the catalyst symmetry influences the stereochemistry of each insertion and  $\alpha$ -agostic interaction stabilizes the transition state.<sup>1</sup> The observation that  $\text{Cp}_2\text{ZrMeNp}$  (Np = neopentyl) complexes activated with borane undergo  $\beta$ -methyl elimination to form isobutene and  $[\text{Cp}_2\text{ZrMe}][\text{MeB}(\text{C}_6\text{F}_5)_3]$ , the microscopic reverse of olefin insertion, provided evidence for this mechanism.<sup>2</sup> Studies detailing the kinetic isotope effect of isobutene elimination from  $(\text{CpR}_n)_2\text{Zr}(\text{CH}_3)(\text{CH}_2\text{C}(\text{CH}_3)_2\text{CD}_3)$  added further support for  $\gamma$ -agostic assistance in the elimination transition state.<sup>3</sup>

Several new  $(\text{ONO})\text{ZrX}_2$  complexes have been synthesized as first steps towards determining whether  $\beta$ -methyl elimination of isobutene occurs in this class of post-metallocene catalysts. Although it has not yet been possible to synthesize  $(\text{ONO})\text{ZrMeNp}$ , activation studies with  $(\text{ONO})\text{ZrNp}_2$  do not show any isobutene formation.

### Results and Discussion

#### *Synthesis of $(\text{ONO})\text{ZrCl}_2$*

$(\text{ONO})\text{ZrCl}_2$  was targeted as a starting point for the desired alkyl complexes. The complex can only be synthesized in the presence of an L-type donor such as dimethylamine, pyridine, or THF which presumably stabilizes the electron deficient complex. Direct synthesis of the amine adduct is possible from  $(\text{ONO})\text{H}_2$  and  $\text{ZrCl}_2(\text{NMe}_2)_2$  but the reaction proceeds in low yields with  $(\text{ONO})_2\text{Zr}$  observed as the major

product. Nonetheless, X-ray quality crystals were obtained from a solution in toluene cooled to  $-30\text{ }^{\circ}\text{C}$  (Figure A.1).

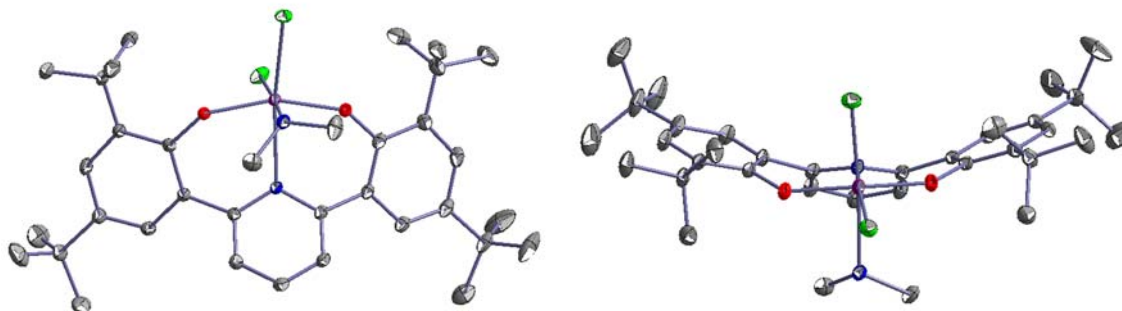


**Figure A.1.** Front (left) and top (right) views of the structure of  $(\text{ONO})\text{ZrCl}_2(\text{HNMe}_2)$  with thermal ellipsoids at the 50% probability level. Hydrogen atoms are omitted for clarity. Selected bond lengths ( $\text{\AA}$ ): Zr–Cl1, 2.4226(1); Zr–Cl2, 2.4540(1); Zr–O1, 1.9469(1); Zr–O2, 1.9702(1); Zr–N(pyridine), 2.3975; Zr–N(amine), 2.3881(1).

A related compound,  $(\text{ONO})\text{ZrCl}_2(\text{THF})$ , can be synthesized in higher yields by reaction of  $(\text{ONO})\text{ZrBn}_2$  and [lutidinium-H][Cl] or  $[\text{H}_2\text{N}^i\text{Pr}_2][\text{Cl}]$  (Figure A.2).

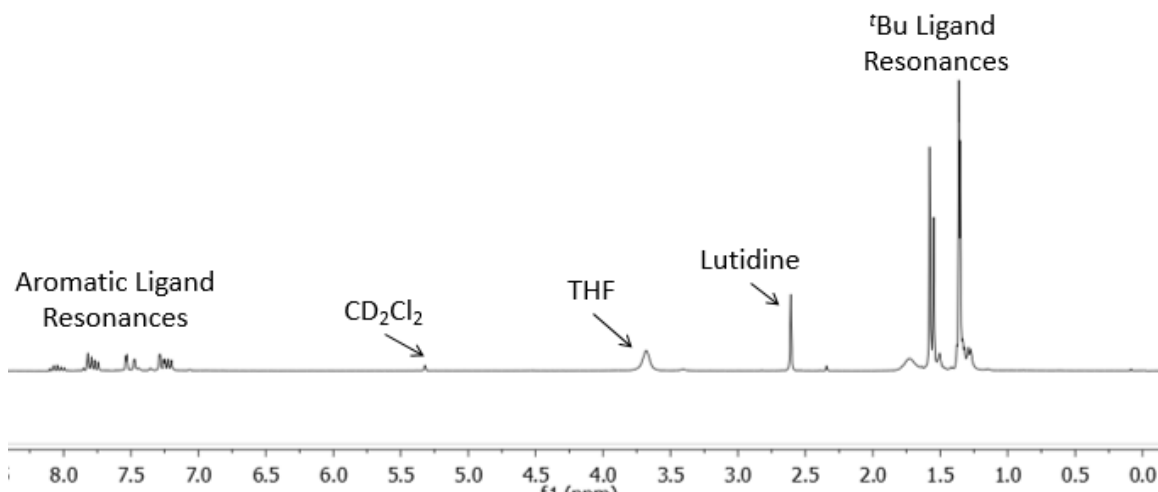


**Figure A.2.**  $^1\text{H}$  NMR spectra of  $(\text{ONO})\text{ZrCl}_2(\text{THF})$  in  $\text{CD}_2\text{Cl}_2$  synthesized from  $(\text{ONO})\text{ZrBn}_2$  and [lutidinium-H][Cl] after the removal of 2 equiv. toluene.

### Synthesis of (ONO)ZrMe<sub>2</sub>

Reaction of (ONO)ZrCl<sub>2</sub>(L) with 2.1 equiv MeMgCl forms the desired bis(methyl) complex (ONO)ZrMe<sub>2</sub> (Figure A.3). Extraction into pentane and filtration through celite removes remaining L-type donors and magnesium salts.

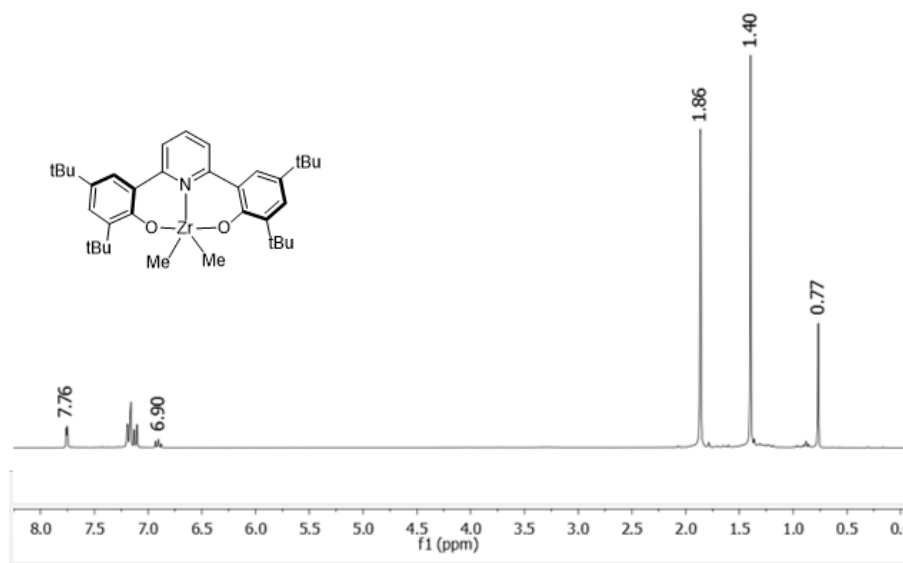


**Figure A.3.** <sup>1</sup>H NMR spectrum of (ONO)ZrMe<sub>2</sub> in C<sub>6</sub>D<sub>6</sub>.

### Synthesis of (ONO)ZrNp<sub>2</sub>

Synthesis of (ONO)ZrNp<sub>2</sub> can be achieved through reaction of (ONO)H<sub>2</sub> with Zr(Np)<sub>4</sub> in toluene or alternatively by addition of Neopentyl Grignard to (ONO)ZrCl<sub>2</sub>(THF) (Figure A.4). The former reaction is lower yielding as it forms substantial amounts of (ONO)<sub>2</sub>Zr in addition to the desired product.

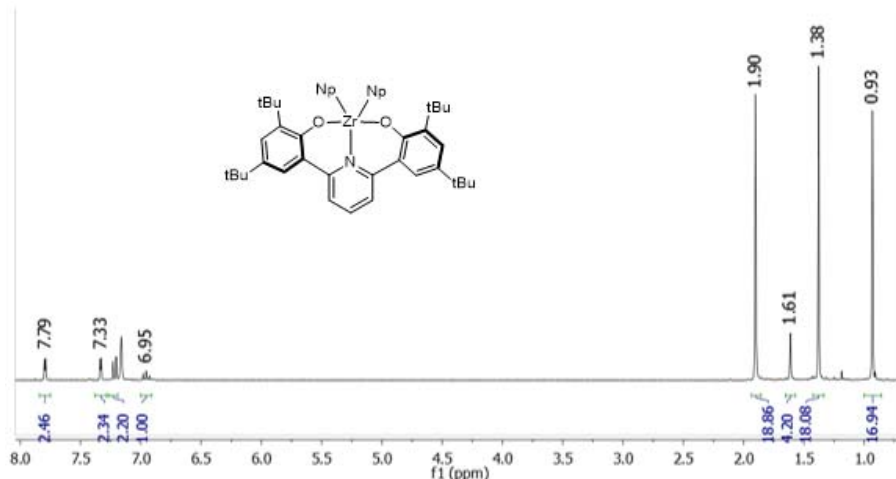


**Figure A.4.**  $^1\text{H}$  NMR spectrum of  $(\text{ONO})\text{ZrNp}_2$  in  $\text{C}_6\text{D}_6$ .

Crystals of  $(\text{ONO})\text{ZrNp}_2$  can be grown from a concentrated solution of toluene at  $-30\text{ }^\circ\text{C}$  but their poor quality prevents anything more than confirmation of the desired complex (Figure A.5).

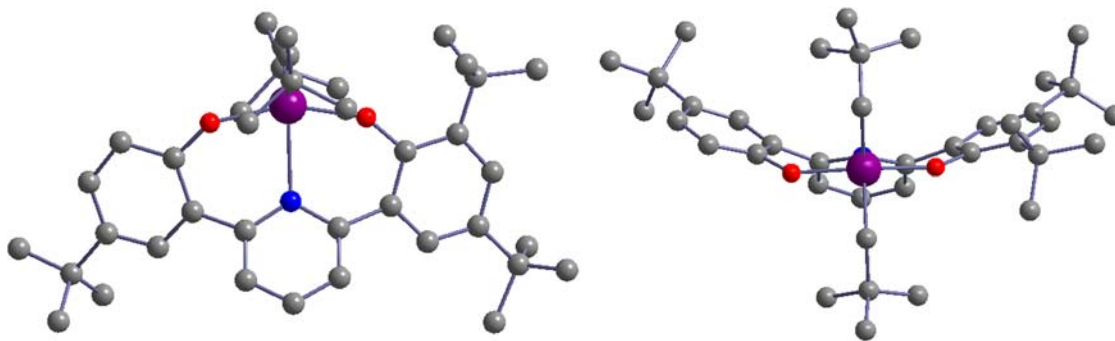
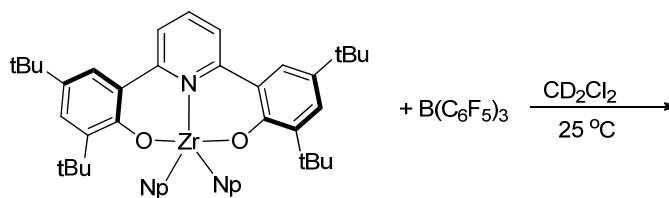


**Figure A.5.** Front (left) and top (right) views of the structure of  $(\text{ONO})\text{ZrNp}_2$ .

#### *Activation of $(\text{ONO})\text{ZrNp}_2$*

When  $(\text{ONO})\text{ZrNp}_2$  is reacted with either  $[\text{Ph}_3\text{C}][\text{B}(\text{C}_6\text{F}_5)_4]$  or  $\text{B}(\text{C}_6\text{F}_5)_3$  (Scheme A.1), new signals slowly appear in  $^1\text{H}$  and  $^{19}\text{F}$  NMR spectra (Figure A.6). Signals for  $(\text{ONO})\text{ZrNp}_2$  remain over 48 hours and the new products have not been successfully identified. Importantly, no isobutene formation is observed during the reaction.



Scheme A.1

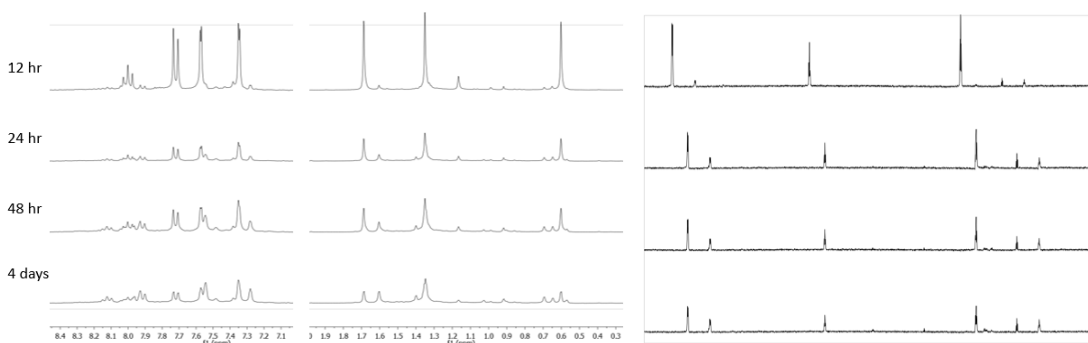


**Figure A.6.** <sup>1</sup>H NMR spectra (right) and <sup>19</sup>F spectra (left) of the reaction described in Scheme A.1.

## Experimental

All air- and moisture-sensitive compounds were manipulated using standard high-vacuum line, Schlenk, or cannula techniques or in a glovebox under a nitrogen atmosphere. ZrNp<sub>4</sub> was prepared according to literature methods.<sup>4</sup> MeMgBr (3M in diethyl ether) and NpMgBr (1M in THF) were purchased from Aldrich. (ONO)H<sub>2</sub> and (ONO)ZrBn<sub>2</sub> were prepared according to literature methods.<sup>5</sup> All other solvents for air- and moisture-sensitive reactions were dried over sodium benzophenone ketyl and stored over titanocene where compatible or dried by the method of Grubbs et al.<sup>21</sup> Benzene-*d*<sub>6</sub> and toluene-*d*<sub>8</sub>, and methylene chloride-*d*<sub>2</sub> were purchased from Cambridge Isotopes, and filtered through a plug of activated alumina. All other materials were used as received. <sup>1</sup>H and <sup>19</sup>F NMR spectra were recorded on Varian Mercury 300, Varian Inova-500 or Varian Inova-600 spectrometers at room temperature unless otherwise indicated. Chemical shifts are reported

with respect to internal solvent: 7.16 and 128.38 (t) ppm ( $C_6D_6$ ); 2.08 and 25 ppm ( $d_8$ -tol); 5.32 and 54 (q) ppm ( $CD_2Cl_2$ ); for  $^1H$  and  $^{13}C$  data respectively.

## References

1. a.) Grubbs, R. H.; Coates, G. W.; *Acc. Chem. Res.* **1996**, *29*, 1412. b.) Piers, W. E.; Bercaw, J. E. *J. Am. Chem. Soc.* **1990**, *112*, 9406. c.) Pino, P.; Cioni, P.; Wei, J. *J. Am. Chem. Soc.* **1987**, *109*, 6189.
2. Horton, A. D. *Organometallics* **1996**, *15*, 2675.
3. Chirik, P. J.; Dalleska, N. F.; Henling, L. M.; Bercaw, J. E. *Organometallics*, **2005**, *24*, 2789
4. ZrNp<sub>4</sub>
5. Agapie, T.; Henling, L. M.; DiPasquale, A. G.; Rheingold, A. L.; Bercaw, J. E., *Organometallics* **2008**, *27*, 6245.

